Stony Brook University

Tissue Engineering Using 3D Template Casting

A Dissertation Presented

by

Travis Kruse

to

The Graduate School

in Partial Fulfillment of the

Requirements

for the Degree of

Doctor of Philosophy

in

Biomedical Engineering

Stony Brook University

December 2016

Stony Brook University
The Graduate School

Travis Kruse

We, the dissertation committee for the above candidate for the
Doctor of Philosophy degree, hereby recommend
acceptance of this dissertation.

Dr. Helmut Strey – Dissertation Advisor
Associate Professor in Biomedical Engineering

Dr. David Rubenstein – Chairperson of Defense
Associate Professor in Biomedical Engineering

Dr. Emilia Entcheva – Committee Member
Professor of Biomedical Engineering at George Washington University
Former Professor in Biomedical Engineering at Stony Brook University

Dr. Yizhi Meng – External Committee Member
Assistant Professor of Materials Science and Chemical Engineering at Stony Brook University

This dissertation is accepted by the Graduate School

Charles Taber
Dean of the Graduate School

Abstract of the Dissertation

Tissue Engineering Using 3D Template Casting

by

Travis Kruse

Doctor of Philosophy

in

Biomedical Engineering

Stony Brook University

2016

One of the major goals of tissue engineering is to develop methods that reliably fabricate tissues and organs *ex vivo* for use/implantation *in vivo*. However, the ability to create large-scale 3D tissues at physiological cell densities is hindered by our inability to sustain cells. The main reason for this is that without an incorporated vascular network, the transport of nutrients and wastes are restricted to molecular diffusion, which is limited to approximately 100 μm in biological tissues. Here we have developed a casting based templating technology to create highly ordered microchannels in polymers for MRI phantom and *in vitro* tissue engineering applications. Existing cell culture and tissue engineering models use two-dimensional substrates to make a three dimensional construct. These types of devices fail to reproduce the microenvironment of the tissue resulting in cells that are not phenotypically similar or adept at culturing in 3D. The three-dimensional tissue cultures that do exist have been limited in size due to the need for a vascular network. Our new technology has the capability to have highly dense microchannels and can be scaled to any size to sustain a tissue construct. This new method for vascularizing hydrogels on chips and in bulk has the fidelity of a bottom-up system with the scalability of a top-down system. By bridging this gap in scale we can create larger tissue constructs to address fundamental and quantitative questions about human tissues.

Dedication Page

To my friends and family who helped and supported me along the way.

Frontispiece

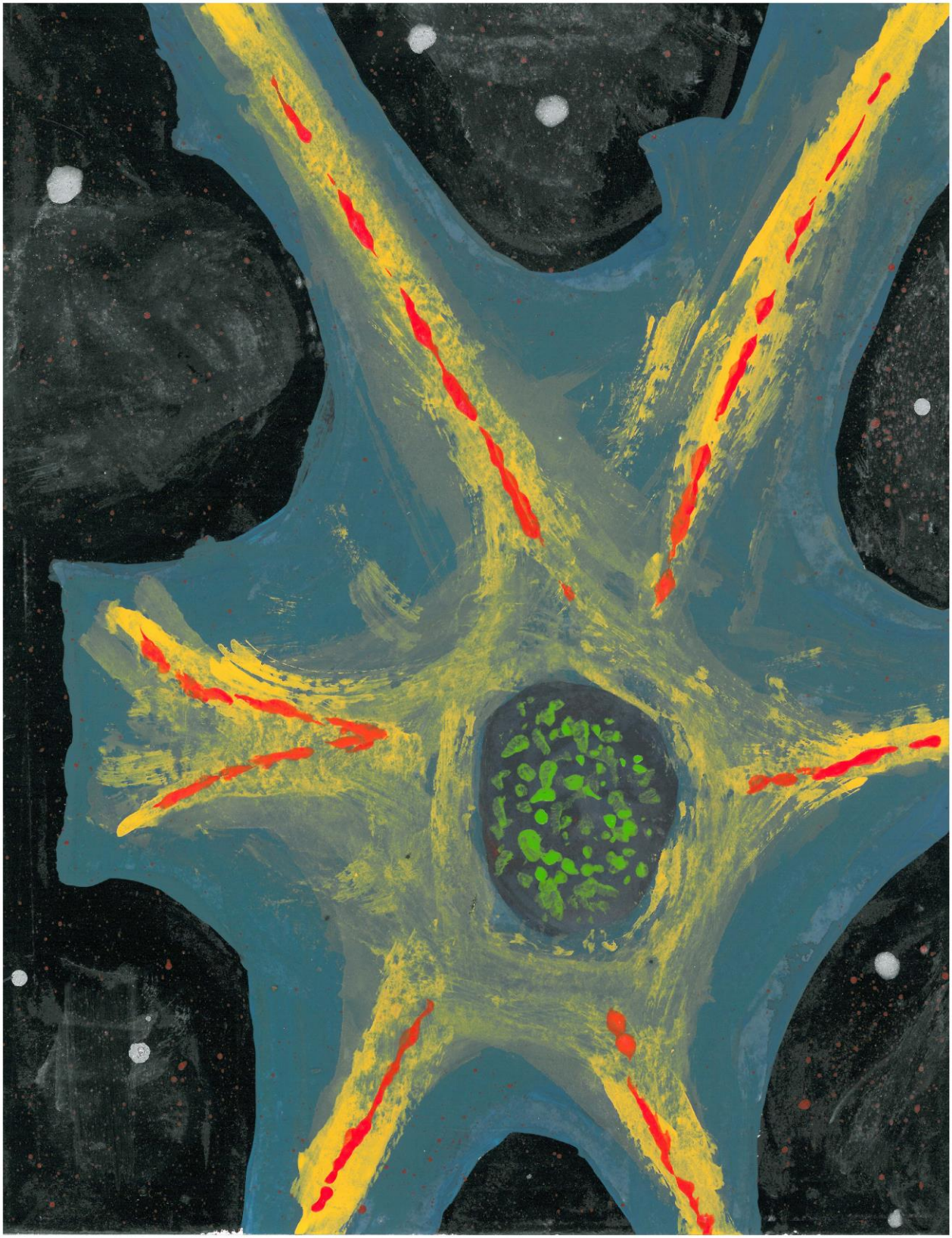

Table of Contents

List of Figures

List of Tables

List of Graphs

List of Abbreviations

Abbreviation	Description
MRI	Magnetic Resonance Imaging
CT	Computed Tomography
PET	Positron Emission Tomography
3D	Three Dimensional
2D	Two Dimensional
QBI	Q-Ball Imaging
FA	Fractional Anisotropy
μCT	Micro-Computed Tomography
DI	De-ionized
ECM	Extra-cellular Matrix
PEG	Polyethylene Glycol
PLGA	Poly(lactic-co-glycolic Acid)
PLA	Poly(lactic Acid)
GelMA	Gelatin Methacrylate
HUVEC	Human Umbilical Vein Endothelial Cells
MMP	Matrix metalloproteinase
AFM	Atomic Force Microscope
UV	Ultraviolet
AIDS	Acquired Immune Deficiency Syndrome
APTES	(3-Aminopropyl)triethoxysilane
GA	Glutaraldehyde
DMEM	Dulbecco's Modified Eagle's Medium
PBS	Phosphate Buffered Saline
HeLa	Henrietta Lacks Cell Line
HDF	Human Dermal Fibroblasts

Acknowledgements

My journey from the first year of graduate school has not been without twists, turns, and unexpected adventures. In my tenure as a student there have been many people from all walks who have contributed to my dissertation both directly and indirectly.

Thank you Dr. Helmut Strey for being my advisor. You graciously let me rotate in your lab for a semester, and it seems I never left. You supported me despite my pranks on labmates and "experiments" that were probably motivated more because I got to set things on fire than on sound scientific rigor. You also entertained my thoughts and questions of graduate school and science. In addition, my committee has been invaluable to me by providing feedback on my proposal and helped shape my work into the semblance of a thesis you see here. Specifically, Dr. David Rubenstein has listened to my crazy theories about how biology only works under a full moon and tried to guide me toward more widely accepted theories.

I'd also like to thank Dr. Eric Brouzes. We started as officemates where you showed me many of the techniques I would later misremember, do improperly, and teach others incorrectly. Your work and ideas were the basis of where my projects stemmed from, and though my works has diverged from yours, you still provide insightful feedback and suggestions.

Thank you to (somehow a doctor) Tomasz Bakowski, who put up with me constantly beating him in prank wars and commiserated with me on project failures. You have been vital in all of my wayward plans to build a snack cabinet (marginal success), finding out how to bypass a locked door (success), determining what the chemical waste consisted of (success), and building drones (not yet a success), among many others. Truly you have been there for me, and this thesis would not have been nearly as entertaining without you.

To my current and former labmates: April Carniol, Smiti Bhattacharya, Danni Wang, Cookie Yu, Dr. Martin Sauzade, and Arun Ajay, thank you for dealing with me day in and day out. We solved all kinds of problems together. You put up with my puns, my daily eye rolling, lack of lunch volume, frequent side projects, and winning personality. Most of you have left for greener pastures, so thank you for your company and help while you were here. To those who have not yet left, I wish you the best, and hope that you too can escape as I seem to have done.

Thank you friends in the BME department. There are too many to name you all, but I'd like to extend a special thank you to Dani, Divya, Yahfi, Dr. Jason, Mariola, David, Dr. Sunny, Stephen, and Dr. Atulya. You all were an amazing group of people and were the best to be around. It was great to be in classes, play volleyball, go hiking and camping, drink, and generally hang out with you all.

Thank you Dr. Samema Sarowar, who bore the brunt of my antics. Your endurance dealing with me is prize worthy. You've listened to my hopes and fears and helped me navigate my thesis. I'd be worse off without your sage advice and guidance at times. Thank you for supporting me and all my inane ideas.

Lastly, I'd like to thank my family: Robert, Cindy, and Spencer Kruse. You guys have been there behind the scenes reading my papers, providing encouragement, and tolerating my relocation from California to New York. I now have an appreciation for cold weather, snow, and more than just one season a year.

1. Introduction to Biologically Relevant Microchannels

In the last few years, rapid developments in microelectronics and biotechnologies have led to advances in applied research of micro-biochips, micro-reactors, and microfluidic systems. Throughout these micro-systems, the common mechanism of fluid transport is via microchannels. Microchannels can be used to: connect different reaction chambers, deliver reactants, separate particles, control fluids, mix chemicals, and for a myriad of other applications.

In biology, microchannels are essential in almost every form of life from the invisible roots in trees and the threadlike hyphae of fungi to within all mammals in the form of vasculature, neural connections, and the lymphatic system. These channels are not simply long intersecting tubes but a vast three-dimensional interconnected network of interlacing conduits through which blood, lymph, ions, and numerous other signals are passed.

The scale of this network is staggering: the length of the blood vessels within your body laid end to end can reach up to 100,000 km with most of that length being made of channels that are less than 100 μm in diameter. Mimicking microchannels for research is therefore vitally important in deepening our understanding of biological phenomenon. To appreciate the difficulty of this undertaking, we must understand the scales that are involved. We will focus on three systems in mammals: vasculature, the lymphatic system, and the nervous system.

Blood vessels and lymphatics are responsible for circulating nutrients and recapturing interstitial fluid within the body. The channels that form these systems have diameters that can range from centimeters to less than 100 μm in diameter. In addition to being extremely small in diameter blood vessels and lymphatics have extremely dense networks throughout our tissues. Any cell is typically no more than 150 μm from one of these channels. This maximal distance is

set due to the limited diffusion length of nutrients within tissues. The diffusion lengths of molecules are primarily affected by their size; smaller molecules can travel farther through tissues.

Axons, a primary unit of the nervous system, translate signals from one end of a neuron to the other. These axons are, in fact, microchannels. They are water and ion filled tubes that range from 2 to 20 μm in diameter. Axons within the brain are especially dense and each axon is a distinct microchannel. Together they form a complicated intersection of channels within the brain.

Each of these systems has complex 3D architectures. They are not simple linear systems of tubes. There is no technique that can create the detailed and complex architecture seen in nature at large scale. Instead, we see systems that either create detailed features in small volumes or large features in large volumes. There is little overlap between these two methodologies. Creating a system to synthetically create both complicated and small channels in large volumes would lay the groundwork for future research platforms. Such a platform will allow researchers to probe the fundamentals of tissue biology and enable accurate study of human diseases without the need for animal studies.

Here we have created a platform to create microchannels in a variety of polymers for applications in neural biology and tissue engineering. We take a simple casting technique of fibers and use it to develop a flexible low cost platform to create microchannels of arbitrary complexity in and sized volume.

2. Fabricating Microchannels in PDMS

A. Biological Background and Motivation

There is currently a push to map and understand the connections in the brain from the Human Connectome Project. The cutting-edge techniques to image and characterize the internal network of connections in the brain *in vivo* include magnetic resonance imaging (MRI), computed tomography (CT), and positron emission tomography (PET). These modalities generate images of living brains by measuring the relaxation of molecular spins, the densities of biological structures, and positron emissions, respectively. Each of these techniques gives information about the internal structures in the brain but their resolution is limited (on the order of millimeters). Large features in the brain can be resolved but miniscule features like individual axons, the structures that connect neurons, are only 4 μm in diameter and cannot be observed.[1] By measuring the anisotropic diffusion of water in addition to the spin relaxation times, dubbed diffusion MRI, we can infer the location, orientation, and connections, of axons in the brain.

i. Diffusion MRI

Diffusion MRI maps the neural connections within the brain by identifying and tracing areas of anisotropic diffusion. The methodology of mapping white matter using diffusion imaging was developed in 1994.[2] It built off early work in magnetic resonance imaging, which measured the movement of water molecules, and exploited the anisotropic tendencies of water diffusion in white matter to detect axon bundles.[3-5] White matter is composed of myelinated axons that connect the various areas of the brain to each other and carry the nerve impulses between neurons (Figure 1). These axons are long cylindrical structures that carry ionic signals

between synapses. They are can be grouped into large bundles of 2000 or more in major areas. As with all cells in our bodies, one of the principle components in axons is water.

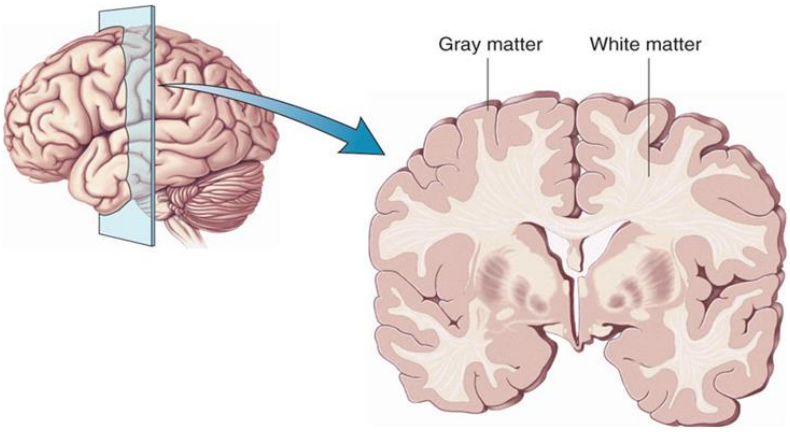

Figure 1: A representation of the brain and the white and grey matter regions.[6]

Diffusion describes the tendency of the random motion of molecules in a solution to move in space on a "random walk". In a featureless container, molecules can diffuse in any direction. But if they were confined to a cylinder, the diffusion would be asymmetrical and more anisotropic. A similar phenomenon occurs within the axons of the brain. The diffusion of water molecules along the white matter fibers is much faster than perpendicular to them.[7-9] Diffusion MRI generates traces of axons by measuring and plotting the differing rates of diffusion in various directions within the white matter of the brain.

Diffusion imaging in MRI utilizes a similar technology to normal MRI. Water molecules are excited with a strong magnetic field causing them to precess simultaneously and to produce signals in MRI. Contrast is achieved by measuring the change in synchronicity between the water protons. Protons that can free tumble, such as those in water, tend to relax faster than those that are more confined and can generate contrast between tissues. To use a MRI to measure diffusion, a magnetic field gradient that is varied linearly is used instead of a homogeneous magnetic field. The rate of precession is proportional to the field strength, and the protons will

precess at different rates as they diffuse along the gradient. Shortly afterwards, another magnetic pulse is applied in the same magnitude but in the opposite direction. The protons that have moved between the two magnetic pulses will not realign perfectly, reducing the signal measured by the MRI. By taking many measurements along different gradient orientations, a tensor map can be generated to extract the diffusivities of a region of interest.[2-5,10,11]

In white matter, the axons are very anisotropic and there is much faster diffusivity along the fibers than perpendicular to them. This anisotropy does not apply to grey matter however, as the high density of connections leads to a similar diffusivity in all directions.[12] In addition to measuring the magnitude of diffusivity in an area, diffusion MRI can measure a fiber's alignment in space. The information from these measurements can be used to create a map of white matter fibers in the brain. The lines are connected between the largest directions of diffusivity in each voxel, assumed to be the direction of the axon bundles, and rendered in 3D (Figure 2).[13-16]

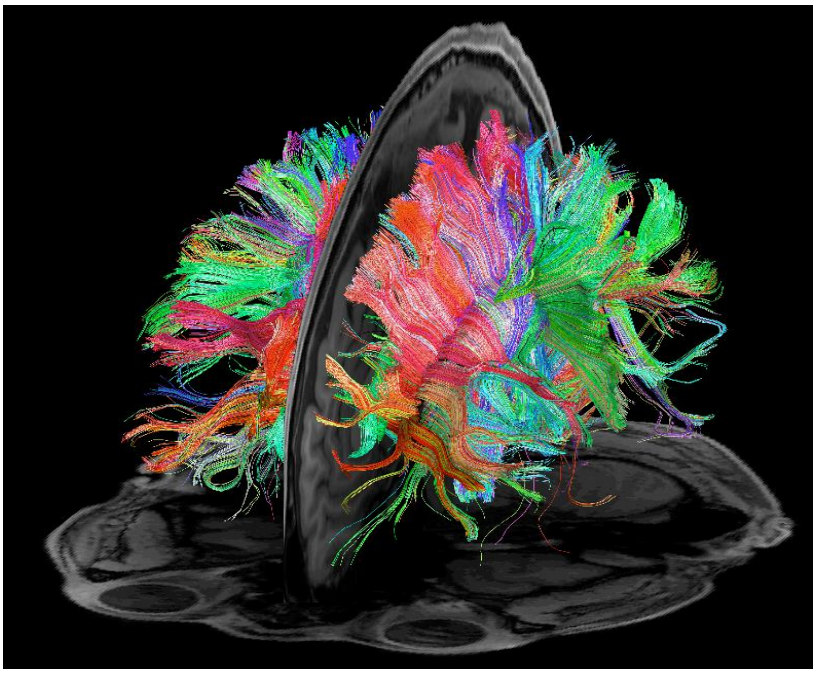

Figure 2: A representation of the axonal connections within white matter.[17]

Diffusion MRI gives a good general sense of the connections within white matter in the brain. Indeed, it has seen use in defining the severity of diffuse traumatic brain injury[18-20], localization of tumors[21-24], and diagnosis of vascular strokes in the brain[25-28]. But there are several limitations to the diffusion MRI model as it relates to white matter tissue. First is that the model assumes that diffusion in the white matter is Gaussian[3], but there are compartmentalization and other effects within the white matter indicating that diffusion in the white matter is non-Gaussian[29-32]. The second limitation is that the use of a single diffusion tensor to describe each voxel is not sufficient. Each voxel in a typical diffusion MRI experiment represents about 2.5 x 2.5 x 2.5 mm of white matter area. This volume of brain matter contains thousands of axons and glial cells. Representing all of these structures with a single diffusion tensor will reduce the diffusion to an average direction and magnitude of the multitude of individual fibers. The basic diffusion MRI model will fail in cases where fibers overlap or share the same voxel area (Figure 3).[33-35]

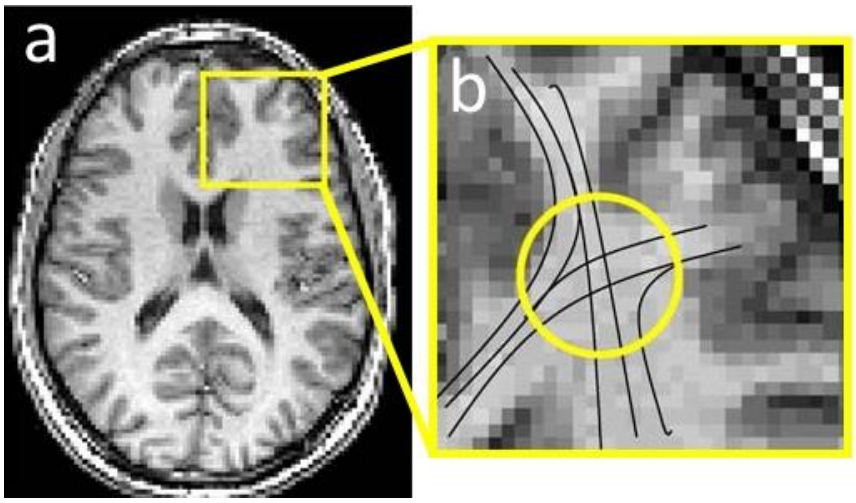

Figure 3: An example of a partial volume artifact in DTI. An anatomical image of the brain (a) with the right frontal region enlarged (d) including line traces of the different fiber systems in the region. Adapted from Assaf et. al.[36]

In order to understand white matter axon fiber crossings, more elaborate techniques such as Q-Ball imaging (QBI) must be used. Q-Ball imaging differs from traditional diffusion MRI in that it assumes diffusion can exist in more than one direction and assigns a direction based on probability calculated from scans. But even this technique is useless without validation. Any validation of these methods requires a phantom to compare the scan to a well-known ground truth geometry. Ideally, the phantoms should be physiologically relevant to the white matter we are measuring. Axons, the primary component of white matter, are <5 μm in diameter and extend centimeters throughout the white matter.[37] There have been several biological phantoms created to validate diffusion MRI and QBI models including rat spinal cords and asparagus stalks. While these phantoms offer a good comparison to *in vivo* diffusion in terms of fiber diameter, length, and fractional anisotropy (FA) they lack reproducibility due to biological variability and suffer from biological degradation over time.[38]

Calibrating a diffusion MRI requires *a priori* knowledge of the internal structures, and currently the only way to validate new diffusion MRI methods on brain matter to compare the scan to a dissected brain.[4] Creating an axonal connection mimic, or phantom, which has well defined ground-truth channel geometries would enable the accurate calibration of diffusion MRI methods and facilitate the discovery of new techniques. A diffusion MRI phantom will necessarily include microfluidic channels in order to copy the water-filled tube-like axon.

ii. Currently used Diffusion MRI Phantoms

Manufactured phantoms for diffusion MRI and QBI offer a solution to the biological phantom's shortcomings. Instead of relying on biology to create diffusion anisotropy, the diffusion in a synthetic phantom can be adjusted to simulate biological white matter. A successful phantom must have aqueous channels that are similar to axon shape and size, have a

large enough volume to fill multiple voxels in the MRI scanner, and be customizable in different geometries. In its most simplistic form, a diffusion phantom uses an array of parallel glass capillaries to create diffusion anisotropy.[39] The anisotropy arises from water only diffusing along the capillaries and not through the glass walls. The glass capillaries used (23, 48, and 82 μm in diameter) created an FA of up to 0.50 (Figure 4a). They saw good agreement between the calculated diffusion path and the capillary orientation. This type of approach is unidirectional, cannot be made into complex geometries, and the capillaries are much larger than axonal diameters.

Artificial fiber phantoms offer more flexibility than their glass capillary counterparts. Individual fibers are bundled together and the bundles are interweaved at specific crossing angles (Figure 4b). Once all of the bundles are woven, the fibers bolts are confined in shrink wrap.[40] This limits the movement of the fibers and restricts and space between them. The FA is relatively high because the water tends to diffuse along the spaces between the fibers rather than into them. With fiber phantoms, hydroscopic fibers tend to have lower FAs. Inherent to fiber phantoms is their flexibility which, in turn, may limit reproducibility as the fibers can shift and twist within the wrapped bundles. In addition, the spaces between the fibers are not accurate models of the hollow cylinder of an axon and the crossing between the fibers are not isolated, minimizing the FA.

A diffusion MRI phantom with high FA was created by winding fibers at high tension around a grooved ball. The grooves of the ball were used as a mold, and molten agarose was cast around the fibers.[38] This fixed the fibers in place while also allowing diffusion to still occur (Figure 4c). Using this technique yielded an FA of 0.9. The spherical nature of the ball created well-defined complex crossing geometries. This technique proved temporally stable over the

course of months. While it did produce a high FA, filling the spaces around the fibers with hydrogel is not an accurate physiological description of white matter.

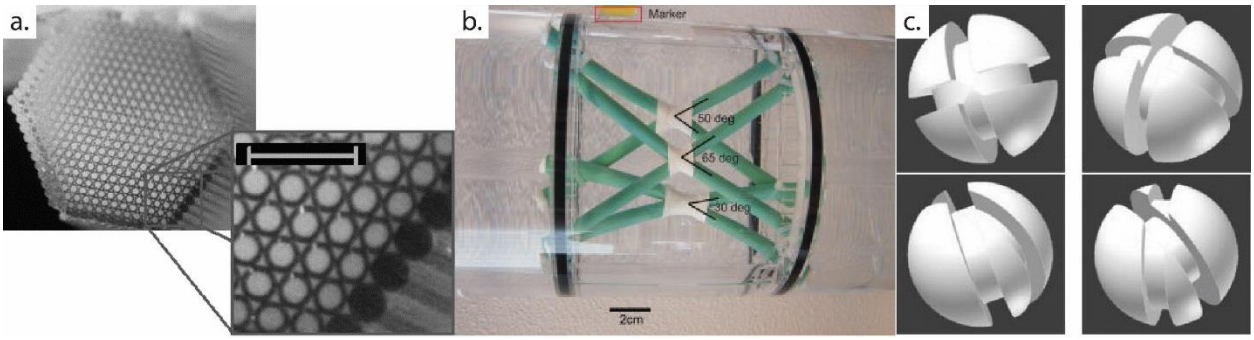

Figure 4: A variety of DTI phantoms: glass capillary based (a), bundled string in shrink wrap (b), and fibers wound around a spherical core (c).

Microfluidics, as a field, emerged in the 1980s and concerns the movement, manipulations, and control of fluids that are confined to small micro-scale channels. Within this scheme, the behavior of fluids is not the same as bulk. Particularly the forces involved in surface tension, energy dissipations, and fluidic resistance, start to dominate the system. One of the most important consequences at this scale is that fluids do not mix as in bulk. Instead fluids that are side-by-side do not necessarily mix because the flow is laminar and not turbulent. By exploiting the features of this system the field of microfluidics has widespread applications throughout biology and physics.

Typically, polydimethylsiloxane (PDMS) is used to create microfluidic devices. It creates an almost exact copy of a silicon wafer template down to the nanometer level.[41] By creating embossed patterns of channels on silicon wafer, a process dubbed photolithography, the PDMS can be used to create a mold of the channels. The minimum size of these microchannels is not limited by the properties of PDMS but by the resolution of photolithography to about 1 μm.[42] Once the mold is made, the PDMS can be permanently bonded to a glass slide to create precisely defined microchannels useful in microfluidics applications.[43] A microfluidic chip, an assembly

of the PDMS mold and glass slide, usually has microchannels with a cross-section area of ~10,000 μm^2 and a length in centimeters and is limited to a single plane of microchannels, or two dimensions. Three dimensional, or layered, microfluidic chips can be created but they require laminating multiple single layers of channels into a final construct. Creating only a few layers is relatively straightforward, but as the number of layers increase so does the need for precise alignment between the layers to ensure that all of the microfluidic channels are connected.

A laminate of thin PDMS layers has been demonstrated as a diffusion MRI scan phantom. Positive channels are created on a silicon master via photolithography and used as a mold for the PDMS layers. The PDMS layers are molded one at a time and then aligned, stacked, and bonded into a block of channels.[44] Different patterns on the silicon master can create different crossing (Figure 5a) or parallel (Figure 5b) microchannel patterns within the PDMS. The required size of the channels is 5 μm which approaches the minimum resolution limit of soft lithography. Delamination and air bubbles between the PDMS layers can also occur and cause aberrations in the scan. The FA can be adjusted to almost any value by modifying the channel spacing. The limitation of this technique is the time required to create a phantom that can fill several voxels on a diffusion MRI scan. We assembled 7 layers of this phantom into a proof of concept device that created a phantom that was only 400 μm thick (Figure 5c)

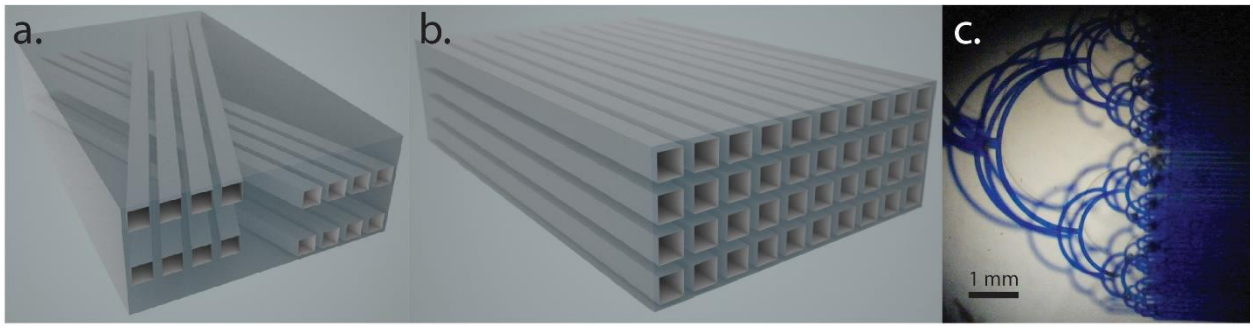

Figure 5: Schematic for laminated PDMS microfluidic channels to mimic axons in crossing (a), and parallel (b) patterns, and a proof of concept assembly of parallel channels (c).

None of these current models are able to provide physiologically relevant channel geometry, construct volume, a volume fraction of greater than 50%, in addition to a high FA (>0.80). Another limitation of these phantoms is that some do not model white matter as hollow channels with water residing inside the axons, but as solid cylinders with water diffusing around them. While this sold cylinder approximation is similar to the physiology of white matter, it does not accurately reflect the diffusion of water within the axons. Our solution to this gap in dMRI phantoms is to create a phantom in PDMS using template casting techniques. Our technique has a well-defined ground truth, is not degradable, accurately mimics the axonal formations in the brain, and is compatible with current MR techniques. The use of this device as a dMRI phantom can lead to new discoveries and facilitate the research into new MRI techniques.

B. Materials and Methods to Create and Validate the Phantom

Some of these phantoms use a polymer to encase the fibers and mimic physiological conditions, typically a hydrogel. Hydrogels are ideal materials to mimic properties of white matter. Typically, the phantoms leave the fibers encased with the hydrogel. Hydrogels are too soft to be able to remove the fiber from them. Instead of using fibers embedded in hydrogel to mimic white matter, we propose using fibers as a sacrificial template in a polymer casted mold to create microchannels that can be filled with water and scanned. Few materials are both MRI compatible and have the strength to withstand the withdrawal of fibers, but PDMS is able to maintain high accuracy casts of fibers and maintain MR compatibility. We will use template casting to fabricate the microchannels in this diffusion MRI phantom. Our template casting technique is a one-shot, negative mold of the small diameter fibers that mimics white matter diffusion properties.

i. Materials

Material	Specs	Source
Replicator 2	500 μm resolution	Makerbot, New York
3D Printing Filament	1.75 mm PLA	MatterHacker, California
Nylon Fibers	20 μm ø	Lowes, Stony Brook
Diisopropylamine	99%	Alfa Aesar, Massachusetts
Polydimethylsiloxane (PDMS)	Sylgard 184	DowCorning, Michigan
Spin Coater	--	Laurell, Pennsylvania
Isopropyl Alcohol	99%	Fisher, New Hampshire
Gadolinium(III) chloride hexahydrate	99%	Aldrich, Connecticut
Sodium Bromide (NaBr)	99+%	Aldrich, Connecticut
Food dye	--	Wilton, Illinois

Table 1: Materials used in Chapter 2.

ii. Fabricating the Diffusion MRI Phantom

To create our diffusion MRI phantom, we must first determine the type of fiber interactions we want to simulate. There are countless ways for fiber bundles in white matter to interact with one another. Here we will simulate to two interaction types: passing through, and looping over. These two interactions are simplistic models of the complex crossing and parallel fibers in the brain but are helpful in calibrating and validating new MR techniques. By first understanding these simple models, we can create models that can more effectively understand the complex interactions within white matter.

After deciding on a fiber bundle arrangement, we 3D print a custom designed mold to hold the PDMS. By using 3D printing, we can create molds to position the fiber bundles in however we choose. Our 3D printed mold has dimensions of 3 x 3 x 3 cm (Figure 6a). We use this large of volume mold to try and maximize the number of voxels the DTI scan has of the fiber crossing region of interest. We are limited to this phantom volume because the solvent we will use to swell the PDMS can only penetrate up to 1.5 cm of thickness.

After constructing the mold, we orient nylon fiber bundles within the mold (Figure 6b). Nylon fibers are used because they do not adhere to PDMS, have a high tensile strength, and are chemically resistant to solvents and can be obtained in roughly the right diameter. Each nylon fiber is approximately 20 μm in diameter, and there are about 2000 fibers in one bundle. Ideally, we would use fibers with diameter approximating that of axons, but there are no commercially available fibers that meet the requirements for this method. The bundle size was chosen because it is large enough to fill several voxels on a diffusion MRI scan, but small enough to be effectively cast using our technique.

As the fiber bundles are placed in the 3D printed mold, we apply tension to them and attach them to the mold with glue to ensure close packing. Using this method, we are able to achieve near 80% volume fraction similar to the physiological size of axon bundles. We physically separate each bundle of fibers that are placed in the mold using a thin (~100 μm) sheet of PDMS. The sheets of PDMS were created by spin coating uncured (10:1 crosslinker : polymer) PDMS on to a silicon wafer at 1000 RPM for 90 seconds, curing at 80ºC for an hour, and then sectioning into squares of 5 x 5 mm. It is important that the crossing bundles of fibers have no crosstalk to maximize the FA and to ensure there is minimal noise in the diffusion MRI readings.

Once all of the fiber bundles are placed in the mold, the mold is filled with PDMS (10:1). The device is degassed to remove any bubbles introduced when mixing the PDMS and then baked at 80˚C for at least 2 hours to cure the PDMS. Once cured, the PDMS block with embedded fibers is removed from the mold (Figure 6c). At this stage, the nylon fibers cannot be removed from the PDMS block. To remove the fibers we must immerse the construct in a solvent of PDMS, diisopropylamine, to swell the PDMS to allow for removal.[45] Our inspiration

to remove the nylon fibers was adapted from Verma et. al where they removed a single nylon fiber cast in complex geometries from a thin sheets of PDMS.[46] Our technique follows the same principle of swelling the PDMS but does it in a construct with much less surface area to volume ratio.

The swelling process is done serially, slowly, and over the course of several days. Immediately immersing the fiber construct in 100% solvent would cause the outside of the PDMS to swell faster than the inside and will shatter the block. Instead, we immerse the block in a serial dilution of the solvent starting at a ratio of 25% diisopropylamine to 75% isopropyl. After 24 hours, we transfer the fiber construct to a 50% diisopropylamine solution, and a 75% solution 24 hours after that. Once the fiber construct has been in 100% diisopropylamine for 24 hours, we can begin removing the nylon fibers (Figure 6d).

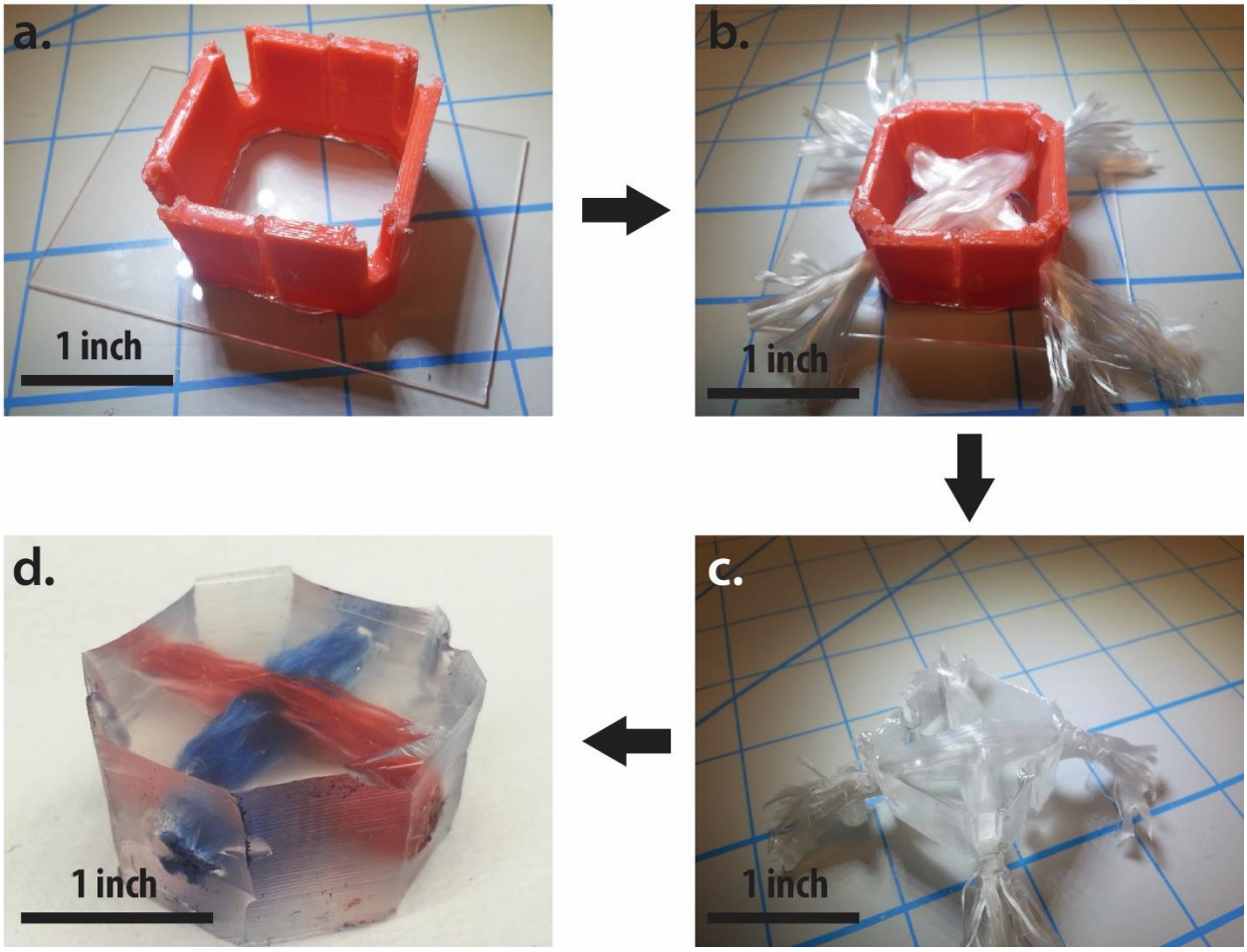

Figure 6: To create the DTI phantom we: print the mold (a), arrange the fibers (b), cast the PDMS (c), and remove the fibers (d).

If placed incorrectly, the ends of the nylon bundles can tangle and as the PDMS block is swollen, rip and tear through the softened PDMS. Therefore, correctly orienting the fiber bundles when casting the PDMS block is paramount. To remove the nylon fibers from the fiber construct, we gently pull small groups of fibers from the construct. Care must be taken during this process to ensure that the highly volatile solvent does not evaporate and start de-swelling the PDMS prematurely, because it will break the construct. Once all of the fibers are removed from the fiber construct, the whole PDMS block is de-swelled in a reverse process of swelling. We let the PDMS block with microchannels, a phantom construct, sit in 100% isopropyl after de-swelling for 72 hours to elute as much of the solvent as possible. Then the phantom construct is baked in

an oven to remove any solvent left within the PDMS. The resulting phantom construct has microchannels of the same diameter as the nylon fibers and in the same orientation.

iii. Validating the Diffusion MRI Phantom

To validate our phantom, we need to confirm microchannel size and orientation, volume fraction, FA, and prove that it can be used as a ground truth device.

To measure channel diameter, we use thinly cut slices of the phantom construct cut orthogonal to the microchannels (Figure 7). We measure the diameter using a calibrated optical micrograph. The orientation of the microchannels within the phantom construct were observed qualitatively by filling the channels with dyed water. From this result, we are able to understand the basic orientation of the microchannels.

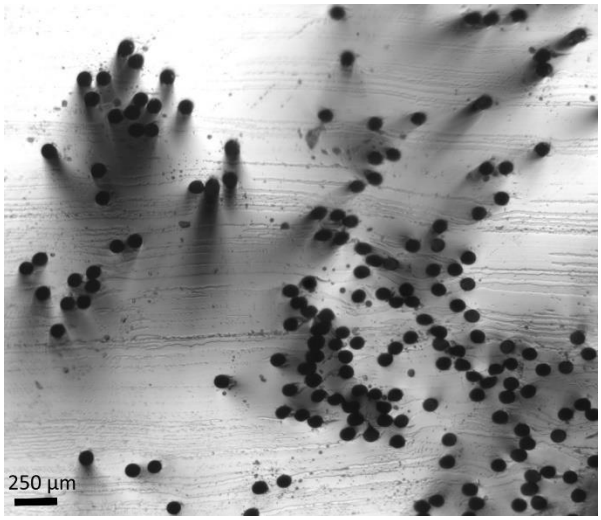

Figure 7: Template molded microchannels after the nylon fibers have been removed from the PDMS.

To find the channel volume fraction, we sectioned a phantom construct and observed the spacing between the channels near the center of the construct in an optical microscope at several locations within the construct. The area we are most concerned with ensuring tight packing is near the intersection of the fiber bundles, as that is where the MRI scan will be focusing.

Directly measuring the FA requires a MRI scan. But we can estimate if this proof of concept phantom construct will have a sufficiently high FA by determining whether there is any connection of crosstalk between the microchannels. Any imperfections in a single microchannel wall will necessarily limit the FA that can be achieved for that microchannel. If there are too many connections between channels within the device, then the phantom construct will not have a sufficient FA required to mimic neural connections. To find any crosstalk between the fiber bundles, we injected dyed water into one set of microchannels (Figure 8) through a pressure connection. Any overlap between the crossing fibers would be evident by the color penetrating the other channels. We repeated this for several single microchannels and microchannel bundles. This procedure was repeated for the other set of microchannels using a different colored dye to have any crosstalk be evident.

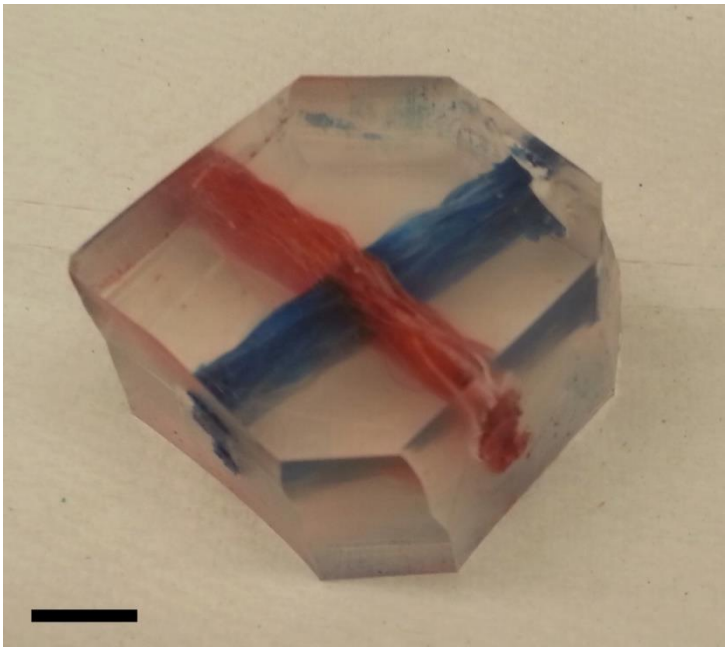

Figure 8: A PDMS phantom construct with nylon fibers removed. Red dye was injected in one direction and blue in the other to observe any cross-talk between the bundles. Scale bar is 1 cm.

For our phantom construct to be a viable phantom for diffusion MRI, we must have a good understanding of the geometry and location of all of the microchannels in the phantom

construct, and create a ground truth scan for comparison. While we have a qualitative idea of the arrangement of the fibers before being cast in PDMS and we can see the microchannels inside of the clear PDMS phantom construct, we cannot precisely identify and localize individual microchannels quantitatively. Even the best optical microscopes only have a working distance of ~1 mm, and our phantom construct is 3 cm in its smallest dimension so we must use a technique with a larger working distance. To construct a quantitative ground truth of the microchannels in the phantom construct we used a micro-computed tomography (μCT) scanner (Scanco μCT 40, Switzerland) which will determine high resolution information of the channel location and orientation. The μCT scanner works much the same as a normal computed tomography scanner, but on smaller objects and with higher resolution. In the same way, the scanner generates contrast in the image by calculating areas that the x-ray signals are attenuated. By filling the channels with a high molecular weight solution, 2M sodium bromide (NaBr), we can achieve the contrast we need to visualize the channels (Figure 9). The channels are filled by immersing a dry phantom construct in the NaBr solution and pulling a vacuum on the container for 30 minutes. The PDMS construct is permeable to certain gases, and by removing the air from the construct and channels we can ensure that the NaBr solution penetrates the entire phantom construct.

To prove that phantom construct can be used in a diffusion MRI setting, we must use it in an actual MRI. To prepare the phantom for scanning, we soaked it in a gadolinium solution in vacuum for several hours. We acquired the diffusion MRI data on a 3T Connectome scanner (MGH-USC, MAGNETOM Skyra CONNECTOM, Siemens Healthcare). The signal from the scan was recorded on a 60-channel “panini press coil”. This coil is made of two flat panels with 30 channels in each. Q-ball imaging protocols were used to acquire the data from the phantom. We used 64 evenly distributed sensitizing directions in a 21 cm x 21 cm field of view resulting in

41 slices with 1.5 mm^3 isotropic voxels. The orientation distribution function reconstruction and fiber tracking were performed in DSI-Studio.[47-49]

C. Results

The nylon fiber we used to as a cast in the fiber construct was 19.8±1.1 μm in diameter and was in good agreement with the diameter of the channels in the PDMS of 19.3±1.2 μm. There were approximately 2000 fibers per bundle of fibers used and each phantom had at least 5 bundles of fibers in each direction.

We calculated the volume fraction of our phantom construct to be 0.78 near the region of interest within the phantom construct. But by applying sufficient tension to the fiber bundles before casting, we found that over the length of the phantom packing constant did not deviate more than 5%.

There are some connections and cross talk between microchannels in the same bundle within the phantom construct. But between bundles, and specifically at the region of interest in the center of the phantom construct, there were minimal connections. Though, most importantly between the two directions within the phantom construct there was no crosstalk.

To visualize the channels, they must have a different x-ray contrast than the PDMS block. Filling the microchannels of the phantom construct with deionized (DI) water does not provide enough contrast to the PDMS for the μCT. Using a high molecular weight solution, 2M sodium bromide (NaBr), gives us the contrast we need to visualize the channels (Figure 9). While we are able to visualize the different groups of channels, the μCT has limited resolution of 36 μm for samples this large and cannot resolve individual microchannels.

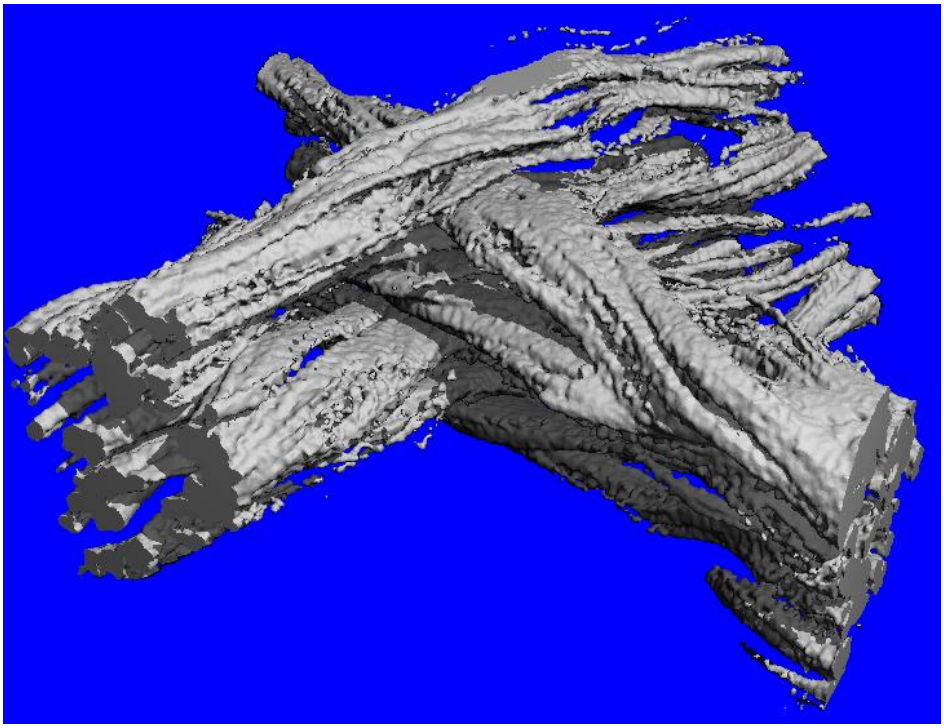

Figure 9: The 3D reconstruction of the microchannels within the phantom construct using µCT.

The diffusion MRI scans were performed at Harvard MGH by Qiuyun Fan, Ph.D. (Figure 9). The scan showed the two directions of diffusion within the phantom. Within the model are points where the diffusion traces are not straight, this is due to the large voxel size and limited size of the fiber bundles. Comparison of the diffusion MRI scan and the µCT reveal good registering between the two.

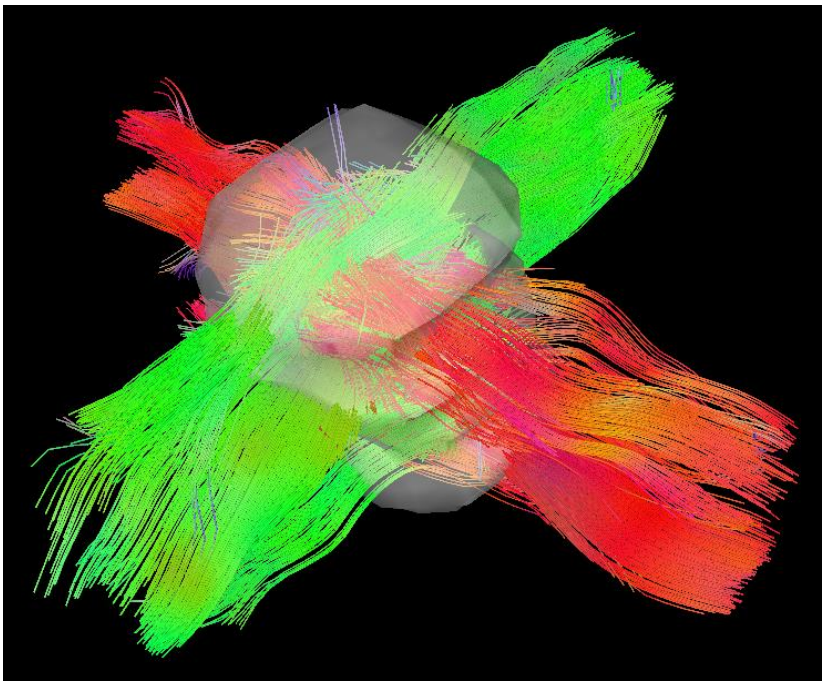

Figure 10: A diffusion MRI scan of the phantom construct showing two directions of fibers through it, green and red.

D. Discussion

We saw that the diameters of the microchannels in the phantom construct closely matched those of the nylon fibers. This agreement is essential in validating this template casting technique. It also proves that the swelling and de-swelling of the PDMS block does not affect the cast of the fiber. This was of concern because diisopropylamine, the solvent chosen to swell PDMS, has the greatest solubility and swelling ratio in PDMS of any solvent.[50] Therefore, the PDMS is still stable through this process and the phantom is able to be used multiple times as a calibration device. The length of microchannels in the phantom construct is set by the 3D printed mold but holds little consequence in the region of interest we scanned with an MRI. The length was chosen because it was as large as we could make it and still reliably swell the PDMS to remove fibers.

The number of fibers was arbitrarily chosen as the nylon rope the fibers were from came in bundles of that number. In the future, knowing the bundle size can lead to more precise phantom construction by mimicking the typical number of axons in a bundle. Here, the 2000 fibers per bundle were ideal for filling the region of interest with the highest density of fibers and also allowed us the most control over their placement. Placing a single fiber at a time into the model would be a time consuming and tedious process. Instead we are able to build up large amounts of microchannels with high density and only minimal crosstalk by using these large bundles.

When placing the bundles into the model we apply tension to them to limit drooping in the middle of the model. There is some inherent helical twist to the fibers as they came from a braided rope and not all of it can be removed. We must put enough tension on the fibers to remove the drooping and minimize the twisting of bundle as well as to increase the close packing of the fibers. Theoretically more tension could be applied, but due to the strength limits of the 3D printed plastic, the fibers maintained some of their twist. While perfectly straight microchannels would be easier to characterize, we believe that the tortuous path that the fibers take can be used to resemble the random orientation of axons within the brain.

More important than number of axons is the volume fraction they represent in the phantom construct. We want the phantom to be as close to physiological as possible. Wide ranges of the volume fraction of axons within white matter have reported, from 30% up to 70%.[51-53] The volume fraction of our microchannels may be artificially high because of the large diameter of the channels relative to biological axons. But the volume fraction can be adjusted somewhat by limiting the tension of the fibers when placing them in the mold. By allowing the

fibers to naturally spread out after being placed in the model we can reduce the volume fraction from what we calculated, 80%, to more physiologically relevant fractions.

In order to create a region in the middle of the phantom construct with a volume that would fill at least a few voxels in the MRI scanner with 1.5 mm^3 sized voxels, we needed to use at least 5 bundles of fibers in each direction in our construct. We have created phantoms with up to 10 bundles of fibers in each direction as well. The danger with putting increasing numbers of fiber bundles into the PDMS block is that it decreases the structural stability and removing that many fibers can cause the construct to rupture.

The μCT results show us a ground truth of the location of the microchannels within the phantom construct. The format indicating the channel locations from the μCT can be directly used in verifying the Q-Ball analysis. While the resolution of the μCT is limited, having a smaller phantom would allow for us to acquire in a higher resolution. The threshold to contrast the fibers from PDMS is also difficult to determine at certain locations. With the scan of the phantom we can clearly see the differentiations between the bundles of microchannels in the PDMS. Harder to determine is any crosstalk of channels within a specific bundle because the resolution of the scan is not enough to resolve a single fiber.

The results of this study have implications for the brain imaging field. By creating well defined phantoms using our template casting methods, arbitrary microchannels in PDMS can be created for a variety of applications.[54] Here we demonstrate its usefulness in dMRI applications, but it can be used as an analog for other biological systems such as capillary beds as well. In addition, the resolving the small diameter fibers is not a uniquely MRI problem, but extends to CT and PET modalities as well. The same phantom can be used in a cross-functional study to

better understand the limitations and advantages of a modality with certain axonal organizations.[55,56]

i. Lessons Learned

To eliminate as much crosstalk between the microchannels as possible, we use thin sheets of PDMS (10:1 polymer : crosslinker) between the bundles of fibers. These bundles can move and shift, especially when using numerous fiber bundles. Adjusting the sheets after more bundles have been placed can be difficult because they become lodged in the fiber bundles. The thin PDMS sheets can also be torn easily so care must be taken when placing and moving them within the mold. The crosslinker ratio of the PDMS sheets being used to separate the fibers must be the same as that of the PDMS block. Different ratios can lead to separation between the two polymers and cause the PDMS block to have gaps within its internal structure.

When assembling the mold, as much of the space between the fibers must be eliminated to create as good of a seal as possible. If the fibers are too loosely placed liquid PDMS can leak through them and out of the mold. When this happens, a second pour of PDMS is required, which may not bond tightly with the previous pour causing the block to split when swollen.

To find the right parameters to be able to remove nylon from a PDMS block was a long process. Using thin sheets of PDMS allows for ubiquitous and rapid swelling of the polymer and easy extraction of the nylon fiber. As the size of the smallest dimension of a PDMS block increases so too does the time it takes the solvent to penetrate into the PDMS. Immediately putting the block of PDMS into the solvent swells the outermost layer of PDMS so rapidly it breaks off from the inner core. Slowing the swelling process is paramount in ensuring the fibers could be removed. We slowed the swelling process by swelling the block in serially increasing concentrations of solvent.

PDMS which is swollen with solvent has much lower hardness than the original block.[57] Fibers which become entangled on either side of the construct may tear through the block rather than being extracted and leaving a microchannel. Still, there must be some fiber extending from the block to pull from. We solved this problem by cutting one side of the fibers even with the block before swelling. During the swelling process, some of the fibers may be pulled into the center of the construct so trimming both sides will result in fibers being left within the block after de-swelling.

Pulling the fibers with an even tension parallel to the block of swollen is key to successfully removing the fibers without tearing. Removing large groups of fibers simultaneously might speed up the process of creating the construct, but leads to more tears through the block. To create a successful phantom, there should be no tears while keeping all the microchannels whole. The problem with removing one fiber at a time is that while the block is out of the solvent, the solvent is evaporating and the block is de-swelling. Therefore, the PDMS block must be re-immersed in the solvent every 5 minutes during the fiber extraction process to ensure that the block does not de-swell too quickly.

Similar to swelling the PDMS block, de-swelling must be done serially. Allowing the solvent to leave the PDMS block too quickly creates a gradient of swelling where the core is swollen and the shell shrinks in and breaks apart.

ii. Limitations

The biggest shortcoming of our phantom is the fact that our microchannel diameter is 20 μm. This is four times the diameter of a single axon. Unfortunately, there are no commercially available nylon fibers that are less than 5 μm in diameter. We have begun investigating the use of carbon fiber threads that have a diameter of 5.9±1.0 μm. These fibers have incredible tensile

strength, but are very brittle and they cannot be removed from the fiber construct. Rather than pulling cleanly from the channel they break within the phantom construct leaving irretrievable pieces in the middle of the cast. We are exploring alternative techniques to remove the carbon fibers without breaking them such as minimizing the size of the construct.

Second, we cannot resolve individual fibers using our μCT scanner. Resolving individual fibers, and understanding their traces through the phantom construct would make our phantom more powerful to any end users and is the first step in calibrating diffusion scans to physiological relevance. Currently, computed tomography, MRI, and other radio-imaging techniques lack the resolution needed to resolve individual 20 μm fibers. This will be even more difficult as we move to more physiologically relevant 5 μm diameter fibers. So far, we have used non-destructive techniques to image the phantom construct because we send our samples to be scanned with DTI after understanding the microchannel structure. If we reversed the work flow, we could section the sample into thin slices and image each of those individually and reconstruct the path of the channels. This is not an ideal scenario for a marketable phantom, because it would mean the phantoms are one-time-use, and would add months of processing.

Lastly, due to the nature of the template casting technique, individual fibers are not protected from touching one another. This can lead to intersections between fibers in a bundle. While there are intersections in white matter, these intersections within our phantom limit the FA. We have explored methods to space the fibers out before casting, but with limited success. It is difficult to know the true number of intersections that occur between fibers because we cannot resolve the individual microchannels in the phantom construct. Adding more PDMS dividers between fiber bundles in addition to those between the layers may increase the division between the fibers.

E. Conclusions

Our novel template casting technique can create high aspect-ratio (>100 length / diameter) microchannels within agarose and PDMS for a variety of applications.

We have shown that this technique can be used in the fabrication of a phantom for MR imaging studies with channels that are 20 μm at a volume fraction of 50%, similar to physiologically relevant numbers. This phantom is both more complex in the fiber crossing and a more accurate model of the white matter. Plans are in the works to create a phantom with even smaller channels over a larger volume to create a crossing phantom to calibrate and understand DTI and QBI studies.

3. Template Casting a Tissue Model System

A. Tissue Engineering Background and Significance

There is a great need for organs for transplants worldwide. Since the creation of organ donor lists in 1987, there have always been more patients waiting for organs than organs available. The discrepancy between the available organs and the need for organs is exacerbated

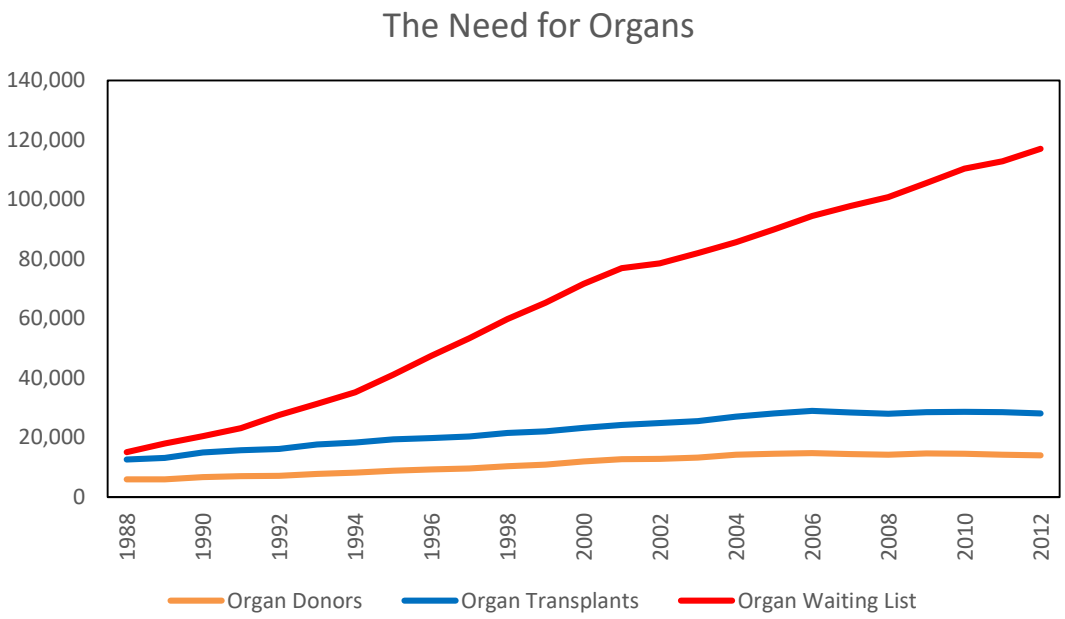

Graph 1: The discrepancy of the organ waiting list with the available organs.

by the increase longevity of patients, and the need for organs rises every year (Graph 1). In the United States, there are 122,432 people on the waiting list as of September 1st, 2015.[58] Of these patients, only around 30,000 will have organs available for them and 8,000 will die this year.

The shortage of organ donors stems from the extremely difficult choice of whether to donate one's organs. Organs are given to those on the top of the waiting list as determined by severity of illness, time spent waiting, blood type, and match potential. To increase the number of available organs, there are programs in place to provide incentives to become an organ

donor.[59,60] However, none of these measures has significantly impacted the ever growing need for organs.

To combat the lack of organs, instead of harvesting organs from donors, tissue engineering seeks to grow organs from simple biological building blocks. Tissue engineering in general employs the natural biology of a system to assist in developing tissues rather than focusing on a fully synthetic approach.[61] The field also has more far reaching applications than organ transplantation including generating tissue cultures for research and drug screening. In addition, engineered tissues can be used by researchers to study human physiology *in vitro*. Currently studies on cells are performed on 2D cultures of cells that do not replicate well the *in vivo* environment. Animal studies, used to bridge the gap between cell studies and human trials, fail to realize important aspects of human biology and are expensive and time-consuming. Creating a 3D culture could enable an accurate study of human diseases on an *in vitro* facsimile of an organ for better prediction of drug and therapeutic effects.

The primary challenge in creating engineered tissues is organizing the myriad of required biological materials in a way that they become self-supporting.[62] The principal requirement in this organization is ensuring that cells are within 100 to 200 μm of any vessel.[63] Capillaries are the smallest of the blood vessels in the body. A capillary is made up of an endothelial sheet, which is only one cell thick, surrounded by a basal lamina, which is a layer of extracellular matrix. The capillaries are around 5 to 10 μm in diameter and help exchange water, gases, nutrients, and waste products between the blood and the surrounding tissue. Capillaries do not function alone; they form a network of vessels called a capillary bed (Figure 11). The more metabolically active a tissue is, the greater need for product exchange, and a denser capillary network is required to sustain it.

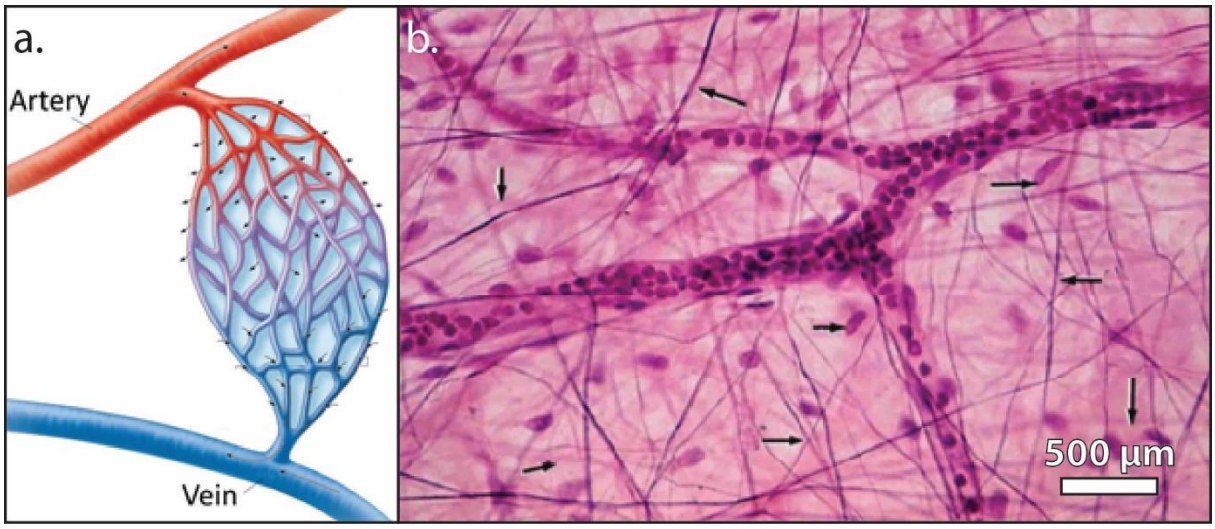

Figure 11: A representative capillary bed. The maximum spacing between any two capillaries is 100 to 200 µm. Adapted from Pearson Education, 2013 and [64]

The reason a denser capillary network is needed for metabolically active tissues is due to the limited diffusion distance of nutrients and waste through a tissue. In typical tissues, there are no cells that are more than 200 µm from a vessel. A simplified model to describe maximal thickness of a tissue without convective nutrient flow is the Krogh model which describes the problem as a function of the diffusion of the solute, the concentration, and the rate of consumption. As an example of this, studies on engineered thick (>200 µm) tissues with encapsulated cells developed necrotic cores within the construct.[65,66] Therefore, any attempt to create a thick engineered tissue requires the parallel development of a perfuse-able vascular network incorporated throughout the construct.[67]

Lymphatic capillaries are similar to vascular capillaries in that they are formed form a lumen of endothelial cells. The lymphatic capillaries are slightly larger in diameter and unlike vascular capillaries, have closed ends. This permits interstitial fluid to flow into them and to lymph nodes. The main functions of the lymphatic system include reabsorbing left over plasma in the interstitial fluid and in support of the immune system. Lymphatic systems are not typically

considered when creating vascularized tissues because in this context it does not contribute to the growth of cells. We consider it here because the system created for tissue engineering can be used similarly for a lymphatic system model.

Typically engineered tissues are constructed by combining cell cultures that were conventionally grown in a 2-dimensional culture flasks, with a scaffold engineered to mimic biological environments. These scaffolds with embedded cells are generally cultured in dishes, stirred vessels, or microfluidics devices. Attempts at creating a thick tissue construct requires micro-structure detail over a large volume and, to date, no technique has effectively accomplished both.

Adherent cells have a need to adhere to a surface, and most tissue cells are not viable when suspended in a fluid, even if the proper nutrients are provided and even if adhesion molecules are present.[68] Clearly fluids differ from solids in the way they respond to a force. Whereas fluids continually deform under a constant stress, solids have a finite deformation under a constant stress. Within the microenvironment of tissues both cells and extracellular matrix contribute to the macro mechanical properties. Each cell within a tissue probes its environment for places to anchor and pull on. The cells transmit forces to their environment using myosin-based contractions through transcellular adhesion sites. The cells respond differently based on the stiffness and elasticity of its environment, forming a feedback where the cells are constantly probing and adjusting their response. This response does not depend on the material the cells are probing; it can occur on natural or synthetic substances, matrix, or even other cells.

When a cell is anchored to a surface and contracts, this is through actin and myosin filament interactions. When the substrate they are anchored to is soft or a thin film it can cause wrinkles in the material.[69-72] Accordingly, the cells respond to the elastic resistance of the

substrate through cytoskeletal reorganization and adapting its overall state. While much attention has been paid to the response of cells to their mechanical environment, there is a feedback loop that couples the cellular mechanics to the mechanical properties of their substrate. Epithelial and fibroblast cells were reported to be able to detect and respond differently depending on the substrate stiffness[73] with similar responses being noted in muscle cells and neurons.[74,75] This begs the question, if typical cell culturing substrates like flasks are basically rigid, does that mean cellular behavior of traditionally cultured cells is different than in their more compliant tissue environment?

i. Tissue Engineering Scaffolds

There are many different systems used to replicate the *in vivo* environment of cells. These scaffolds for the cells to grow on are engineered to be compatible with cell growth and proliferation. Scaffolds typically mimic the extracellular matrix of the cells' native tissue. A successfully engineered scaffold fulfills all of the following functions: allowing cell attachment, migration, and modification, delivering cellular signals, enable diffusion of nutrients and cellular products, maintaining a specific mechanical and biological environment.

One of the most ubiquitous material used in this type of tissue engineering are hydrogels. Hydrogels are networks of polymer chains that are dispersed in water. Hydrogels are used because of their biocompatibility, similarity to extracellular matrix (ECM) components, and tunable chemical and physical properties.[76-78] There are two categories of hydrogels used in engineered cellular scaffolds, natural and synthetic.

Natural hydrogels are made of proteins, polysaccharides, and hybrids of the two. Principal among this class of hydrogel are collagen, gelatin, and agarose. A study embedded endothelial cells within collagen tubes of 116 μm diameter.[79] The endothelialized tubes had

microvascular-like properties, supported leukocyte adhesion and responded to inflammatory mediators. The same technique of embedding endothelial cells within collagen was used to study the effect of cyclic AMP on microvessels. Collagen is considered a good hydrogel for artificial blood vessel development because of its integrin-binding and low inflammatory response.[80] Gelatin is a hydrolyzed product of collagen and retains some of the same cell-binding sites such as RGD and matrix metalloproteinase degradation sites.[81] By post-crosslinking gelatin with some naturally occurring enzymes, it can generate cytocompatiblity for murine mammary epithelial cells.[82]

Agarose, and other polysaccharide hydrogels such as carrageenan, hyaluronic acid (HA), alginate, and chitosan) have excellent gel-forming properties as well as good biocompatibility and biodegradability.[83-85] They also have a variety of crosslinking mechanisms including polymerization, chemical conjugation, and esterification. An agarose based system has been used to create microfluidic channels that demonstrated efficient delivery of nutrients to the encapsulated cells.[86] It uses a layer-by-layer approach to first define the channels and then to layer them on to another sheet of agarose to seal them. Building a whole tissue this way is not feasible because of time and cellular life constraints, but it does prove that such a system could work. Microfluidic channels have also been formed in calcium alginate to detect mass transfer and to monitor the chemical environment of cells.[87] Composites of protein and polysaccharide hydrogels can also support cellular encapsulation and some flow.[88]

The main limitation of these natural hydrogels is that it can be difficult to tune and control their mechanical properties.[89,90] The processing methods required to obtain the natural hydrogels can affect their mechanical properties. Though a hydrogel may have high mechanical strength *in vivo*, harvesting, isolating, and purifying the protein, removes some of the natural

crosslinks and negatively impacts its mechanical properties. Further, it may be necessary to use chemical modification or other strategies to provide control over the intrinsic mechanical properties that are difficult to modify. This leads to naturally sourced hydrogels having batch-to-batch variation, a greater potential for contamination, and being generally more difficult to control and tune than specifically synthesized synthetic polymers.

Synthetic polymers seek to have more reproducible physical and chemical properties than the natural hydrogels. The synthetic scaffolds primarily used in tissue engineering include polydimethylsiloxane (PDMS), polyethylene glycol (PEG), and poly(lactic-*co*-glycolic acid) (PLGA), and polylactic acid (PLA).[91-93] Some of these synthetic polymers are hydrophobic which can inhibit their biocompatibility. There has been some research into creating hybrid versions of the synthetic and natural polymers to get the structural integrity of the synthetic and biocompatibility of the natural polymers.

For example, PDMS is easily pre-vascularized but because it is not permeable to water, cells can only be grown on the surface of the channels. Instead of using pure PDMS to make the construct, the surfaces of the PDMS construct can be coated with peptides to minimize nonspecific adsorption and improve biocompatibility.[94] Some of the other hydrogels like PLGA has been used to fabricate complex microfluidic structure and culture endothelial and hepatocyte cells.[95] But by far, the most widely used synthetic hydrogel for tissue engineering is PEG. PEG is used because it is soluble in many liquids, has low protein adhesion, and is non-immunogenic.[96,97] It can also be synthesized with functional end groups or be combined with bioactive agents. This system has been used to investigate 3D cell behavior and cellular growth and connectivity along microchannels.[98,99]

There are also hybrid synthetic and natural hydrogels. PEGylated fibrinogen hydrogels which integrate the natural bioactive molecules into PEG hydrogels or gelatin can be electrospun with poly(L-lactic acid) to form vessel-like tubes.[100] Natural hydrogels can also be synthetically modified to fit specific crosslinking or mechanical specifications.

Most prominent among these is gelatin methacrylate (GelMA) which can be synthesized by replacing the amine groups with methacrylic groups in gelatin (Figure 12a), making it photopolymerizable (Figure 12b).[101] This hydrogel has seen use in drug delivery, wound dressing, and bio-printing applications. It has compatibility and has been used with fibroblasts, chondrocytes[102], endothelial cells[103], and human umbilical vein endothelial cells (HUVECs)[104].

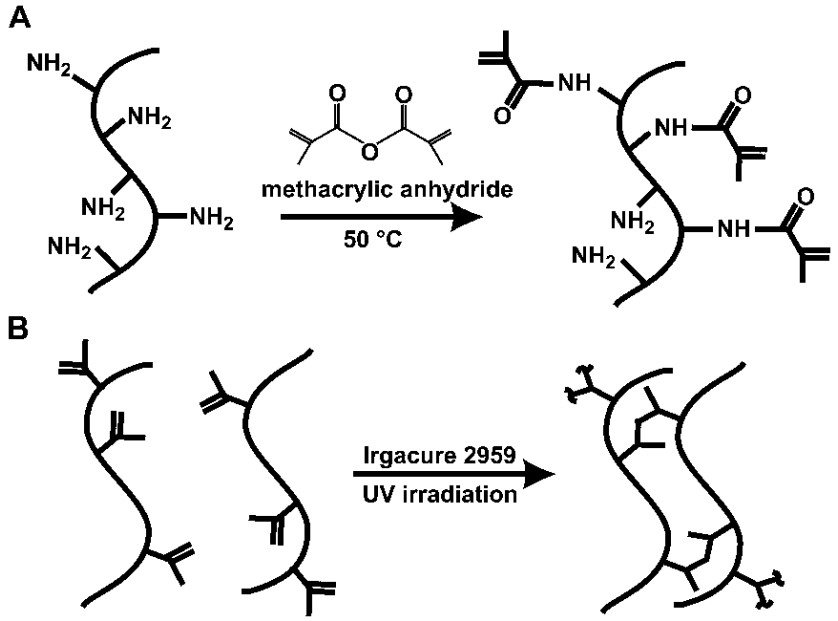

Figure 12: The synthesis of GelMA through reacting amine groups methacrylic anhydride (MA) to add methacrylate pendant groups(a). Irgacure 2959 is added to permanently crosslink the gel (b).[105]

GelMA has many useful cellular interactions including its hydrophilicity, integrin binding, and degradation sites[104]. Because it is highly hydrophilic, it can be dissolved in water to create a highly biocompatible hydrogel with good cellular encapsulation qualities. Because of the binding sites of the gelatin it has high cellular adhesion properties and has a degradation pathway

from its matrix metalloproteinase (MMP) sites. Without a curing agent, the gelling of GelMA is thermally reversible. With the addition of a photo-initiator such as Irgacure 2959, GelMA can be permanently crosslinked via exposure to specific light wavelength due to the release of free radicals which interact with the methacrylate groups (Figure 12b). Care must be taken when photo-crosslinking cell-laden GelMA because the released free radicals as well as the light exposure can damage cells and DNA. Importantly, the mechanical properties can be tuned by varying the degree and methacrylation and the concentration of the gel. Similar methacrylations can be done on other natural hydrogels including chitin[106], agarose[107], and PEG[108]. The main drawback to using the synthetic polymers is that, despite their superior physical and chemical properties, they can be prohibitively expensive. Creating a tissue construct of any appreciable size using such an expensive polymer is not feasible.

ii. Hydrogels in Tissue Engineering

A hydrogel scaffold for tissue engineering should provide a comparable mechanical stiffness to that of the native ECM it is trying to replicate, have non-cytotoxic gelling properties, support cellular growth, and maintain perfusion.

The substrates that cells adhere to cover a wide range of stiffnesses, thicknesses, and topographies. The resistance of a solid to being deformed is measured in elastic modulus, *E,* which is the change in stretched length depending on the force applied. A simple method for measuring the *E* of a tissue is to hang a weight to a section of tissue and measuring the relative change in length. More recently, atomic force microscopes (AFMs) and micro-indenters have been used to probe the elastic modulus of tissues.[109] Many tissues have relatively linear stress strain ratios within low strains, of about 10 to 20%. Within the scale of forces that a cell can produce, *E* is relatively linear.[110] The trouble with some studies is they probe the response of

cells in a high-frequency manner[111], which is in contrast to the time scale that cell exert strains[112]. There is a general consensus that brain tissue is softer than muscle[113], and muscle softer than skin[114]. In all, understanding the macro mechanical properties of a tissue does not necessarily correlate with the mechanical microenvironment of groups of cells within the tissue.

Cells probe the mechanical properties of a substrate which feeds back on the adhesion, cytoskeletal, and contractile properties of a cell. Specifically, adherent cells show dynamic and limited adhesion on soft substrates (E ~ 1 kPa) and stable dense adhesions on hard substrates (E ~ 30 to 100 kPa)[73] with a similar phenomenon occurring in 3D matrix[115]. Simply, cells on soft substrates need to be less contractile than on stiff substrates and if they are less contractile, their adhesions do not need to be as strong.[113] The cell-to-cell interactions have similar effects as those induced by substrate stiffness. Indeed, when grown to confluency, endothelial cells have the same morphology on soft and stiff substrates.[116] Similarly, epithelial cells, fibroblasts, and cardiomyocytes prefer to form cell-to-cell contact than adhere to a soft gel. Increases in cell contractility, which changes based on cell type, can lead to different arrangements of cells[117] with individual cell clusters forming by pulling into a ball[118]. This type of self-organization has been explained through the "differential adhesion hypothesis", where the different number of adhesions on each cell give it an imaginary surface tension.

In terms of mechanical properties, in most soft tissues the Young's modulus ranges from 0.1 kPa to 1 MPa depending on the tissue (Figure 13).[119,120] Rheological studies of liver tissue found an elastic modulus of 1.7kPa.[121] The stiffness of hydrogels can be varied by changing the polymer concentration, increasing the degree of crosslinking, and adjusting various environmental conditions. Typical gel stiffness range from 19-32 kPa for 3% agarose[122], to 60-500 kPa for PEG-based hydrogels[123], and 5.4 to 11.8 kPa for HA-tyramine hydrogels[124]. It is

important to choose a hydrogel for the tissue being replicated. The mechanical properties and pore size of hydrogels play an important role in cellular behavior.

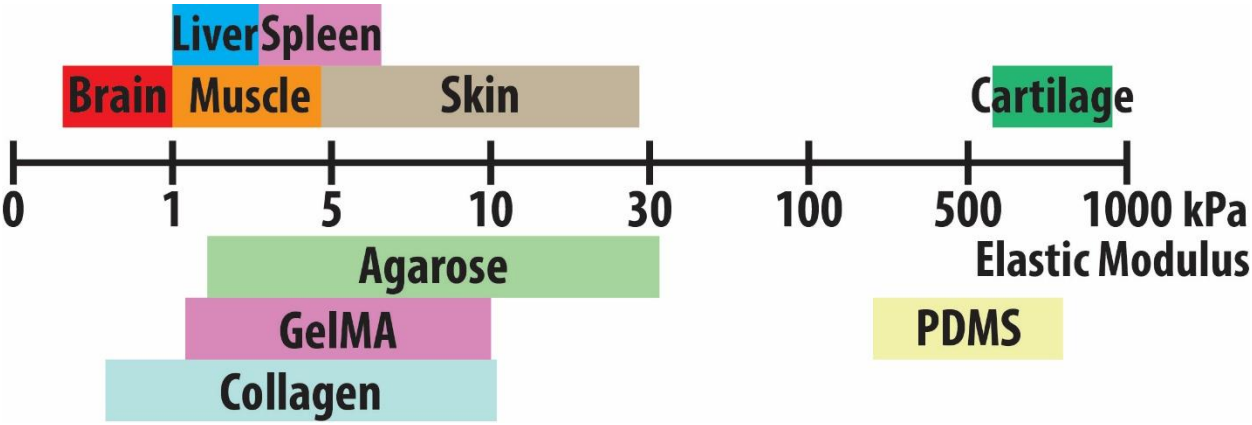

Figure 13: Elastic modulus of various organs and hydrogels used in tissue engineering.

The gelling method is a critical factor in hydrogel selection. The hydrogel needs to be able to gel in conditions that support cellular growth. Gelling should be done is as short amount of time as possible to limit oxygen and nutrient depletion at a temperature that does not harm cell viability. This is especially important in some organizational specific cell types, as certain cells cannot survive a long time (> 30 minutes) without perfusion.[125] But appropriate working conditions for the gel should be found that fit the specific methods being used.[126]

Crosslinks within hydrogels must be present to prevent their dissolution back into solution. There are many different ways crosslinking has been achieved in hydrogels, categorized into physical and chemical crosslinking methods. When used in biological applications, biodegradability must be considered, and therefore labile bonds are frequently involved in either the polymer background or crosslinks used in the hydrogel. These bonds must be able to be broken under physiological conditions due to either enzymatic or chemical triggers, typically hydrolysis.

Chemical crosslinking can be broken down into a few major categories: radical polymerization, reaction of complementary groups, and high energy irradiation. In radical polymerization the polymer is formed through the addition of free radical building blocks. The free radicals are usually created through separate initiator molecules. After initiation, polymerization is induced until termination occurs. Certain initiators can also be induced using ultraviolet (UV) illumination, which is becoming more popular in hydrogel preparations.

With reactions of complementary groups, the functional groups of a hydrogel (mainly OH, COOH, and NH_2) are covalently linked between the polymer chains. Hydrogels can be crosslinked this way using glutaralydehyde. Without it crosslinking can occur, but low pH, high temperature, or other harsh conditions are required. Even so, glutaralydehyde is a toxic compound that inhibits cell-growth even at low concentrations.

High-energy radiation, such as gamma and electron beams, is used to polymerize unsaturated compounds in hydrogels. This type of reaction requires water-soluble polymers with vinyl groups. While this type of reaction can be done with mild conditions, it cannot be used when laden with biologically active material. In addition, if the crosslinks include C—C bonds, the gel will not be biodegradable.

Physically crosslinking can be achieved through ionic interactions, crystallization, and hydrogen bonds. This method of crosslinking is used because it can avoid many of the cytotoxic agents present in chemically crosslinking methods. Crosslinking with ionic interactions can be performed at physiological temperatures and pH making it ideal for cell-laden experiments. Crystallization crosslinking, however, requires the gel to undergo several freezing cycles to form the hydrogel. Hydrogen bond crosslinking requires a connection between oxygen and protonated carboxylic groups. Typically gels formed through hydrogen bonding are thermally reversible.

Choosing a gel and an appropriate crosslinking method is critical in ensuring cell survival. With hydrogen bond crosslinking, such as that in agarose, high temperatures are required to melt the polymer into the water and cells must be added after the temperature has decreased. Whereas with free radical crosslinking, the level of UV a cell-laden hydrogel is exposed to must be limited. Too long an exposure will cause damage to cellular function and an exposure not long enough will limit the crosslinking of the gel.[127]

Cyto-compatibility and cellular attachment are requisite for cells to survive being embedded in a hydrogel. If a hydrogel were toxic to cellular growth, it would be a poor candidate for use as a tissue engineering scaffold. Agarose has been used extensively in tissue culture applications. [128-130] Cellular attachment must also be taken into account, because it is a prerequisite for endothelial cells to populate a channel wall and is important in cellular behavior and function.[131] Cell attachment varies between different hydrogels and also for hydrogels of differing concentrations.[132] The level of attachment can be modified by introducing attachment sites into the hydrogel.[133]

Degradation is also important to consider when designing any engineered scaffold. As the cells take hold, they need room to move and expand. A gel that does not degrade will limit cellular growth, and could kill the cell population.[127] On the other hand, a gel that degrades too quickly may not be able to bear the mechanical forces being put on it by the perfusion. The biocompatibility of the degradation products must also be considered. This means ensuring that the compounds created can either be metabolized or excreted with minimal cytotoxic effects. Ideally, a gel will maintain its strength until the cells can produce their own functional ECM to replace the scaffold. Hydrogels are generally degraded through hydrolysis, an enzyme-mediated

reaction, or a combination of both.[134] For synthetic hydrogels, degradation can be "programmed" to start occurring after a set time and at a certain rate.

An ideal hydrogel for a vascularized tissue construct will have the strength to support flow and to mimic the target tissue, a short gelation time to minimize oxygen and nutrient depletion, gelation conditions that are not cytotoxic, be cyto-compatible, support cellular attachments, and allow the cells to degrade their environment so they can remodel it to their liking.

iii. Biomolecule Mass Transfer

The field of understanding the transport of oxygen in tissues was pioneered by August Krogh. He was interested in tissue metabolism and the role oxygen played. He determined the capillary network density in various tissues[135], focusing on skeletal muscle and also studied the diffusion coefficient and consumption rate of oxygen[136]. Using this information, he was able to model the oxygen transport in tissue in the Krogh cylinder model. In it, he concluded that a gradient of oxygen was needed to ensure that the tissue received the necessary amount of oxygen.

His model for oxygen transport was based on several assumptions: that oxygen diffused passively and uniformly, that blood in capillary was a homogenous fluid, and that oxygen consumption rate in a tissue was homogenous. Therefore, there was a longitudinal oxygen gradient within the capillaries and a radial gradient within the tissue. The oxygen gradient within a tissue is determined by the metabolism and diffusion coefficient of oxygen in the tissue space. The diffusion coefficient for oxygen within the tissue space is relatively stable, so the gradient is dependent on the metabolism of oxygen within the tissue. Skeletal muscle has a wide metabolic range due to its two states: contracting and relaxed. More oxygen would be consumed during

contraction and the gradient of oxygen would be steeper. In reality, the Krogh model is a simplified version of a complex system. Oxygen can diffuse between any two areas with a concentration gradient and therefore the radial gradient of oxygen concentration within a tissue may not be linear or consistent. Indeed, capillaries are no longer thought to be the only contributor of oxygen to tissues but now includes arterioles and venules.

Even so, we can use this simplified Krogh model (Equation 1)to help understand some of the basic needs of a tissue where λ_K.is the length at which nutrients diffuse from a channel, D_s is the diffusion constant of the solute, c_0 is the concentration in the channel, and R is the consumption rate of the solute.

$$\lambda_K = \sqrt{D_s c_0 / R}$$

Equation 1: The Krogh length.

Understanding human physiology is vital in uncovering the reasons behind bodily dysfunction and pathogenesis as it is connected to medicine, drug development and toxicology. Experimentation on humans *in vivo* is the most direct method to study physiology. But the macro phenomena of the body that occur depend on and interact with lower level systems like tissues, cells, and genes. Untangling these interactions is difficult in a system as complex as the human body using only *in vivo* testing. To limit these outside factors, biologists have taken a reductionist approach to understanding bodily systems. They take single populations of cells and proliferate 2-dimensional cultures of them for study outside the body. These *in vitro* models are robust and repeatable, making for advantageous models. However, this simplistic take on physiology is also a disadvantage because it does not reproduce physiologically relevant factors.[137,138]

By adding some of these missing factors back in to the system it becomes more relevant but also more complex. If these factors are not carefully added back into the system they can produce unpredictable results.[139] Using key aspects of the *in vivo* environment to enhance the *in vitro* experiments can lead to experiments that would not increase the biological complexity or unpredictability but be more physiologically relevant. The difficulty is in elucidating which aspects of the microenvironment are important to mimic. To date, several geometrical, mechanic, and biochemical factors, have been identified to steer cells towards a more realistic phenotype.[140-143]

Concentration gradients of biologically relevant molecules exist within all 3D tissues due to the production and consumption from cells. The gradient comes from the competition between diffusion, convection, consumption, and production, within the tissue space. The consequences of this gradient are that the different molecular concentrations can cause cells in different locations to behave differently, and it can induce a migration of the cells or a cellular response depending on the gradient.

The basic molecules that cells require in culture are oxygen, glucose, and various amino acids. Oxygen is the most readily depleted molecule because it has low solubility in culture medium. The effects of oxygen gradients on cell viability has been studied on various systems.[144,145] With high cell density models, such as epithelial cells, oxygen depletion becomes an issue when the aggregate diameter exceeds 0.25 mm in culture media, whereas with low cell density models, the oxygen depletion gradient is not as steep.[146,147] An additional barrier to dissolved oxygen in media is in unstirred vessels. Even in 2D monolayer culture the oxygen concentration under 2 mm of media is only 10 to 50% of the concentration at the air interface. Differences in oxygen concentration go beyond basic cellular respiration. High concentrations of

oxygen can be toxic to cells where low concentrations can cause differentiation of stem cells.[148,149] On a molecular level, changes in oxygen concentration can change the activity of signaling molecules, leading to DNA damage.[150]

There are several efforts to control the delivery of oxygen into 3D cultures including controlling the dimensions of the tissue and lifting the cells near the air-liquid interface to minimize diffusion distances. Due to these constraints much of development of 3D cultures has moved toward microfluidic systems that can better control these parameters. In determining molecular gradients, consumption and production rate of a molecule must be determined. But there is a lack of available data on these rates for biomolecules.

Our understanding of biomolecules involved in 3D tissues is also limited. It was previously thought that autocrine loops were a hallmark of cancer but it is emerging that they are primary regulators of cell-signaling networks. Cells that use autocrine loops examine their environment based on recapturing the emitted signal, and possibly help defining tissue boundaries.[151-153] The loss of this autocrine signal has been theorized to explain why using high flow rates in 3D tissues, intended to improve nutrient transfer, can actually limit cell survival and proliferation.[154]

Not only is the bulk media flow important, but interstitial flow can play a role in cell signaling as well. In tissues, fluid is forced from the capillaries and into the tissue due to Starling forces.[155] The fluid that does not return is drained into the lymph. This interstitial flow into the lymph can be stimulated by mechanical forces on tissues coupling the mechanical stress and signaling in a 3D matrix. The larger the molecule the lower the diffusion coefficient and the more important convection is conveying the molecule to the target tissues with the physiological range for interstitial flow being 0.1 – 1.0 μm/s.[156,157] Cells and thus tissues respond to local

gradients of chemokines rather than the absolute amount. Engineering proper control over scaffold materials, biomolecules, and flow rates in essential in ensuring cellular viability in 3D environments.

To model the mass transfer of nutrients or waste in a tissue construct system, there are several parameters that need to be defined to model the system. These include: diffusion coefficient in the media, diffusion coefficient in the gel, flow rate, channel size, construct size, concentration of the solute in the media, rate of consumption of the solute by the cells, the number of cells, and the size of the construct. For our system several of these parameters predetermined. The channel size is 100 μm in diameter, the size of the tissue construct is 5 mm x 25 mm x 500 μm, and we use approximately 3×10^6 cells per mL in the gel.

For other values we must look to the literature for measurements of molecular properties (Table 2). The diffusion coefficient of oxygen in water can be calculated using the Stokes-Einstein equation to be 1.97×10^{-5} cm^2/s.[158] This diffusion coefficient must be adjusted for diffusion within the hydrogel, which depends on the concentration density and mass fraction of the gel. With this adjustment, the diffusion coefficient of oxygen in GelMA is 1.968×10^{-5} cm^2/s, which is less than 1% different than the free diffusion of oxygen. The concentration of oxygen in media can be estimated to be similar to that of in water, 9.03 mg/L, but we will use values calculated in literature of 6.772 mg/L.[159] The consumption of oxygen by various cell types have been calculated, but are specifically concerned with HeLa cells. Values ranging from 0.1 to 0.5 mmol O_2 per liter-hour at cell densities of 3×10^6 cells per mL have been reported.[160-164] For our model we use an average of these values.

The values for glucose levels in media are readily obtained, because glucose is added specifically for cell growth at 4.5 g/L (DMEM, Sigma-Aldrich). The diffusion of glucose has

also been well documented and defined at 0.9×10^{-5} cm^2/s.[165] Determining the consumption of glucose in cells is more difficult. Each cell type has different consumption rates, and these rates vary based on the phase of the cell cycle. We used several literature sources to estimate the glucose consumption rate of HeLa cells to be 2.5×10^{-4} mol / m^3 s.[166,167]

Lastly, we need to determine the properties of calcein-AM as they relate to our tissue construct model. The diffusion of calcein was determined to be 2.4×10^{-5} cm^2/s.[168] While calcein is not necessary for cell growth, we can use it as a marker to directly assess the diffusion, flow rates, and other parameters of our system. Therefore, the initial concentration is something that can be adjusted. Previously, 5×10^{-3} mol/m^3 has been used to identify cells. Additionally, the reaction rate, the rate at which calcein-AM is converted into a fluorophore by the cells, was calculated to be 1.5×10^{-7} mol/m^3 s.[169]

	Oxygen	**Glucose**	**Calcein**
Consumption rate (mol / m^3 s)	2.22E-04	2.50E-04	1.50E-07
Initial concentration (mol / m^3)	2.18E-01	25	5.00E-03
Diffusion coefficient (m^2 / s)	1.968E-09	6.70E-10	2.40E-10

Table 2: Values used in the tissue construct model.

iv. Cell Sources

When building a tissue mimic device, it is important to consider the source of the cells that should be used. Sources for cells include immortalized cell lines, primary cell material, stem cells, and induced pluripotent stem cells. Immortalized human cell lines are widely available and well established but have slight phenotype mismatch with *in vivo* tissues and are genetically homogenous. Primary cells do not have this mismatch or homogeneity, but are more difficult to

keep in culture. Using stem cells or inducing pluripotent stem cells gets around this problem, but steering the cells towards a well-differentiated state and maintaining that state can be difficult.[170]

HeLa cells, an immortalized cell line, is one of the oldest and most commonly used human cell line. These cells are derived from a cervical cancer taken from Henrietta Lacks. These cells were the first human cells grown in the lab that did not die after a few cell divisions and saw use in vaccine, cancer, AIDS, and other research. The durability and prolificity of HeLa cells lend themselves to proof-of-principle experiments. These cells have seen use in novel carbon nanotube arrays[171], newly developed hydrogels[172], new hydrogel preparation methods[173], and in 3D printing gels[174,175].

v. APTES and GA Surface Modification for Gelatin Immobilization.

The inherent properties of PDMS allow for easy molding as defined by a master and the properties can be changed and adjusted. One of the drawbacks in using PDMS with hydrogels is that PDMS surfaces are highly hydrophobic which can limit ability of gels and biologicals to effectively adhere.[176-178] Because the wettability of PDMS is a critical factor affecting adhesion, previous research has focused on reducing the hydrophobic nature of PDMS with plasma treatment, but this effect only works for a limited time.[179,180] There are efforts to create a stable covalent linkage of protein to the PDMS surface using an amino-silane, such as (3-aminopropyl)triethoxy silane (APTES), and a homobifunctional aldehyde, such as glutaraldehyde (GA).

A surface treatment of APTES and GA act as a spacer that minimizes the interactions of proteins with the PDMS surface and to overcome the steric hindrance from the vicinity of the support to create stronger protein attachment. The process of creating a silane layer the PDMS surface requires four steps. First, hydrolysis of the PDMS leads to the formation of a reactive

silanol group. Next the silanol groups condense and form a siloxane linkage over the surface. Hydrogen bonds are then formed with the –OH groups on the surface. Lastly, a covalent bond is formed between the silicon groups. In the presence of water, multiple layers of silane can be crated, so it is advantageous to produce the silane in a non-aqueous solution.

The silane layer has amine functionality on the surface and when treated with glutaraldehyde, can gain aldehyde functionality (Figure 14). These aldehyde groups can react with biomolecules to form amine linkages. The glutaraldehyde can crosslink gelatin such as that found in GelMA. While this reaction is heterogeneous and can happen in a multitude of ways, it produces a stable covalent bond between the two groups.[181]

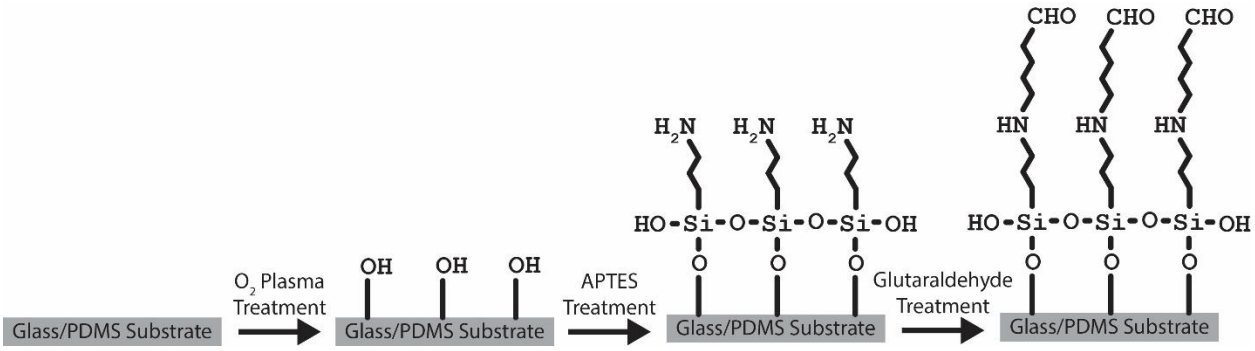

Figure 14: Chemically generated surface groups from the APTES and GA surface treatment protocol.

B. Materials and Methods to create a Tissue Model

There are a multitude of engineered tissues using pre-vascularized hydrogels. But these methods do not have ability to scale into larger tissues, they are typically set in their scale. Here we present a method to create a pre-vascularized hydrogel that is in keeping with the template casting method used in creating a diffusion MRI phantom. Creating the tissue construct with this method allows greater flexibility in terms of molding, channel size, geometry, and can be used as a test bed for larger scale tissue constructs created using the same basic method.

i. Materials

Material	Specs	Source
Gelatin	Porcine, Type A	Sigma, Missouri
Methacrylic anhydride	94%	Aldrich, Connecticut
PDMS	Sylgard 184	DowCorning, Michigan
Needle	30G x ½	BD, New Jersey
Nylon	Invisible	Gutermann, Germany
(3-Aminopropyl)triethoxysilane (APTES)	99%	Aldrich, Connecticut
Gluteraldehyde (GA)	50% EM Grade	Electron Microscopy Sciences, Pennsylvania
Glass slide	80 x 50 mm	Fisher, New Hampshire
Tubing	30G	Small Parts Inc., Indiana
HeLa cells	--	ATCC, Virginia
DMEM	--	Gibco, New Hampshire
Magic tape	--	Scotch, Minnesota
Dialysis tubing	12,000 – 14,000	Fisher, New Hampshire
2-Hydroxy-4′-(2-hydroxyethoxy)-2-methylpropiophenone (Irgacure 2959)	98%	Sigma, Missouri
Calcein-AM	96%+	Sigma, Missouri
Ethidium bromide	95%	Sigma, Missouri
96-well plate	--	Fisher, New Hampshire

Table 3: Materials used in Chapter 3.

ii. Fabrication of the Microchannel

The culture device is composed of a section of PDMS bonded to a glass slide. The PDMS section is 8 mm thick, 25 mm in length, and has a 500 μm x 5 mm trench running through its length. The trench is created in the PDMS by casting liquid PDMS (10:1 polymer : crosslinker) around a 500 μm high by 5 mm wide by 25 mm long rectangular structure. The PDMS with trench is irreversibly bonded to a glass slide through oxygen plasma bonding at 500 mTorr for 30 seconds. Immediately after bonding the PDMS to the glass slide, the APTES solution is injected into the slit. The APTES is allowed to bind to the surface groups for 15 minutes at room temperature to form an even monolayer of silane. The APTES is washed out of the slit with room temperature 100% ethanol three times. The remaining ethanol is blown out of the slit and the slit

is left to dry and set the APTES in an 80ºC oven for 2 hours. The slit is then cooled to room temperature and the glutaraldehyde solution is pipette to fill the slit and incubated for 20 minutes at room temperature (Figure 14). The slits are washed out with phosphate buffered saline (PBS, pH 7.4) three times and air-dried.

The nylon fiber is then threaded through the slit. On one side, three layers of tape are built up to provide an elevated platform for the needle. The nylon thread is threaded through the needle. The needle is bent to approximately 30º near the base and ~ 3 mm is inserted into the center of the slit. The needle is aligned into the center of the slit both vertically and horizontally and glued into place. On the other side of the slit, the nylon fiber is threaded through the length of exit tubing. The fiber is attached in place on the needle side with glue. The exit tubing is then attached into place 3 mm into the PDMS slit with glue. The string is pulled taut through the tubing and glued into place. It is paramount that the string has some tension on it or it will droop and the microchannel will not be straight. Once all of the parts are secured with glue, the readied device is placed in an incubator to attain 37ºC.

iii. Synthesizing GelMA

To synthesize the GelMA we follow an established protocol.[105] Briefly, gelatin was mixed at 10% (w/v) into PBS pH 7.4 at 60ºC until fully dissolved, about 20 minutes. Next 15% (w/v) Methacrylic anhydride (MA) was added dropwise while stirred at 50ºC and allowed to react for 1 hour. Varying the amount of MA would affect the fraction of lysine groups that were reacted and changed the material properties. The solution is diluted 5x to arrest the reaction. The resulting solution is dialyzed against distilled water for 7 days using 12 – 14 kDa dialysis tubing to remove salts and unreacted methacrylic acid. Lastly a foam was formed by lyophilizing the solution for 1 week and then stored at – 20ºC until use.

iv. Cell Culture

The tissue construct we use relies on embedding cells from traditionally culture sources. We use HeLa cells in this tissue construct cultured in appropriate media: 10% fetal bovine serum, 0.5 U/mL penicillin, and 0.5 µg/mL streptomycin in Dulbecco's Modified Eagle's medium (DMEM) and are cultured at 37ºC and 5% CO_2. The cells will be passaged at confluence for use in the experiment through trypsin digestion. Each experiment uses 1 flask of cells, approximately 5 million cells.

v. Casting the Cell-Laden Hydrogel

The foam GelMA is dissolved into 1 mL of DMEM for use as a cell-laden hydrogel and kept at 37ºC to ensure it is still liquid. Next 10% (w/v) of the photoinitiator, Irgacure 2959, is added to the GelMA. After the cells are in suspension, we spin them down and suspend the 5 million cells in 0.5 mL DMEM. This 0.5 mL is then added to the 1 mL of GelMA for a final cell count of approximately 6.6 million cells per mL. The gel is then pipetted into the PDMS slit with fiber assemble using heated pipette tips to ensure good flow. The cell-laden GelMA mixture is allowed to incubate for five minutes with the GA surface groups to promote attachment. The slit as a whole is then exposed to a 500W Hg lamp (Oriel, ~78 mW/cm^2) for 10 seconds to polymerize the gel. Excess gel is removed from both the inlet and outlet side, with some extra removed from the outlet side to allow for expansion of the gel. The gel is sealed into the slit on both sides using cyanoacrylate (Superglue) and the glue is allowed to set for 20 minutes.

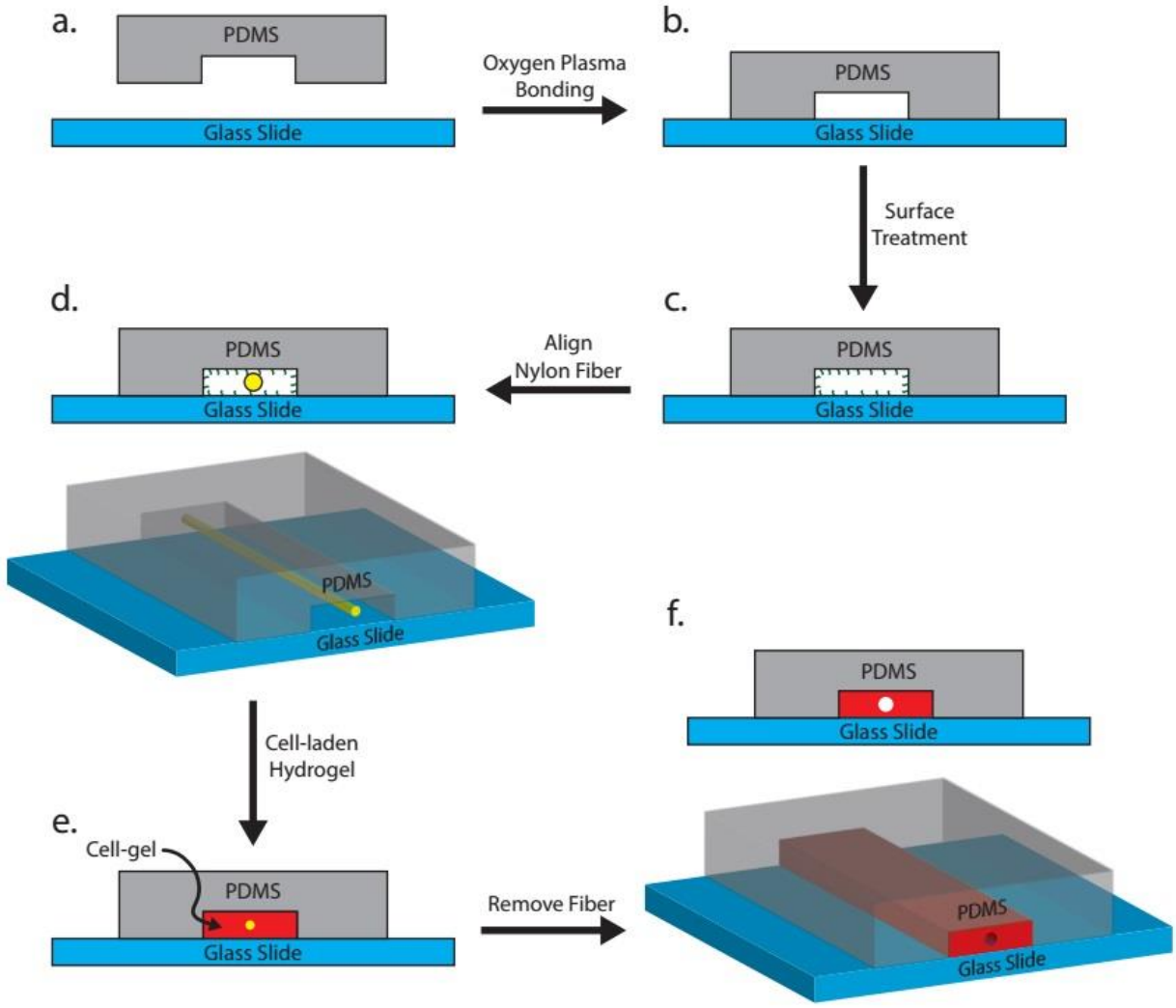

Figure 15: A schematic of the fabrication of a tissue construct using template casting. A glass slide is bonded with a PDMS slit (b), a surface treatment is applied to the inside of the slit (c), a fiber is aligned into the middle of the slit (d), a cell-laden gel is cast around the fiber (e), and the fiber is removed leaving a microchannel (f).

vi. Sustaining the Tissue Construct

To sustain the tissue construct we will be flowing heated DMEM through the central microchannel at a rate of 25 µL/min. The DMEM is perfused using a syringe pump (New Era Pump Systems, Inc.) which is connected to the luer lock of the inlet needle. A syringe heater is used on the tubing nearest the inlet needle to ensure the media and therefore the construct is maintained at 37ºC. The outlet tubing is connected to a sealed collection container so the media

can be reused (Figure 16). The temperature of the slit is maintained at 37ºC in a closed box with a heating element and fan. The temperature is logged throughout the experiment to identify any inconsistencies. We used a microscope to identify regions of interest within the micro-slit, specifically those near the microchannel, as areas to look at over a long period of time. After a suitable location was chosen, having good number of cells and minimal contaminants, we focused and set up a time lapse program to take an image every 5 minutes. Changes in focus were handled manually throughout the experiment.

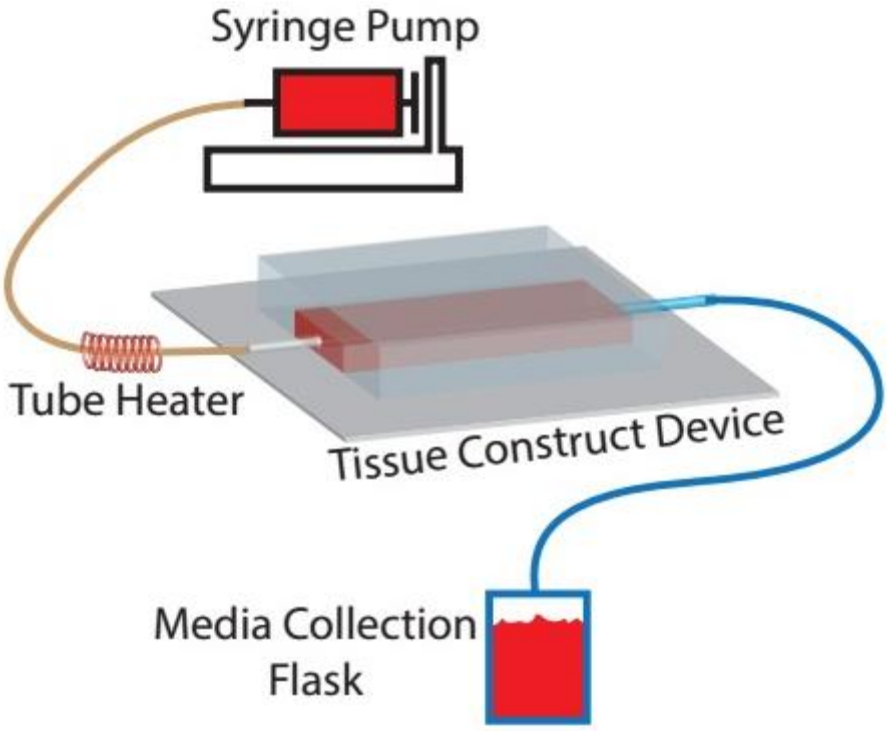

Figure 16: A schematic of the tissue construct setup. Media is perfused from the syringe pump through heated tubing into the tissue construct device and out into a media collection flask.

As a control, we used the same cell-laden gel as is used in the flow group. We pipette 100 µL of the gel into several wells of a 96-well plate, to make a thin (~300 um) layer of gel within the well. The gel was polymerized in the same way as the flow group, but media was added on

top of the gel rather than flowed through. The wells were washed with PBS and the media was exchanged every day. Images were taken at 1 day intervals to monitor cellular proliferation.

vii. Staining Protocol

Immediately after the experiment ends we need to stain the cells to determine cellular viability. We will assess the cellular viability with 2 µM calcein and 4 µM ethidium in PBS solution. For the flow tissue construct, we will extract the thin hydrogel from the PDMS and place it on a cover slip. Approximately 500 µL of the staining solution will be added and incubated at 37ºC for 5 minutes. Afterwards, the stain will be washed off of the sample with PBS two times and imaged using FITC (live) and TexasRed (dead) fluorescence filters. The viability of a sample is quantified by dividing the living cells (stained alive) over the total number of cells (stained alive or dead) to find the percentage of cells alive and viable. A similar protocol is followed to stain the control hydrogel sample, except the gel is left in the well.

C. Results

In this proof-of-principle experiment we are looking for several markers to determine the success of this tissue construct as a model for human tissue. We must ensure that cast we make of the nylon fiber is exactly reflected in the microchannel of the hydrogel in terms of diameter and orientation. In addition, the tissue construct must be able to support flow over the course of days. The process to cast the cells in a hydrogel must not prove lethal to the cells we use. We will be modeling the flow of key nutrients to determine the radial distance cut-off of cell survivability. We will also look at the viability of cells after being sustained in the tissue construct for several days and assess the impact of diffusion gradient on the cell viability.

i. Fiber Casting in Hydrogel

The diameter of the nylon fiber was determined using a calibrated micrograph to be 97.6±0.94 μm (Figure 17a). After casting in hydrogel, the diameter of the channel was measured to be 105.1±1.1 μm in diameter over the 2 mm length of microchannel (Figure 17b). Qualitatively, the microchannel was smooth with no tear-out or obvious defects along its length. As we observed the nylon fiber being removed from the hydrogel, we saw no new defects being created.

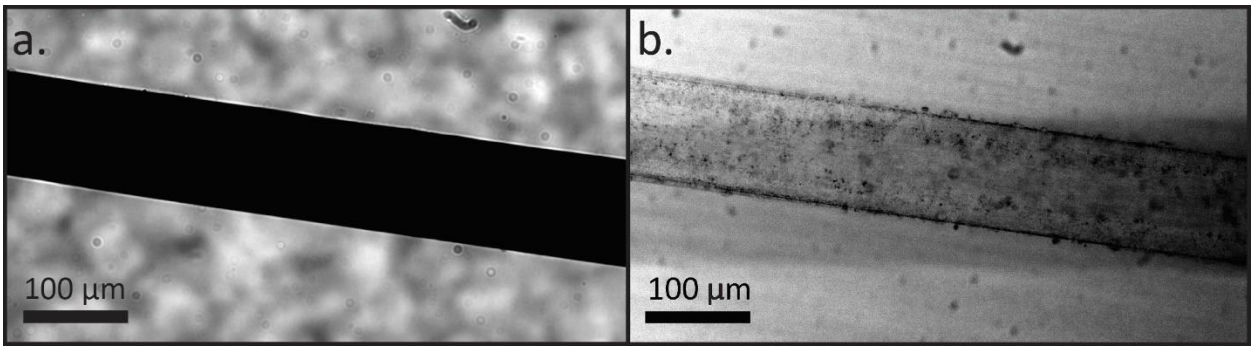

Figure 17: A hydrogel with embedded fiber (a) and after the fiber has been removed (b).

To test the flow of the channel, we connected a 60 mL syringe with dye to the luer lock of the input needle. Under normal flow rates, from 0 to 50 μL/minute, we observed the dye flowing through the channel and diffusing into the gel but not deviating around the channel. Long-term flow was tested by flowing an aqueous solution through the gel at 25 μL/minute over 3 days. Over that time period there was no degradation within the gel and the flow was sustained and collected.

ii. Modeling Nutrient Flow

Important in characterizing this tissue construct is in understanding the nutrient gradients created by having only a single central channel in a relatively large ($>>\lambda_k$) tissue construct. Here we modelled oxygen, glucose, and calcein, transport through model of our hydrogel. The

gradient is created by the competition between diffusion and consumption of the molecules. Here we model two molecules essential to cell survival, oxygen and glucose, and one larger molecule that is used in staining, calcein.

Using relevant cell concentrations, we model the concentration of oxygen at distances radial to the channel in a 100 µm diameter channel and 500 µm tall slit (Graph 2a). At our initial seeding density of HeLa cells, 3 x 10^6 cells per mL, there is some depletion of oxygen within the hydrogel space. At 5 times the population, approximately 2 doublings, there is a sharp drop off of oxygen concentration, reaching conditions that are used in hypoxic experiments 750 µm from the channel wall. At 10 times the initial cell population, approximately 3 doublings, the cells reach hypoxic conditions 250 µm from the channel wall.

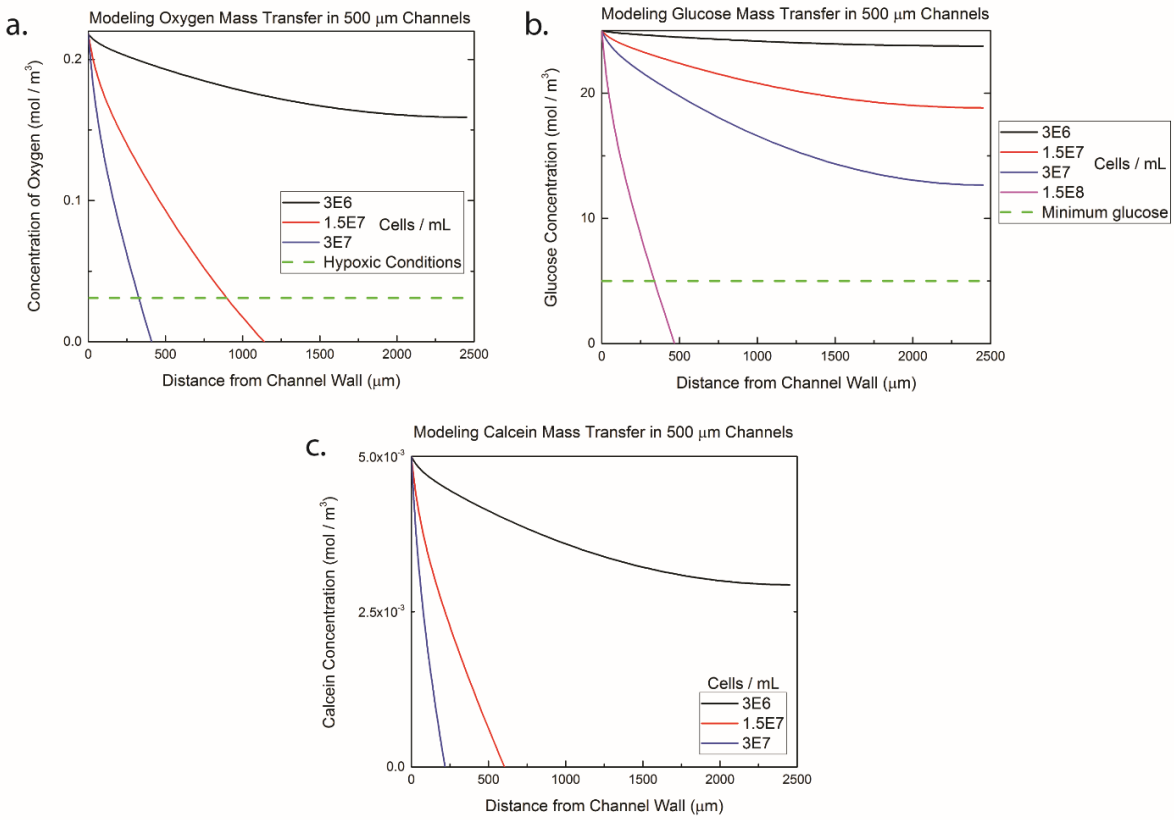

Graph 2: Mass transfer modeling of several relevant molecules to the microchannel slit tissue construct including oxygen (a), glucose (b), and calcein (c).

We find similar results when modeling the mass transfer of glucose in our microchannel and slit (Graph 2b). The concentration of glucose does not reach low-glucose concentrations within our tissue construct until 50 times the original cell population, or 6 population doublings. Lastly, we modeled the mass transfer of calcein in our system (Graph 2c). The relatively high consumption rate and low initial concentrations means that the concentration of calcein drops steeply with increasing cell number. When limiting the slit height to 300 µm rather than 500 µm, we see an increase in the decay length of the molecules within the slit (Figure 18).

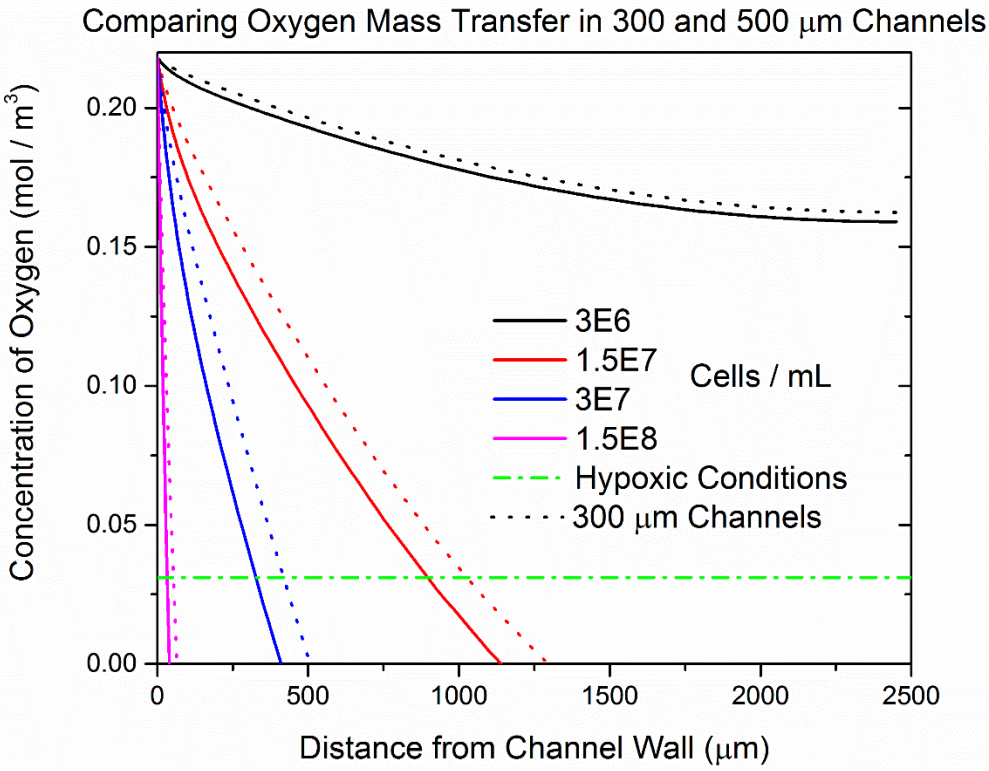

Figure 18: A comparison of the mass transfer decay curves in 300 and 500 µm high slits.

When considering all of the hydrogel within the slit as a 3D object rather than a 2D idealized approximation, we can better observe the decrease in molecule concentration both axially and lengthwise along the microchannel (Figure 19). Cells further from the source of nutrients will see a shallower gradient of concentration as well as a lower initial concentration.

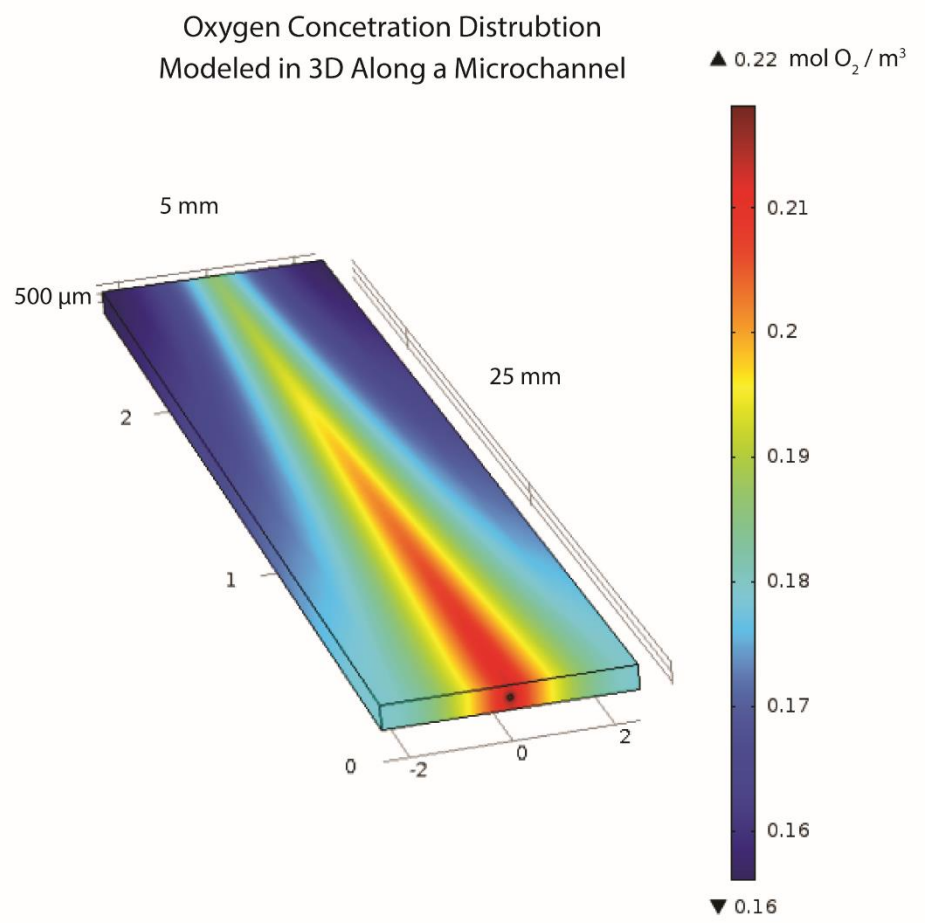

Figure 19: The distribution of oxygen in a model tissue along a microchannel.

iii. Viability and Proliferation of Cells

To better understand how our system reacts over time we used took images every 5 minutes of a region of interest in the tissue construct. Through these we were able to see any morphology or phenotypic changes in the cells as they happen. Over 24 hours we saw a 34% change in cell population within 100 µm of the microchannel and a -1% change of cell population 500 µm from the microchannel (Graph 3).

Importantly, after 48 hours we quantified the viability of the HeLa cells near the channel, within 100 µm, near the edge of the slit, great than 1000 µm, and somewhere in the middle of these two zones (Graph 4). Nearest the channel we saw the highest viability of the HeLa cells

and saw decreasing viability of cells away from the channel. The differences in viability between the cells near the channel and those at the wall were statistically significant. Similarly, the difference in viability of the cells near the channel were statistically significant from those in the control sample.

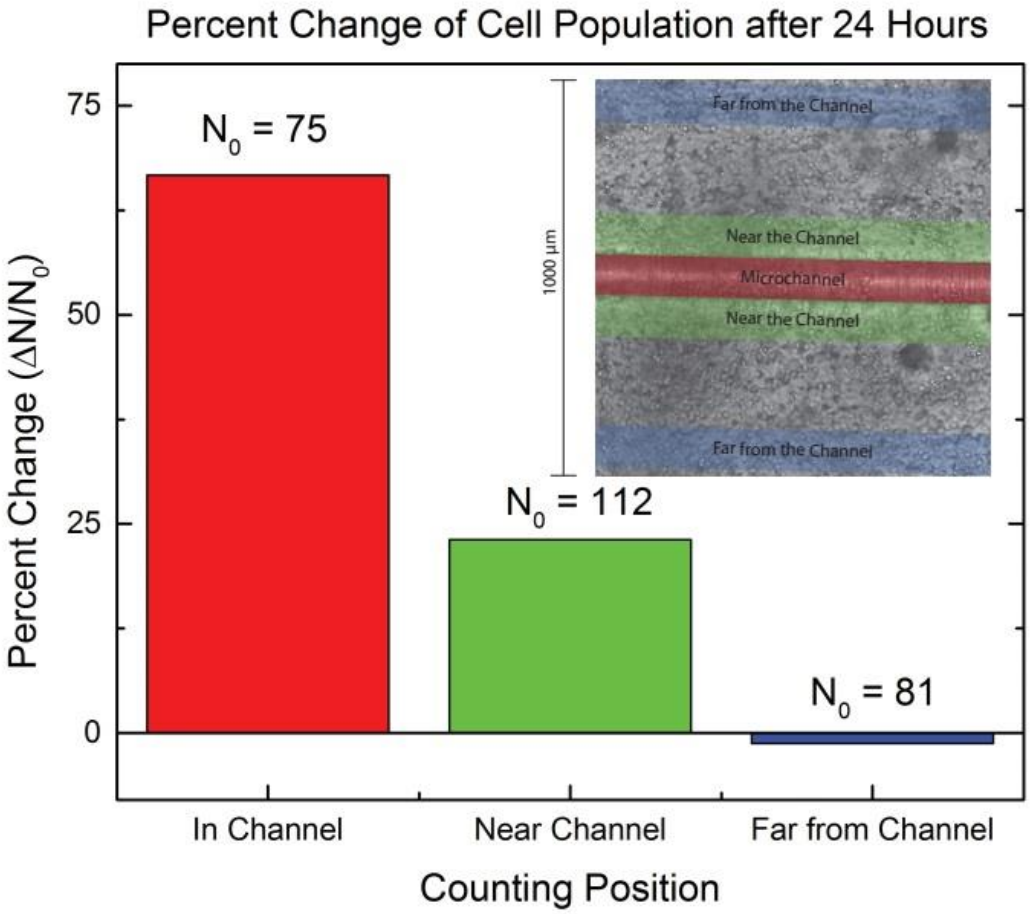

Graph 3: The percent change of cell population at three locations shown in the inset: in the channel, near the channel, and far from the channel.

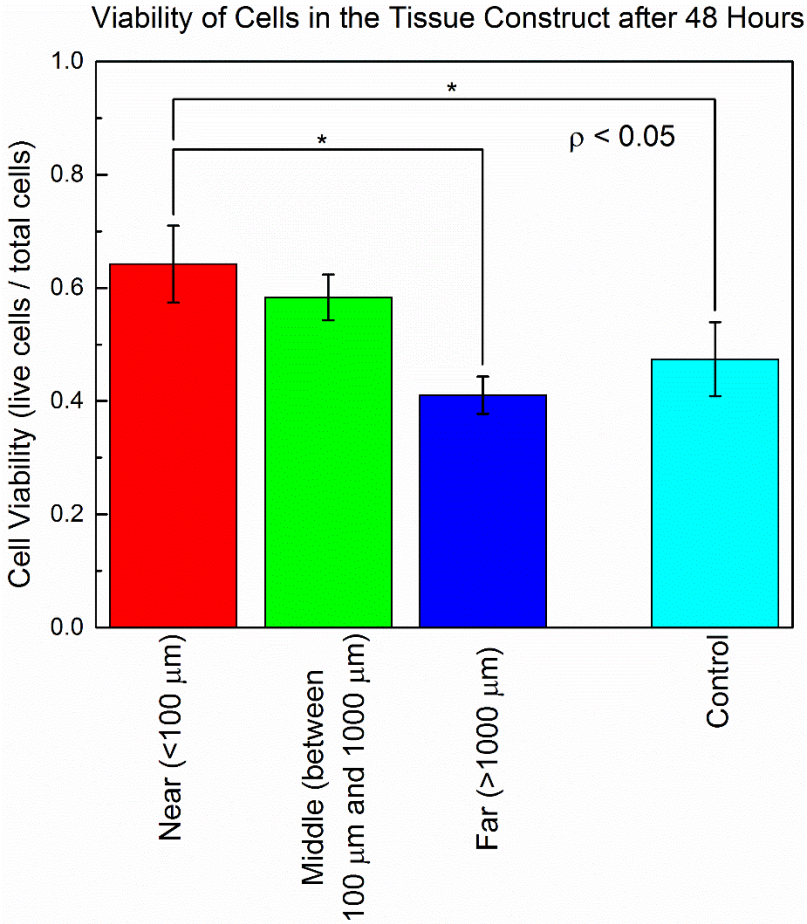

Graph 4: Measuring the viability of HeLa cells in our 2.5D tissue construct in 3 zones after 48 hours of flow.

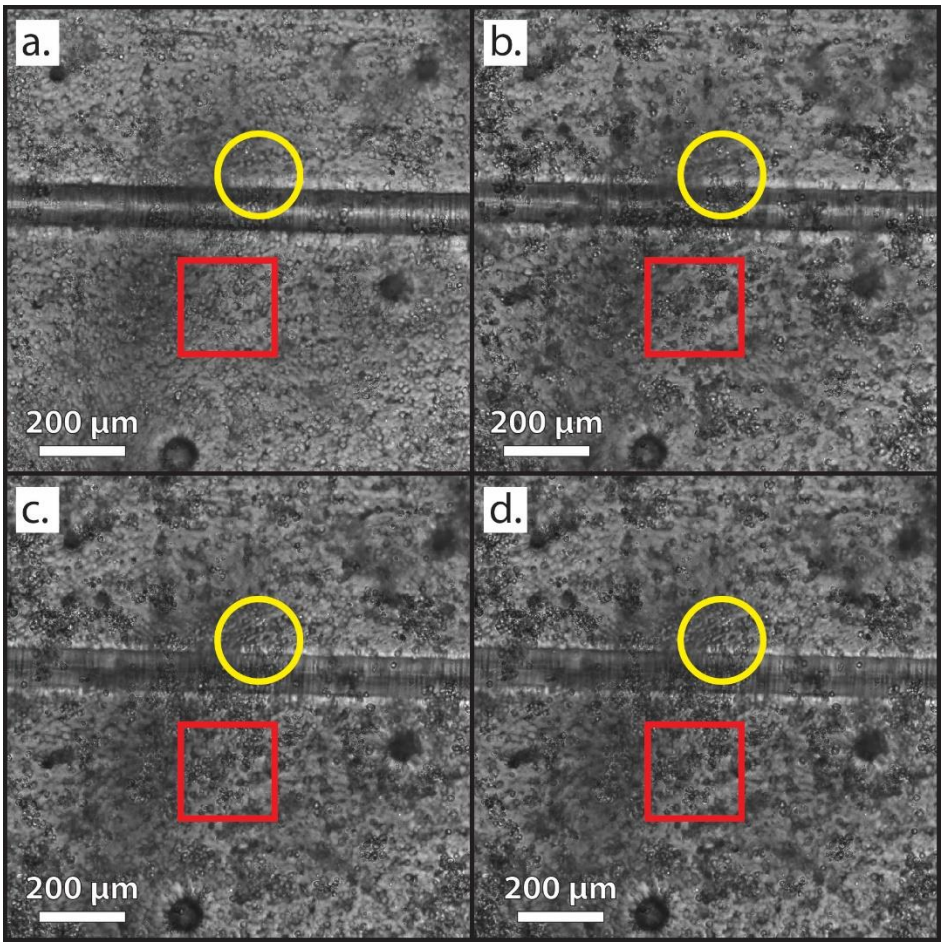

Figure 20: Selected time lapse images over a 24-hour period showing cellular proliferation. Images were taken at 0 hours (a), 8 hours (b), 16 hours (c), and 24 hours (d). Significant areas of growth are highlighted in a yellow circle and red square.

D. Discussion

In this proof-of-principle experiment we proved that our tissue construct created an almost exact cast of the fiber, that it could sustain flow over the course of several days, and that the viability of the cells embedded in the construct are correlated to mass transfer models we have.

i. Materials Justification

In our tissue construct experiment, we used GelMA as a scaffold for the cells. We used GelMA because of its material properties, previous use in tissue engineering, and its

photopolymerizability. The mechanical properties of GelMA can be tuned to specific applications and tissue targets (Graph 5). In this case we wanted to create gel that could withstand several processing steps as well as flow over the course of several days. It is important that our tissue construct can survive flow over the course of several days so that there we can observe cell proliferation. The HeLa cells we used have some of the fastest division times among adherent mammalian cells, around 24 hours, and are therefore suited for this application.

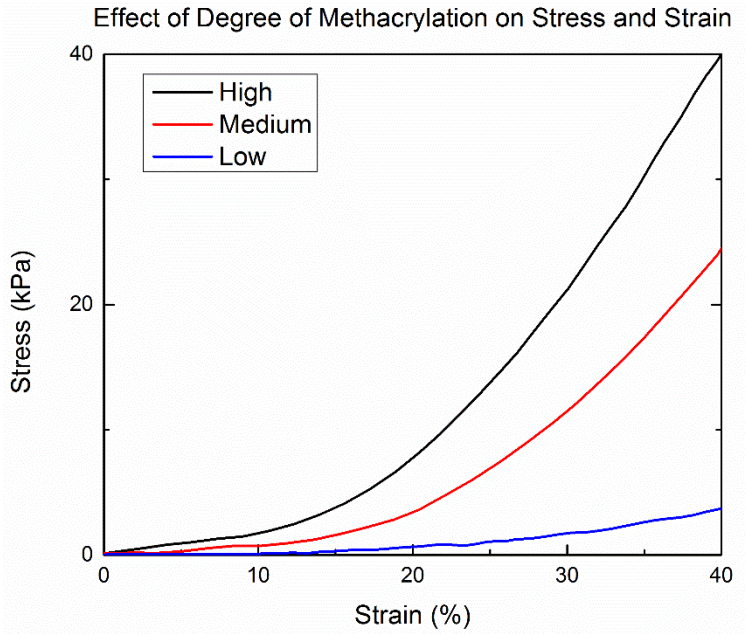

Graph 5: The effect of various degrees of methacrylation on the elastic modulus of GelMA. Adapted from Nichol et. al.

By synthesizing the GelMA ourselves we could control the degree of methacrylation and therefore the stiffness of the final gel. The GelMA has also seen extensive use in tissue engineering applications, primarily in 3D printing tissues and that work supports that the GelMA we used is degradable and attachable by HeLa cells.[182,183]

As discussed previously, allowing for cells to modify their environment is important in sustaining a culture especially in 3D. Lastly, the ability to photo-polymerize the gel makes fabrication of the device straightforward. While there are some hydrogen bonding effects as the

GelMA cools, it is thermally reversible. In contrast we can permanently crosslink the GelMA using UV light. There is noted damage to cells via UV exposure, but by limiting the exposure time and power the effects on cell viability are minimized.[184,185] By minimizing the need for drastic temperature control, we improve our chances for success.

The PDMS and glass model we used to create the slit was used because it is a well-defined system used for casting. The casting of the slit makes as close as a 1:1 mold as possible, increasing the accuracy of our model and the oxygen plasma bonding step exposes surfaces groups that allow for surface modification of both the glass slide and the PDMS slit. The addition of the APTES and GA surface treatment is to ensure that the GelMA bonds to the glass and PDMS, two hydrophobic materials. The ATPES-GA system is a well-defined surface modification system used in organ-on-a-chip applications.[186] While GA is toxic to cells even in low concentrations, the bulk of the GA is washed out in the fabrication steps leaving only those molecules that are bound to the surface.

We use a 30G needle as our inlet because it is smaller than the 500 µm slit height and can be bent and centered within the slit with relative ease. The luer lock on the needle is also ideal for connecting the media syringe pumps to the tissue construct, without the need for glues or other complex fluid connections. As the outlet, 30G PTFE tubing is used for its large inner diameter and non-stick properties limiting the potential for clogs. A 100 µm diameter nylon fiber is used for its minimal interactions with the gel, and its diameter which is large enough to minimize resistance but small enough to mimic physiological capillaries.

Creating our tissue construct in this way, with template casting, we can understand our system to scale it to a larger tissue construct with more channels. Other 2.5D tissue engineering methods are either expensive, tedious, or not feasible in large scale. By using our template

casting technique with other hydrogels and other cell types, previous work can be expanded to include more in-depth studies.

In our proof-of-principle experiments we used HeLa cells due to their rapid proliferation and general heartiness. Several processing steps in the fabrication of this tissue construct could be detrimental to cell viability and we needed a cell line that could be used without fear of affecting phenotype or viability. In addition, as an adherent cell it readily grows in GelMA. When sustaining the tissue construct we used a flow rate of 25 µL/minute because it is within the range of physiological flow rates and should be fast enough to allow for replenishment of nutrients within the gel.[187]

ii. Setup Justification

We used a syringe heater at the inlet tubing to ensure that media going in was as close to 37ºC as possible. In addition to heated inlet media, the immediate area around the tissue construct was heated with resistance heater and fan. This allows even distribution of heat throughout the space, and the temperature was monitored with a thermocouple to ensure proper heating. Because the tissue construct was enclosed in PDMS, moisture level was not considered because there should be minimal water loss in this sealed construct.

When imaging the construct with time lapse, the focus has to be adjusted due to change in focus of the sample over time. This is due to thermal fluctuations and vibrations from the fan on the sample. The change in focus is subtle and non-linear so constant monitoring is required to ensure that all images are at the same focal plane over the whole time lapse. We directly imaged the cells during flow to better understand what morphological and phenotypic changes occur in our system. In addition, we can monitor the experiment for any leaking or change in flow rate. The staining protocol we used is a simple system to determine the viability of a cell culture. The

gel traps some fluorescence because of the limited convection to the sample and therefore there is always a relatively large background single. During image acquisition, the same exposure time is used in all images to allow for more direct comparison of fluorescent levels. While there are many different methods used to sustain a tissue culture, our setup is similar to previously used perfusion systems.[125]

iii. Making Sense of the Mass Transport Model

The values for initial concentration, consumption rate, and diffusion, were gathered from extensive literature search. Within the literature, however, values for the same parameter can vary by orders of magnitude. Here we presented a model based on our best guess of what the parameter was for a given molecule. We can approximate the number of cells per milliliter for a solid tissue to be 1×10^8 cells/mL. Our starting density of cells, 3×10^6 cells/mL, is well below those levels, but still can but substantial strain on the nutrient level.

Previously, oxygen was indicated as being the essential molecule in modeling survival in limited tissue systems. This is due to the rapid use of oxygen by cells and the limited amount of oxygen that can be dissolved in media, which is less than in water. When we estimate oxygen consumption for HeLa cells, we averaged the measurements in literature. In addition, the amount of oxygen in the media was not measured directly, but instead determined through a literature search. The minimum oxygen threshold was set based on previous experiments on the effect of hypoxic conditions on cells. Oxygen levels less than 15% of the oxygen naturally dissolved in media were considered to be detrimental to cell survival and proliferation. An important complicating factor in our system is the fact that PDMS itself is permeable to oxygen and may affect results, but this was not modeled. This effect should be limited by the thickness of PDMS used in the construct. We see that our model of the oxygen consumption matches the

assumptions that we have made, at approximate cell densities in tissues we see a sharp decline in oxygen in distances > 200 μm away from the channel, matching what we see in physiology and the Krogh model.

As we look at the model of glucose transport in our channel we notice the same trend of consumption as oxygen but at lower level. It is not until much higher cell densities that there is a sharp drop in available glucose. The concentration of glucose in the system affects the rate of cell proliferation but it is not until approximate cell densities of tissues that we such an effect. This is in contrast to oxygen, because the solubility of glucose in media is greater than that of oxygen while their consumption rates are similar.

Here we model calcein because it can give us an indication of the diffusive properties of our gel and allow us to directly compare our model to the tissue construct device. By flowing calcein-AM through the channel, we expect the cells to convert it to calcein, a fluorescent molecule. By measuring the distance over which fluorescence decays we directly measure the diffusion and rate parameters of our system rather than relying on literature values. In addition, as the cell number increases we expect to see decreasing amounts of fluorescence in the channel. But such an experiment would require a higher cell density than our initial density to see an effect.

In our model we use a slit height of 500 μm, the same as our device. However, if we could decrease the slit height of our device to 300 μm, we see an increase decay length (Figure 18). Due to limitations in placing the needle with our current system this is not possible, but by moving to a micro-fabricated device it may be possible to limit the device in this way. Indeed, when we compare the oxygen models with the two channel heights we can see the difference in

decay length. This allows us to design the chamber according to the range of parameters that we want to study.

iv. Understanding Cell Viability and Proliferation

We measured the change of cell population using time lapse bright field imaging and not fluorescent imaging because our setup was not compatible with continuous fluorescent imaging. Instead, at the end of the experiment we extracted the gel from the slit and stained the gel with a live/dead stain to determine cell viability. Additionally, exposing the cells in the construct to ethidium for prolonged periods of time causes apoptosis and should be avoided. The location to record the time lapse images was chosen so as to have the largest field of view without aberrations or abnormalities in the gel. In general, we recorded within the first centimeter of the channel if possible. The farther along the microchannel the lower concentration of nutrients is provided by the microchannel (Figure 19).

We expected that the proliferation near the channel (within 100 μm on either side of the channel) would be highest. The farther from the channels the cells are the less likely it is that sufficient nutrients will diffuse there. The field of view was limited to approximately 1 mm^2 at the magnification required to resolve individual cells, which limits the amount of data we can compare cells near the channel with. With the time lapse protocol, we imaged the tissue construct every five minutes. Watching the time lapse, we can qualitatively see proliferation of the HeLa cells in the construct, specifically in zones near the microchannel (Figure 20).

As expected, cells that were $>>\lambda_k$ from the microchannel did not see the same proliferation as those that did near the channel. In fact, there was a loss of cells from those sections. While in bright field, we would not expect cells to disappear, localized changes in focus or shifting of the gel may have obscured cells that were counted previously. Over most of the

time lapse images we saw increasing or no gain in cell number, not loss in number, supporting this hypothesis.

The initial counts of cells in the channel were lower than those near the channel and were similar to those far from the microchannel. This low count may be due the fiber removing some of the thickness in the gel in that area. Wetting effects of the gel on the nylon fiber may also account for the localized increase in cell numbers near the fiber than in the surrounding gel. Despite the low starting number of cells in the microchannel, they showed the highest percent change in cell population over the 24 hours. This is consistent with the hypothesis that cells nearest the microchannel will have the most access to nutrients and will have higher proliferation rates than those farther away.

We expected that the viability of the HeLa cells to follow a similar trend of that in the cell population. More specifically, we expected that the cells nearest the channel would have the highest viability and that there would be decreasing viability moving away from the channel wall. That is the effect that we observed, with the difference in viability between the cells nearest the microchannel and those far away (> 1000 μm) and in the control being statistically significant. While none of the populations had near 100% viability, as might be expected in a traditional cell culture environment, the processing steps or nutrient gradient could have affected their survival.

Even the control sample, which had a uniform 500 μm thickness of gel and saw relatively low viability. This may be due to the majority of cells being embedded more than 100 μm into the gel and therefore not be within the decay length of nutrients. Cells that were far away from the channel were somewhat viable, over 50%, but this may not indicate good health of the cells.

Combined with the results of the proliferation study, these cells maybe in a state of quiescence and not actually proliferating, potentially due to serum withdrawl.[188]

v. Lessons Learned

To get to the point where we could sustain flow through the tissue construct over prolonged periods of time took many iterations of designs and included many lessons learned. Here we will describe some of the obstacles encountered making the device and how they were solved.

The order of assembly of the tissue construct is important. The GA should not be incubated in the slit with the nylon fiber and needle. Initially we thought that we could functionalize the needle tip to facilitate the gel adhering to it. Instead, some of the GA remained on the nylon fiber and the gelatin was then crosslinked to the fiber. When removing the fiber, some of the GelMA came with it causing tears and unevenness in the microchannel. Now the nylon fiber and needle assembly are added after the surface treatment of the slit. The surface treatment can be disrupted when touched and care must be taken when threading the fiber through the slit to minimize contact with the treated parts of the construct.

The timing of the surface treatment is important to creating a stable functionalized area. As mentioned previously, allowing APTES to polymerize in the presence of water can cause multiple uneven layers of silane to form. Even the natural moisture in the air can cause this to happen so care must be taken to ensure that no water can enter the channel during APTES treatment. In addition, allowing the GA to APTES reaction to take place for too long can cause crystallization of the chemicals in the channel. Not only does this obscure the slit from viewing but can let excess GA leech into the gel when cast. The GA should be incubated for a maximum of 20 minutes in the APTES treated slit to avoid this.

The most important piece of the tissue construct is the nylon fiber. It is what defines the geometry and placement of the microchannel in the final tissue construct. Therefore, the alignment of the fiber within the slit is paramount. The fiber must have tension on it to prevent drooping through the center of the slit. While a microchannel can be cast with arbitrary orientations of the fiber, having the fiber make a tortuous path through the cell can allow it to contact the wall. Any contact the microchannel has with the sides of the device can cause leakage around the gel rather than through the microchannel. While the gelatin is crosslinked to sides of the channel, sometimes enormous pressures are generated and fluid can be forced around the gel rather than through it.

In a similar vein, the needle needs to be exactly centered in the slit before casting. We center the needle by creating a platform for the needle to rest on and take as much human alignment out of the process as possible. Even still, having the needle touching the top or bottom of the slit can create areas of leakage around the microchannel in the tissue construct.

Despite a perfectly aligned needle and fiber through the channel, leaking of media out of the slit and not through the microchannel can occur. In this case, it is due to incomplete sealing of the channel with Superglue. The superglue sealing is required on both the inlet and the outlet side to bond the gel with the PDMS and glass. The preferred path of media is not through the high resistance microchannel but instead around the water layer formed around the hydrophobic needle and out of the inlet side. We ensure sealing of the inlet and outlet by using multiple layers of Superglue and an accelerant to complete bonding.

We must take care when injecting the gel into the slit to minimize air bubbles. The high viscosity of the gel and the constraint of the slit prevent any effective measure to remove the bubbles from the gel before polymerizing. The bubbles typically form when pipetting the gel into

the slit but are also commonly seen at the precipice of the outlet tubing. The air within the outlet tubing combined with its large inner diameter means that some gel can slip in and the air is forced out creating an air bubble near the outlet. Air bubbles that do not come into contact with the microchannel have minor consequence on the system, but if they are in the microchannel path they can affect the path of least resistance and the localized shear.

With even the most ardent bonding of the inlet and outlet, if there is no path through the gel, the pressure build-up from the syringe pump can cause media to force itself out of the sealed slit. The path in the microchannel can be blocked for a variety of reasons and need to be checked prior to flowing media through the channel to ensure longevity. The most obvious blockages occur within the microchannel itself. Sometimes these can be resolved with persistent slow flow. More commonly blockages occur in the outlet tubing. The outlet tubing has a relatively large inner diameter which can fill with that can shift and occlude the outlet. To facilitate identifying these type of blockages we moved to using clear tubing for the outlet.

Within the outlet tubing blockages typically occur at the initial exit, or within the media collection vessel. If the outlet tubing does not drip directly into the vessel but instead runs down the wall of the vessel, the large surface area of the media can hasten drying which can block the tubing. This type of blockage is more common in overnight experiments where the device is not continually monitored. Especially concerning is the contamination of media within the channel, at the outlet. If any part of the microchannel system is not sterile, it can lead to biofilm formations within the device that can cause blockages within the microchannel (Figure 21).

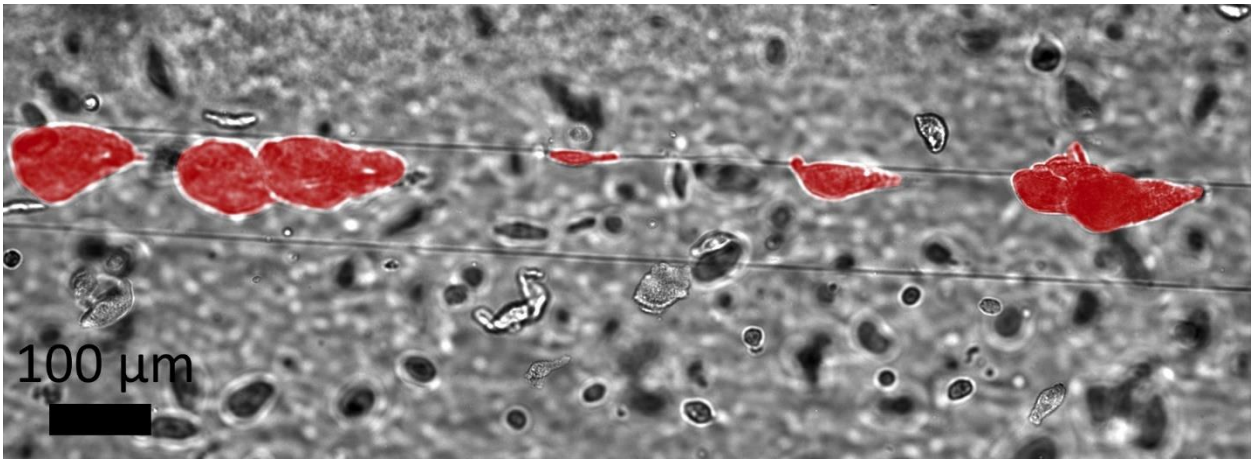

Figure 21: Bacterial colonies, highlighted in red, growing within the microchannel.

The lynchpin for the tissue construct is the gel that the cells are cast in. Synthesizing the GelMA for casting is a two-week process, but errors can occur in this process. It is vital to test every batch of GelMA to ensure that it polymerizes properly before use. Prolonged time above freezing can prematurely degrade the gel and cause problems when casting a microchannel.

When casting a hydrogel, especially in applications that the gel will be immersed in water, swelling must be accounted for. Using lower concentrations of GelMA when casting the tissue construct (<15%) can lead to the gel swelling in the slit from the flow of media through the channel and the channel being constricted closed. Higher concentrations of GelMA (>20%) eliminates this effect in cell-free gels. However, when cells are used in the gel, they are naturally inclined to modify their surrounding ECM. As the GelMA is modified and the linkages within the gel are degraded by the cells, the gel can continue to swell and constrict the microchannel. Important then, is leaving several mms of space near the outlet of the slit to allow for gel expansion.

A consequence of the microchannel variation over time is that the pressure through the system can change. When using a pressure controller to control flow, which provides constant pressure, the flow rate changes as the microchannel changes (Figure 22). This can be especially

troublesome in our system because the gel and microchannel can minutely change, affecting the flow rate through the microchannel, and thus minimize the nutrients delivered to the gel. To resolve this, we use a syringe pump to set a particular flow rate. The syringe pump bypasses the need to understand the minute resistant changes within the system. We have found that we must maintain pressure within the assembly to ensure flow when changing syringes. To do this we use a system of 3-way valves to build pressure in the replacement syringe before introducing it into the flow stream.

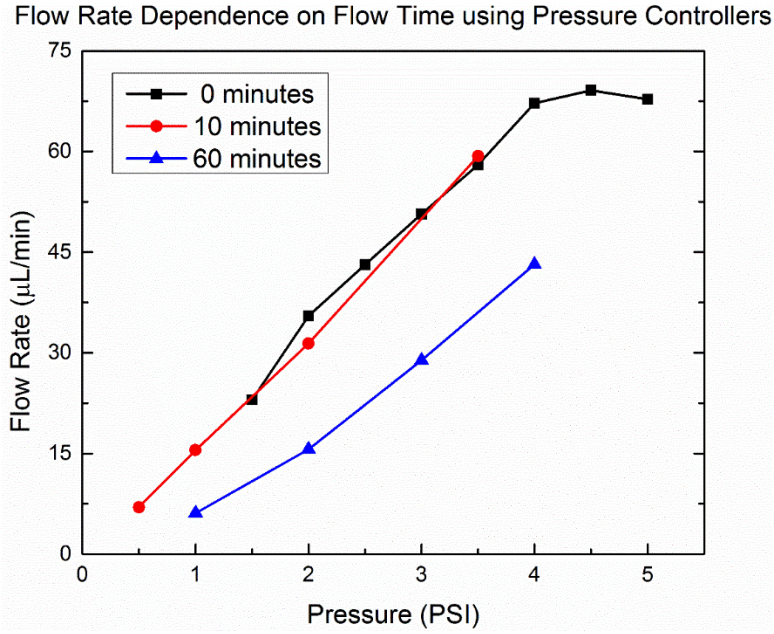

Figure 22: Analysis of the flow rate dependence on flow time when using pressure controllers. The swelling in the channel decreases flow after 30 minutes.

The shifting of the gel occurs due to swelling, temperature effects, and localized pressure build-up. This shifting can affect the field of focus within the gel as well as the field of view. The only way to combat these changes is to monitor the acquisition of images and manually adjust the focus or field. Even still, the shifts in gel may not be isotropic and the field of view may

change over time. The quantification of cell number in images should not be taken as a given as the focus and location of the counts can differ throughout the time lapse.

vi. Limitations

There are of course some limitations to this study on 2D tissue cultures. Determining the edges of a cylinder in a microscope can be especially difficult because of lensing effects in the hydrogel. Measurements were done at the focused that showed the sharpest line for the wall of the microchannel, assumed to be extents of the channel and compared to the diameter of the fibers which were measured in the same way. *En face* measurements the microchannels and fiber would provide more accurate measurements but they remained elusive for this slit based tissue construct.

Modelling the microchannel in the tissue construct used an idealized scenario of all parameters involved. In reality, the channels were never exactly straight and of course the consumption rate of molecules not equal, but it should provide a good starting point for understanding of the mass transfer within the tissue construct. The simplified model also does not take into account discontinuities in the concentration profile at the boundaries between the liquid and hydrogel, which should not impact the general understanding of our model.

Counting of cells in bright field, as well as in fluorescence are slightly biased by the specific person counting them. As of yet, this process has not been automated and still requires counting by hand. To mitigate some of the bias from this count multiple people were used to count the number of cells in a given image. Adding to this problem, the live/dead stain we used tended to show cells fluorescing both fluorophores simultaneously. Our analysis of this is that the cells were in the process of dying; the membrane was permeable to the ethidium but there were still active enzymes to activate calcein-AM. A different contrast agent such as CellTiter-

Glo Luminescent Cell Viability Assay (Promega, WI) which measures ATP may help with quantifying the level of viability of the cells.

Additionally, when creating control samples, we wanted the gel to be as thin as possible to see how well the HeLa cells proliferated in it. Unfortunately, making the gel fluid enough to make thin meant bringing it to higher temperature which would have affected cell growth. As a compromise, we used a spin coater to spread the gel out as thin as possible, which we estimated to be ~ 500 μm. When imaging the control samples, it was impossible to differentiate between cells that were embedded in the gel and cells that had migrated out of the gel and adhered to the bottom of the dish. We counted all stained cells rather than try to differentiate the two populations.

E. Conclusion

Here we have expanded our template casting technique from use in PDMS, a commonly used casting polymer, to use with a hydrogel. Most notably, we can create microchannels on size order of capillaries and place them in arbitrary geometries with high fidelity in the tissue construct.

First, we ensured that the casting of a nylon fiber in the gel, GelMA, produces a reliable and accurate cast. We saw that the difference between the embedded fiber and microchannel it creates is less than 1%. Next we constructed a PDMS slit with a nylon fiber threaded through the center to mimic one of many channels in a vascularized hydrogel. To this we had to iterate our design using different materials and methods in order sustain flow through the device. Once optimized, we created a finite element model of our system to determine whether such a system could support cells within it given its limited perfusion of nutrients.

We saw that the gel could indeed sustain cells near the microchannel, where the transport of molecules is not as limited by diffusion. Additionally, we noted that nutrients are drained from the microchannel and the decay length shortens further down the channel. We can exploit these decay curves to design experiments to study our system and also to design competition experiments between different cell types.

Once our model proved that our system was viable, we created a cell-laden hydrogel with GelMA and HeLa cells. We used this photo-polymerizable gel in conjunction with our assembled slit with a nylon fiber to create a tissue construct confined to a PDMS chamber. We flowed heated media through the system to sustain the cells and recorded their proliferation and viability. Cells nearest the channel saw the most growth, almost 70%, and were the most viable population. Taken together, this shows that our system is capable of sustaining cells.

Using this 2D model of a tissue as a research platform has several advantages over creating a 3D tissue. First, it allows for easier study as the preparations are less complex and there are not as many variables when designing studies. Second, the thin nature of the construct allows us to have continuously observe the cells within and to measure the morphologic or phenotypic changes that are happening. By flowing a cell stain within the media, this platform could conceivably take time lapse fluorescent images to increased contrast and looking at more specific markers.

4. Template Casting a 3D Tissue

Mammalian biological tissues are heavily reliant on the microarchitecture of 3-dimensional networks of fluidic channels, that can be divided into vasculature (ø cm to <100µm)[189], the lymphatic system (ø cm to <100µm)[190], and the nervous system with axons (ø 2µm to 20µm)[191] that conduct electrical signals between neurons. The coverage of the capillary network (both vasculature and lymphatic) is especially dense – typically cells are no more than 150µm away from a capillary to ensure proper transport of oxygen, nutrients and waste products.[192]

These channels networks have complex 3D architectures that have been difficult to replicate *in vitro.* Having a well-established vascular network is vital to sustain tissue that have features larger than 200 µm due to limitations in diffusion lengths of cell required biomolecules. A 3D tissue scaffold needs to be pre-vascularized with well-defined structures because points within the construct that are more than a decay length from the vasculature will turn necrotic. Microchannels need to be created every 300 µm to ensure proper nutrient gradients in the construct.

There are techniques that can create these dense microchannels in a scaffold using both directed and undirected fabrication techniques. Directed techniques can produce highly dense microchannels but they generally can only do this in small volume (< 1 cm^3) tissue constructs. There is an unmet need for a directed microchannel fabrication technique to pre-vascularize tissue constructs with highly ordered microchannels that have less than a 300 µm pitch in large volume (> 1 cm^3) tissue scaffolds.[63,65,66]

Un-directed fabrication techniques include methods that process scaffolds in bulk, and can tune the internal microchannel diameter, density, and other parameters of the scaffold, but lacks precise control over placement and geometry of the microchannels. Conversely, directed fabrication of microchannels involves the deliberate creation of microchannels in a scaffold in a precise dimensions and orientations. Directed fabrication can be further broken down into top-down and bottom-up techniques. Top-down techniques build the tissue construct all at once, usually through the subtraction of material, while bottom-up techniques build up the construct layer by layer.

Here we will focus on the gap between these two methodologies in terms of feature resolution and construct volume. Top-down methods can create large tissue constructs ($\nu \sim 1$ cm^3) but lack feature resolution ($\zeta \sim 1$ mm) while bottom-up methods exhibit high feature resolution ($\zeta \sim 1$ μm) but lack construct volume ($\nu \sim 1$ mm^3). Here we are proposing a technique to bridge this gap.

The goal of this project is to develop a platform technology that can create an intricate vascularized tissue construct with a scalable one-shot technique in cost-effective manner. Previous methods are expensive, time consuming, or lack the mechanical properties to be used as a tissue engineering technique. This work will address the shortcomings of previous work by creating a highly adaptable technique that can create microchannels with physiological spacing in a cost effective and straight-forward manner. Completing this work will be a major step forward in advancing tissue engineering techniques.

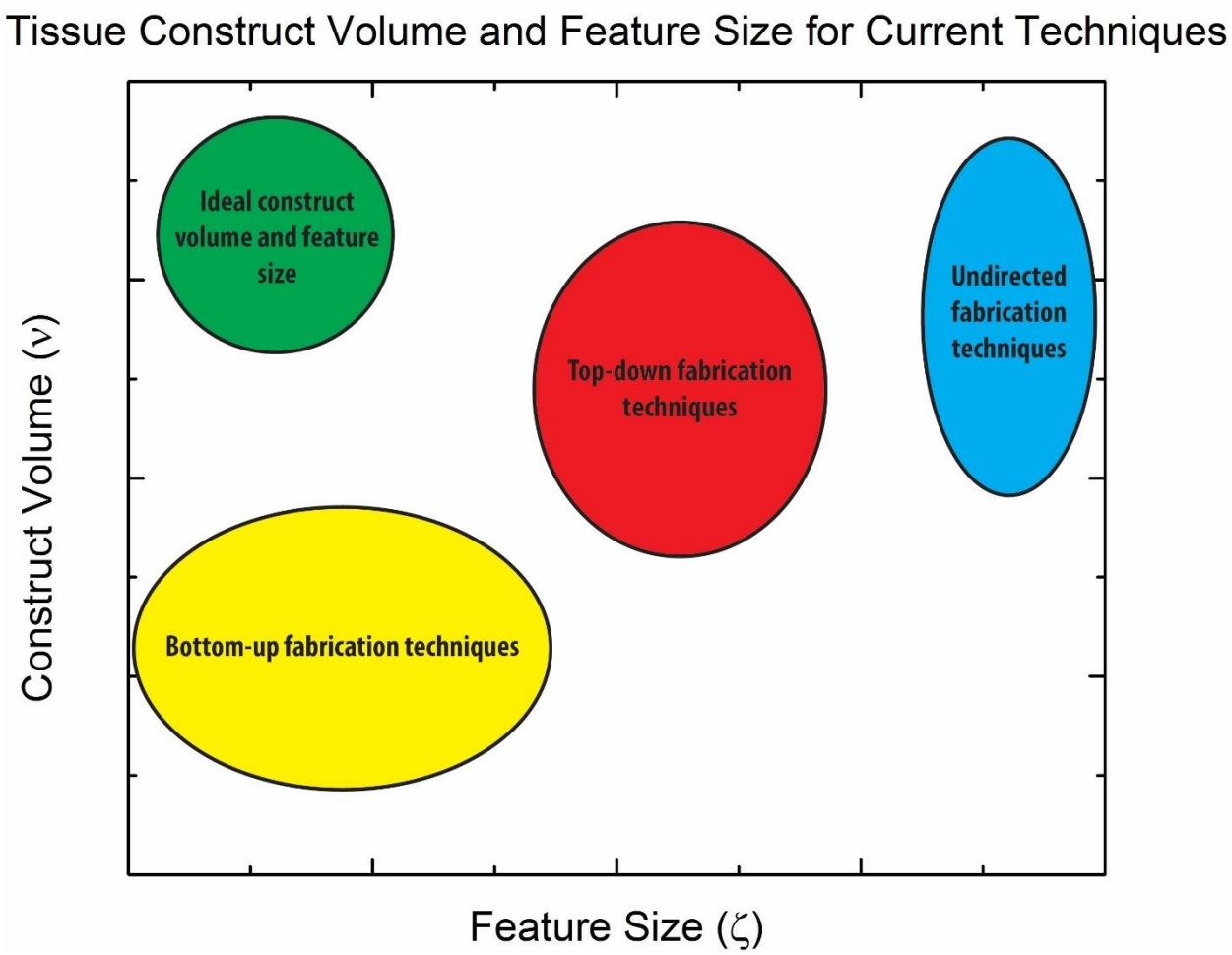

Graph 6: The scale gap between top-down and bottom-up fabrication techniques currently being used in tissue engineering applications.

A. Large Scale Tissue Engineering Background

The goal of vascularizing hydrogels is to create a construct that can support cellular growth. The microchannel size and spacing within the construct is vital in ensuring proper tissue growth. If the channels are too small, it can limit the mass transfer to the cells and there can be occlusions blocking nutrients to whole areas of the construct. Conversely, if the channels are too large it can decrease the mechanical strength of the construct and limit cell motility while not increasing the decay length of nutrients into the construct. Tissue constructs have perfused channels from 10 to 300 μm in diameter with channels of 100 μm diameters being used most

often.[193-195] Additionally, the channels should also be strong enough to support flow, while also able to be degraded by the encapsulated cells. Finding a compromise between all these requirements is needed to create a viable tissue construct.

For a tissue engineered scaffold to be successful it must have several features. It must have interconnected pores or a method that allows for perfusion. It must be made from a material that is bio -degradable or -resorbable so cells can replace the scaffold. The scaffold should have some way to bind or interact with the cells to ensure that the cells can survive. The scaffold should have mechanical properties that match or approximate the target tissues they are replicating. There should be no adverse cytotoxic response from the scaffold being degraded. And the scaffold should be able to be fabricated in various shapes and sizes.[196,197]

i. Undirected Microchannel Fabrication

Undirected scaffold fabrication techniques use bulk physical processes to create a scaffold. These techniques have limited control over pore size, microchannel geometry, interconnectivity, and scaffold stiffness, in bulk scaffolds. The fabrication methods used to make these scaffold exploit physical processes to create random pore structures within a scaffold material. Gas foaming ($\nu > 2$ cm^3, ζ = N/A)[198], melt molding ($\nu > 0.5$ cm^3, ζ = N/A)[199], and emulsion freeze drying ($\nu > 2$ cm^3, ζ = N/A)[200], have all been used to create this type of scaffold and can all create large volume scaffolds quickly.

Some techniques garner more control over the network of microchannels in the scaffold than others. In one instance, a construct was created using a random nest of dissolvable sugar fibers embedded in hydrogel. Once the gel is set around the fibers, the construct can be soaked in water and the fibers will slowly dissolve and be eluted out ($\nu > 1$ cm^3, ζ = N/A).[201] A single inlet and outlet are connected to the nest of channels and perfused (Figure 23a). Currently, the

technique uses the biocompatible, but non-biodegradable, PDMS. While this method can create large volume constructs, it lacks control over the order within the microchannels.

Scaffolds can also be created using molding processes. By compressing a PLGA powder with gelatin microspheres into a Teflon mold and heating it above the glass transition temperature of PLGA, the gel assumes the form of the mold ($\nu > 0.5$ cm^3, ζ = N/A).[199] The gelatin particles can then be leached out by soaking the scaffold in water. Emulsion freeze drying can also create micro-structures in scaffolds. Two immiscible liquids are homogenized to form a water-in-oil emulsion and freeze dried to produce a porous structure ($\nu > 2$ cm^3, ζ = N/A).[200]

Solvent-casting particle leaching techniques have also been used. A hydrogel is mixed with a specific diameter of salt particles to achieve a uniform suspension. After the gel has been cured, it can be immersed in water to dissolve the embedded salt particles ($\nu > 2$ cm^3, ζ = N/A).[202] The resulting hydrogel has a porous structure that can support cells. A similar method to create this porous scaffold utilizes a CO_2 saturated gel that is degassed during curing. This creates cavities within the curing gel for tissue engineering.

Other techniques do not focus on the creating channels within hydrogel but creating subunits of hydrogel that have pores between them. Rather than creating microchannel networks, cell-laden collagen units were assembled together within a tubing ($\nu > 1$ cm^3, ζ = N/A).[203-205] The porous structure between the cell-laden collagen units allowed media to perfuse through the construct and sustain the cells (Figure 23b). Randomly orienting the pillars within the perfusion chamber is not an efficient use of space, and other shapes have been tried.[206,207] However, this assembly of collagen units lacks cohesive strength. It would not withstand sustained flow without the structure of the tubing supporting the construct.

Another technique that has been used to create tissue scaffolds is electrospinning. Electrospinning of hydrogels has also been used to create a large porous network that cells can attach to and proliferate. A large electrical potential is applied to a precursor hydrogel solution that is dripping on to a surface. When the electrostatic repulsion overcomes the surface tension of the charged droplets, a continuous stream is formed (Figure 23c). The stream of hydrogel gels as it falls on the surface. This technique has been used to embed embryonic kidney cells inside of fibers and the electrical potential from the spinning did not adversely affect the cells ($\nu > 1$ cm^3, ζ = N/A).[208] While the scale of this technique is impressive it lacks a well-defined channel system as well as an inlet and outlet.

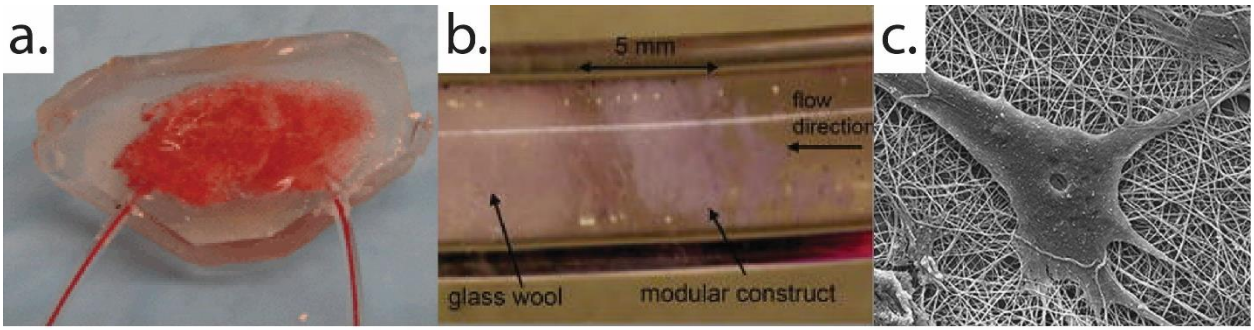

Figure 23: Undirected methods to create microchannels in tissue scaffolds including: sugar nests (a)[201], collagen units (b)[203], and electrospinning (c)[209].

These undirected microchannel fabrication techniques are able to create large scaffolds with microscale channel networks that have been used for tissue engineering applications ($\nu >$ cm^3, ζ = N/A). However, there is a lack of control in the precise microchannel placement, orientation, and density to create an effective tissue mimic.[210] Instead we will focus on directed techniques to fabricate microchannels for tissue engineering applications.

ii. Directed Microchannel Fabrication

Counter to the undirected methods, directed microchannel fabrication methods deliberately create microchannels within a scaffold with precise geometry, orientation, placing,

and spacing. This type of technique has been limited in scaffold volume due to the precise nature of the microchannel placement but the advantage is a more well-defined system.[67,211]

There are two schools of thought regarding the directed micro-fabrication of tissues: bottom-up layer-by-layer fabrication or top-down one-shot techniques. The bottom-up fabrication of an organized tissue of one layer is straightforward, but generating multiple aligned layers and forming them into a tissue is daunting. The main limitation of such bottom-up fabrication methods is the time and cost involved in creating a tissue construct of sufficient volume. Conversely, top-down methods can create the whole microarchitecture in one shot. Top-down techniques allow researchers to create larger volume constructs relatively quickly, but these constructs lack the necessary micro-structure detail to truly mimic the physiological environment of a tissue.

a. Top-down Techniques

Current top-down 3D culture technologies generally rely on using macro techniques to create micro-structures in a scaffold. The simplest form of a top-down tissue construct involves casting needle in hydrogel ($\nu > 0.25$ cm^3, ζ = N/A, Figure 24a). After removing the needle, media can be flowed through the cast, perfusing the construct.[212] Cells embedded in the hydrogel can be sustained when using this technique. This single hollow tube construct cannot sustain a whole tissue construct due to its limited diffusion.

To create a similar structure, cell sheeting engineering uses rolled sheets to overcome the insufficient mechanical properties of other constructs ($\nu > 0.25$ cm^3, ζ = N/A).[213] Cells were cultured to over-confluency so they could be removed from the whole dish as a complete sheet. The sheets were then rolled and cultured with constant perfusion through the hollow core (Figure 24b). While this technique is quite effective at creating hollow cylinders of tissue, it is difficult to

create other geometries. Additionally, only cell types that are proliferative and that can create excess ECM can be used.

Rather than casting a hydrogel around a single needle, some techniques have adopted the use of casting hydrogel around multiple well-defined spindles. ($\nu > 0.5$ cm^3, $\zeta > 0.5$ mm, Figure 24c).[214] While this technique does allow for more precise control over channel geometry, it is still limited in construct volume due to the mechanical properties of PDMS.

Top-down techniques also involve repeating a process over a large construct. Laser ablation uses high power lasers to ablate scaffold in precisely defined areas ($\nu > 0.1$ cm^3, $\zeta > 0.5$ mm, Figure 24d).[215] This technique has been used with porous poly(glycerol sebacate) hydrogel, but the lasers cannot penetrate very deeply and it is difficult to scale this technique up to any appreciable tissue construct volume.

Most recently, sacrificial molding has been combined with a 3D printing platform that can create precise 3D networks of carbohydrate filaments (1mm to 200μm diameter). After the cell laden aqueous ECM is poured over the carbohydrate networks, the carbohydrates dissolve and leave a hollow channel network through which the tissue can be perfused (Figure 24e, f). By doing this Miller et al ($\nu > 1$ cm^3, $\zeta > 1$ mm)[125] were able to form several square centimeters of vascularized solid tissue that supports positive pressure and pulsatile flow of human blood.

There have been several successes in the generation of thin or vessel-less tissues using the top-down approach. But overall, top-down approaches have lacked the fidelity to properly generate 3D constructs in a physiologically relevant size and shape.

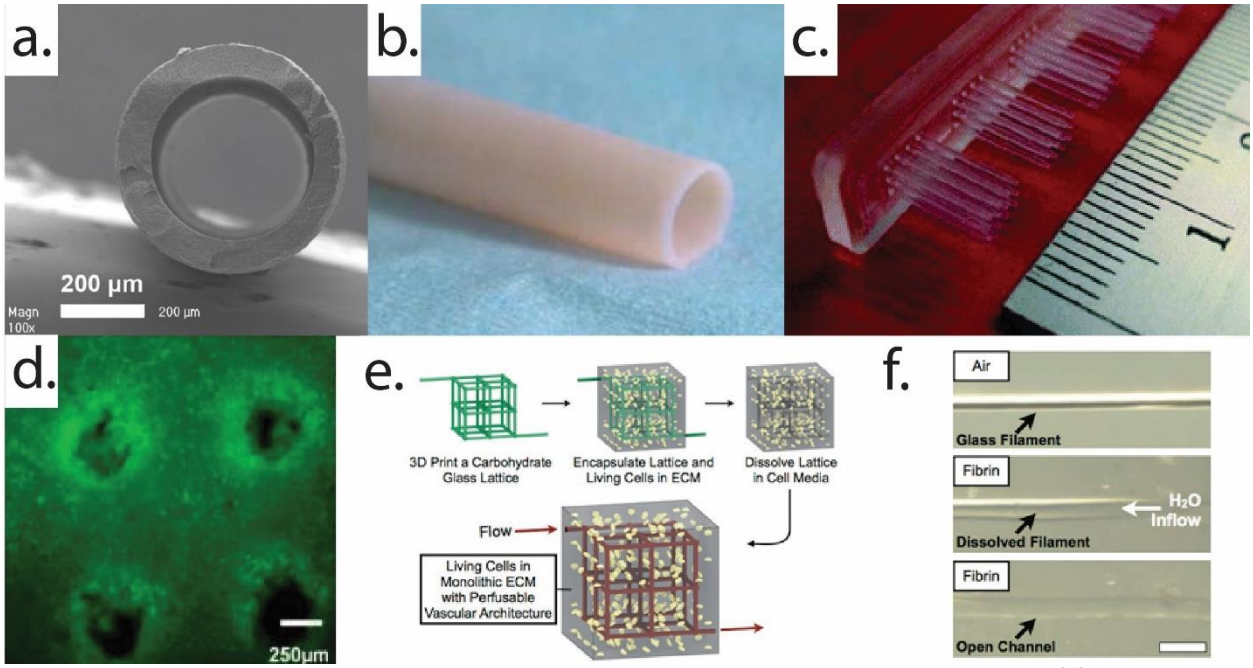

Figure 24: Top-down methods to create tissue constructs including: needle molding (a)[212], cell sheets (b)[213], PDMS molding (c)[214], laser ablation (d)[215], and carbohydrate networks (e, f)[125].

b. Bottom-up Techniques

The bottom-up approach to 3D cell culture relies on using small building blocks to create a larger tissue construct.[216] The principle of bottom-up 3D culture is to pattern an engineered tissue as close to native tissue as possible. This way, upon implantation, the implanted construct will be guided toward maturity.

The most basic of the bottom-up methods use photolithography to fabricate discreet polymer sheets that are aligned and bonded into a laminate with a common inlet and outlet forming a scaffold with 3D architecture. This methodology is the basis for most micro-molding techniques used in vascularization due to of the precise control over channel geometry it affords. After fabrication, the channel networks can be seeded with cells and can be given tissue specific functionality.

Such platforms can mimic the microvascular geometry of organs. Typically, these constructs use polydimethylsiloxane (PDMS) molded on a silicon master to create a single layer of the tissue construct ($\nu > 0.25$ cm^3, $\zeta > 0.1$ mm).[217,218] The layer is removed from the silicon mold and added layer-by-layer to the previous layers of PDMS (Figure 25a). Each additional layer must be aligned with the previous layers to ensure vascular continuity. PDMS is used extensively in soft-lithography and offers high accuracy replicas of the molded structures. However, it lacks the natural extracellular matrix (ECM) that provides support for cellular growth and cannot be used as a scaffold in tissue engineering.

To increase the versatility of the PDMS scaffolds, a technique was created using molded PDMS as a stamp for hydrogels. This technique creates a PDMS stamp from a silicon mold and selectively adheres hydrogels to the stamp ($\nu > 0.25$ cm^3, $\zeta > 0.25$ mm).[219] The stamp can then be used to stack layers of hydrogel where they can be bonded to create a complete structure (Figure 25b). While this addresses the lack of biological ECM of the PDMS constructs, it still requires a high degree of precision to successfully align and assemble they layers into a construct.

Another technique uses cell-laden hydrogel soft lithography where a PDMS master is used to stamp the gels in specific geometries. Hydrogels can also be programmed for use in photolithography. The cell laden hydrogel is thinly poured over a surface and a photo-pattern is exposed on to the surface. The exposed pattern crosslinks the hydrogel and the rest can be washed away ($\nu > 0.2$ cm^3, $\zeta > 0.2$ mm).[132] This can be repeated many times to create a whole tissue.

Selectively illuminating and photo-crosslinking hydrogels can increase the accuracy of the scaffold architecture. This technique uses a pool of photo-reactive hydrogel, proteins, and cells, to build a 3D structure. It has been used to create a honeycomb structure around an

engineered hepatic micro-tissue ($\nu > 0.2$ cm^3, $\zeta > 0.2$ mm, Figure 25c, d).[220] While they were able to create modular tissues similar to liver lobules, the polymerization penetrated the whole depth of the chamber restricting it to 2.5D rather than 3D structures. This limits the techniques to a single pattern and reduces the ability for it to be perfused and sustained over days.

The limitations of bottom-up techniques is their lack of scalability. While they can create intricate vascular networks in hydrogel, this can only be done with small volume construct. A key factor in designing a tissue construct fabrication technique is whether it can create a construct in a physiologically relevant size.

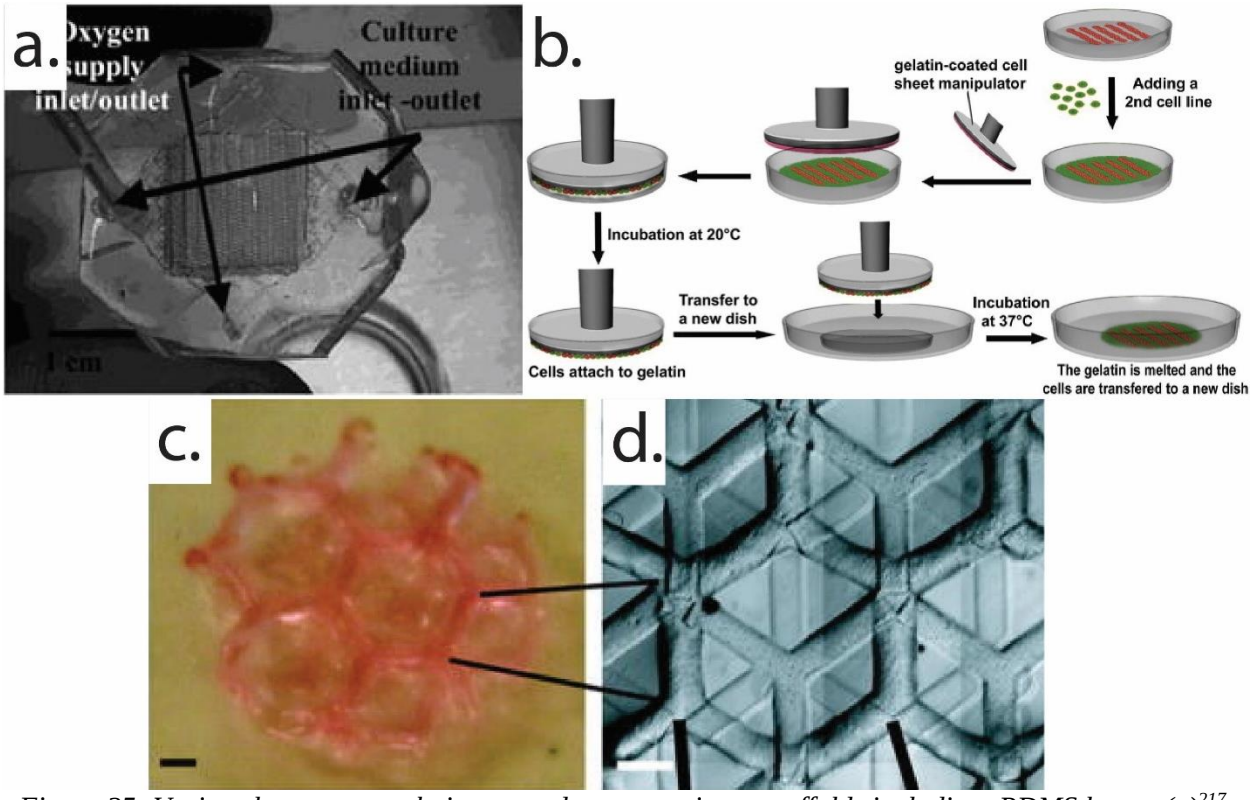

Figure 25: Various bottom-up techniques used to create tissue scaffolds including: PDMS layers (a)[217], hydrogel stamping (b)[219], and photo-crosslinking hydrogels (c, d)[216].

iii. Bottom-up Cell-laden Hydrogel Technologies

Tissues are a heterogeneous mix of cells embedded in an extracellular matrix with interspersed vasculature. Tissue develops based on specific spatial and temporal signals. Engineering live tissue requires multicellular geometries to replicate the form and function of the biological form. Typically engineered tissues are constructed by combining cultures of cells that were grown in two dimensions with an engineered scaffold.[221] These scaffolds are cultured in dishes, stirred vessels, or microfluidics devices.

A vascular network is critical in the success of any engineered tissue as it provides cells with nutrients and removes waste. But it has proven difficult to engineer a microcirculation that supports efficient perfusion of a construct.[222] The optimization of vascularization within an engineered tissue has focused on two main strategies: spontaneous angiogenesis from the host into the scaffold and the formation of capillaries before implantation. Spontaneous angiogenesis relies on the response from the host. It is due in part to the inflammatory wound healing response induced by the surgical procedure. In addition, the center of the scaffold is hypoxic and stimulates the endogenous release of angiogenic growth factors. The vessel growth from this process is generally too slow to provide adequate mass transfer to the cells within the scaffold. By forming the capillaries *in vitro*, the host vessels do not have to grow into the entire construct but only to the outer regions. As the vessels connect to the vascular network, the scaffold would be perfused with blood. With either spontaneous angiogenesis or pre-fabricated capillaries, the time it takes for vascularization can lead to cell death within the scaffold. Therefore, patterning scaffolds with microarchitectures can be used to sustain the embedded cells until implantation. It is not just the geometry of the target tissue that is replicated, but specific cell types as well. There are several ways that cells have been organized for implantation and culturing.

There are a multitude of approaches to fabricating tissue engineering scaffolds for perfusion. Methods include: molding soft lithography, photopatterning, 3D bioprinting, and sacrificial molding. Molding is a basic and commonly used technique to create microchannels within hydrogel constructs. Typically micro-needles or fibers are fixed in a chamber and then a hydrogel is poured in and gelled.[223] The channel is created by gently removing the needle of fibers. This technique has been used with collagen hydrogels to create channels from 100 to 500 μm in diameter with endothelial cells seeded on the channel walls.[224] They found that within the channels, the cells had self-organized and had similar function to human microvessels. This methodology can be adapted to almost all tissue scaffold hydrogels. However, these simple molding methods are confined to very simple channel architecture with straight and parallel microchannels.

Cell sheet technology uses cells grown on a polymer substrate that are induced to form excess ECM. The ECM that is formed around the cells helps them to form a cohesive cellular monolayer. The monolayer of cells can be detached from the polymer and form the building blocks for a tissue construct.[225] Each sheet of cells can be layered on to other sheets to form a whole tissue. Sheets of endothelial cells have been rolled up and used as blood vessels as part of a tissue construct in this method.[213,226] Also, researchers have used this method to assemble different cell types together using PDMS micro-patterning techniques (Figure 25a).[227] However, each layer of cells is very thin, and creating a whole tissue construct is not feasible without scaffold spacers. Furthermore, the process to create multiple sheets is complex, and the handling of the sheets must be done delicately.

Soft lithography uses templates with predefined patterns as molds to hydrogels. After patterning each layer, the layers are fused together to form a complete channel. This approach

has been used with collagen, gelatin, and agarose gels. After sealing the layers together, the inlet and outlet can be plumbed and the fluidic channels perfused. Endothelial, hepatic, and cardiac cells have been seeded in soft lithography created channels.[228-230] A soft lithography approach gives greater control in the channel geometry, but is limited to individual layers. The approach requires complex steps to make a single layer, which is not conducive to cell-laden hydrogels, and limits its applicability to tissue engineering.

Hydrodynamic focusing has also been used to create mono-disperse spheroids of gel with embedded cells. Two liquids phases are focused on to a central flow. At the proper flow rates, the two focusing flows induce the center flow to break off and create small droplets of gels.[231] This technique has been successfully demonstrated for use with fibroblasts and endothelial cells. In another flow regime, jetting of an alginate gel through a crosslinking solution. This jetting can create continuous solid or hollow cylinders of cell-laden hydrogel (Figure 26a).[232]

3D cellular printing uses a pneumatic device to build a scaffold using a cell-laden hydrogel.[67,233] With 3D cellular printing, scaffolds can be designed on the computer to include any geometry and multiple cell types can be used simultaneously to achieve complex tissues. This technology has been used in vascular and nerve grafts.[234] Similar to this process is inkjet-based cell printing which uses a commercial inkjet nozzle to spray biological materials on to a surface. Due to limitations in the printing nozzle, however, only low cellular concentrations can be used.

Laser-assisted bio-printing is based on laser-induced forward transfer of energy.[235,236] A layer of cells is placed on the underside of a glass slide that has laser-absorbing materials deposited on it. The cells are “printed” when the pulse laser reacts with the laser absorbing materials the cells are deposited on, creating a cavitation and propelling cells from that area to a

surface below (Figure 25b). By precisely positioning the slide above the surface and picking specific spots on the slide, the cell printing can be guided to create any tissue structure.[237-239] However, some of the laser absorbing material is transferred with the cells and speed of "printing" is limited by the availability of cells on the glass surface.[240]

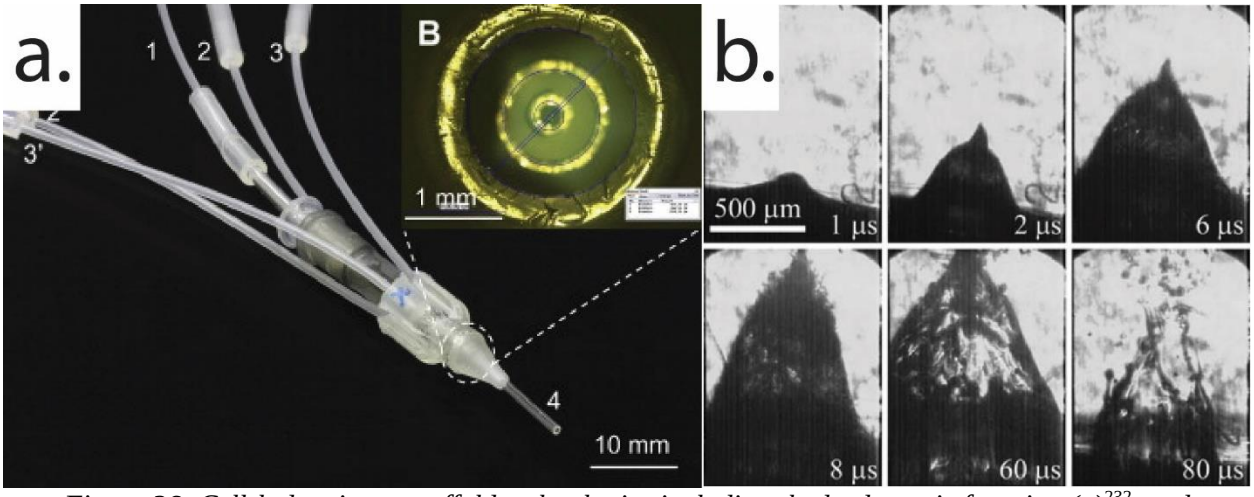

Figure 26: Cell-laden tissue scaffold technologies including: hydrodynamic focusing (a)[232], and electrospinning (b)[235].

3D bioprinting is similar to 3D printing of polymers, but uses cells and biomaterials to create a layer-by-layer additive fabrication of a tissue construct.[241] The 3D bioprinters can use phase-changing hydrogels, minimizing the use of cytotoxic chemicals. The printer uses either one or multiple nozzles to dispense different hydrogels at precise points on a surface. It builds one layer at a time to organize a 3D functional living macro-tissue and organ construct. Similar to sacrificial supports used in 3D printing, 3D bioprinting can use sacrificial hydrogels that can be preferentially removed as support. This methodology has been used to create a collagen gel with seeded HUVECs, as well as vascular tissue constructs using thiolated HA and GelMA.[132,242] This approach is limited by the resolution of the printer of 300 µm, as no finer features can be created, and the length of time it would take to generate a whole tissue construct.

There are many tissue engineering techniques that utilize cell-laden hydrogels, but they lack the scalability required to create a whole tissue. Instead they focus on creating organelles, or organs on a chip for small-scale applications. Larger volume constructs, then, must use a technique to bridge the gap in scale between the small features in a bottom-up and the large volume of a top-down method.

iv. Physiological Relevance of Fibroblasts and Endothelial Cells

While the target tissue will always dictate one major cell type that will be embedded in the scaffold, it is equally important to consider the supporting cells in a general tissue engineering technique. Supporting cells are used to try and mimic the natural tissue as closely as possible in the organization of the tissue. These cells can create vessels, put down ECM, and provide factors relevant to cell growth that are difficult to synthetically apply. Two of the most important cells that support and help a target tissue grow are endothelial and fibroblast cells.

Endothelial cells play a vital role in tissue engineering as they are the cells that form the vasculature *in vivo*. Vascular endothelial cells line the entire circulatory system. They act as a barrier, selectively filtering flow between the vessel lumen and the surrounding tissue. Endothelial cells are critical in the formation of new blood vessels and are therefore used in virtually all tissue engineering modalities to line pre-vascularized scaffolds.

Fibroblasts are heterogeneous and found in multiple tissues. Fibroblasts from different anatomic sites have unique gene expression, phenotypes, and produce different ECM and cytokines. Dermal fibroblasts have multiple functions not only in creating ECM but also proliferating and migrating in response to biological and chemical signals. Culturing fibroblasts in an air-liquid interfaces promotes differentiation resembling that of skin. Dermal fibroblasts

play a key role in ECM deposition, cell interaction, and wound healing. They are readily cultured in 2D and can easily be incorporated into engineered tissues.

B. Materials and Methods

We propose a top-down approach to create a hydrogel scaffold to support cells. The advantage of this method is that the density and spacing of channels in our large volume construct is higher than previous top down methods while simultaneously also allowing us similar architectural control as bottom-up methods.

i. Materials

Material	Specs	Source
Replicator 2	500 µm resolution	Makerbot, New York
3D Printing Filament	1.75 mm PLA	MatterHacker, California
Nylon fiber	"Invisible", 100 µm ø	Gutermann, Germany
Wire mesh	Stainless steel, woven wire cloth 70 x 70 mesh	McMaster, Illinois
Agarose	Type II-A, Medium EEO	Sigma, Missouri
PEEK tubing	Blue 1/32" OD x .010" ID	IDEX, Illinois
Fibroblast media	--	Sciencell, California
Endothelial cell media	--	Sciencell, California
PDMS	Sylagard 184	DowCorning, Michigan

Table 4: Materials used in Chapter 4.

ii. Fabrication of the Tissue Construct Template

The tissue construct is a cell-laden pre-vascularized hydrogel and relies on a cast of nylon fibers to create the microchannels. Our template uses nylon fibers (100 µm ø) oriented with a wire mesh (300 µm pitch) strung in a custom 3D printed mold.

We begin by 3D printing the custom model frame pieces using PLA or ABS plastics (MakerBot). The printed template consists of a frame attached to a support structure and a detachable frame. To each of the frames we attach a wire mesh to act as a guide for the nylon

fibers. We then temporarily attach the two frames, mesh-side in, together with the holes within the mesh aligned.

Within each pore of the mesh we place a pre-knotted pre-cut length of nylon fiber. The order of placing the fibers within the mesh is vitally important. The nylon fibers were placed row by row. After each row was threaded through the mesh it was glued into place as horizontally as possible. We repeated this process for however many fibers were required for a mold. For high density molds, with a fiber pitch of less than 300 µm, an appropriate mesh was used and we threaded approximately 200 x 200 fibers to create a cross-sectional area of 5 mm x 5 mm.

After all of the fibers have been threaded through the mesh in the frames, the frames with meshes are separated and pulled apart to create a section within the model of straight highly oriented fibers. The fibers need to be glued as horizontally as possible to maximize the area within the frames that can be used as tissue construct mold. Once the frames are as separated as possible, the free frame is glued into place and excess nylon fibers are trimmed. This assembly is the template for the hydrogel mold (Figure 27, Figure 28a).

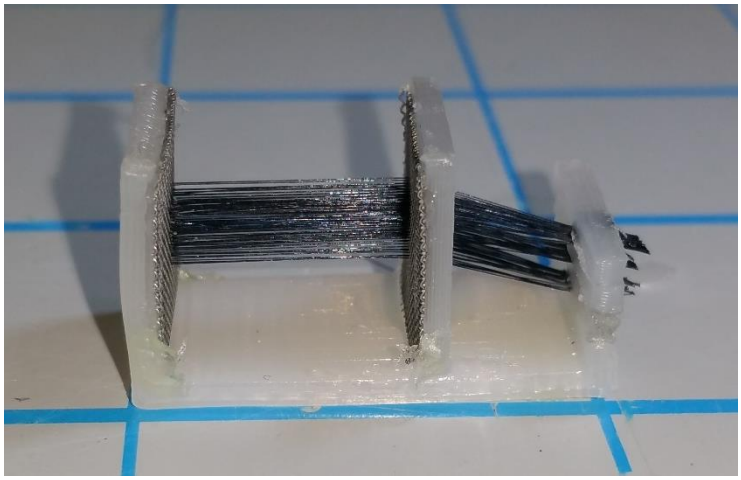

Figure 27: A fiber template made of 100 µm ø fibers strung between two meshes with 300 µm spacing.

iii. Perfusion Cap

The perfusion cap is a PDMS piece that sits on one end of the tissue construct to provide a pressure seal and facilitate profusion. We create the perfusion cap by molding PDMS around a custom 3D printed PLA mold of the cap negative. The mean feature of the cap is posts that allow for media pooling within the cap to maintain equal perfusion through all the channels. A hole is punched in the center of the cap for PEEK tubing to be inserted. The dimensions of the cap are exactly that of the tissue construct for proper sealing.

iv. Cell Culture

The tissue construct we propose relies on embedded cells from traditionally cultured sources. We propose the use of human umbilical vein endothelial cells and human dermal fibroblasts to validate our construct (both cell lines are from ScienCell). The cells will be used between passages P2 and P8 for the HUVECs and P2 to P10 for the human dermal fibroblasts (HDFs). We will maintain the cells in the appropriate media: 5% fetal bovine serum, 50 µg/mL endothelial cells or 50 µg/mL fibroblast growth supplement, 0.5U/mL penicillin, and 0.5 µg/mL streptomycin. They will be cultured in a 37˚C and 5% CO2 environment. The cells will be passaged at confluence through the use of trypsin digestion. We are using 4 flasks of cells, each with approximately 700,000 cells, for each experiment.

v. Assembling the Tissue Construct

To prepare the template for casting we have to prepare the agarose, and all of the perfusion equipment. The agarose is melted and sterilized in an autoclave in PBS (pH 7.4) and maintained in a liquid form in an 80ºC water bath. The peristaltic pump, PEEK tubing, and perfusion cap are washed in 70% ethanol to sterilize them.

To cast the template in cell-laden hydrogel, four flasks of cells will be dissociated, centrifuged, and re-suspended in 6 mL of media. Simultaneously, the agarose will be removed from the 80˚C bath and allowed to cool. As the gel reaches ~40ºC (after 2 minutes) the 6 mL of cell solution will be mixed with 6 mL of 3% agarose to make a 1.5% cell-laden agarose solution. We invert the tube several times to mix thoroughly and immediately pour the cell-laden hydrogel into the template mold (Figure 28b).

After pouring the gel, we immediately transfer the rapidly gelling construct to a sterile incubator at 37˚C. We wait approximately 20 minutes to ensure that the entire construct is gelled before removing it from the mold. We then use a sharp razor blade and cut the nylon threads from one side of the mesh. With one end freed, we can either use sharp forceps to remove the fibers individually, or slide the gel off of the fibers to do it all at once (Figure 28c). High density channels at this spacing may not affect the strength of the hydrogel significantly (~5%), but we must take care in ensuring they do not rip the hydrogel when being pulled from it.

Once the gel is freed from any stray fibers, we will cut it in half. Half of the tissue construct is used as an experimental control, while the other half is used as an experimental section. The experimental tissue construct is placed into the perfusion cap and glued into place (Figure 28d). Gluing the construct into the perfusion cap is an important step in ensuring there are no leaks and that the channels will be perfused. We wait 30 minutes for the glue to dry completely before inverting the tissue construct into a perfusion chamber (Figure 28e).

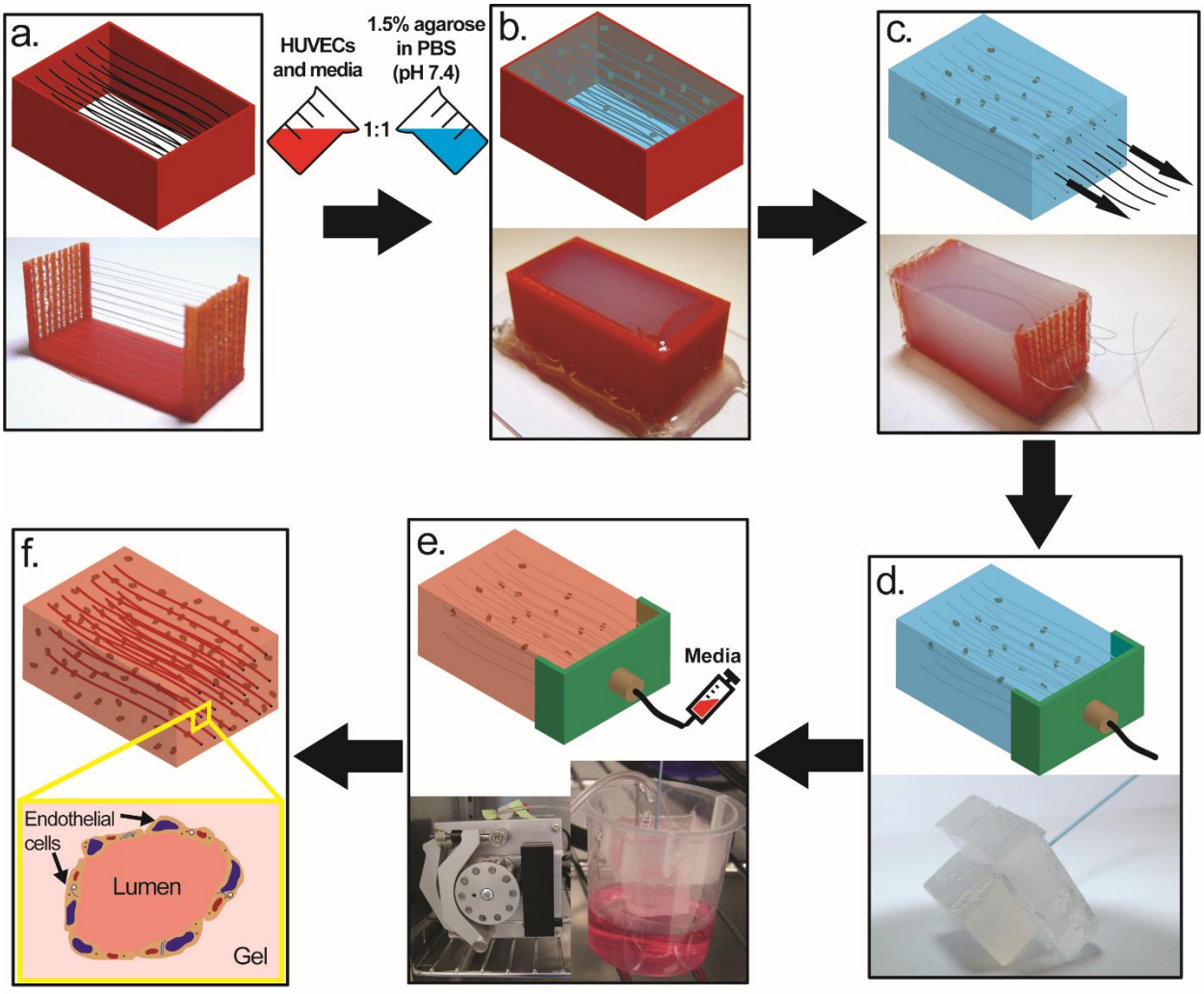

Figure 28: To create a hydrogel tissue construct we: thread a template (a), pour a cell-laden agarose mixture into a mold (b), remove the fibers from the cast gel (c), attach a perfusion cap (d), use a peristaltic pump to perfuse the gel construct (e), sustain the cells within the construct (f).

vi. Sustaining the Tissue Construct

We sustain our template casted tissue construct in a 37ºC incubator through pressure-based flow through the perfusion cap and into the microchannels within the hydrogel. After travelling through the hydrogel, the media drops out into a collection vessel for recirculation of the media through the device. The pressure of media into the construct is created using a peristaltic pump with its tubing is connected to the PEEK tubing in the perfusion cap. We

maintain a flow rate of 150 µL per minute through the construct. The control construct is immersed in media with now flow for the duration of the experiment.

vii. Staining Protocol

Immediately after the experiment ends we need to stain the cells to determine cellular viability. We will assess the cellular viability with 2 µM calcein and 4 µM ethidium in PBS solution. For the flow tissue construct, we first extract the tissue construct from the PDMS perfusion cap. Next we section the construct into thin (~ 500 µm) slices and place it on a cover slip. Approximately 500 µL of the staining solution will be added and incubated at 37ºC for 5 minutes. Afterwards, the stain will be washed off of the sample with PBS two times and imaged using FITC (live) and TexasRed (dead) fluorescence filters. The viability of a sample is quantified by dividing the living cells (stained alive) over the total number of cells (stained alive or dead) to find the percentage of cells alive and viable. A similar protocol is followed to stain the control hydrogel sample.

C. 3D Cell Culture Results

We determined the maximal spacing of the microchannels using our oxygen model from the previous chapter. We found that for a physiologically dense tissue, the maximal spacing of microchannels is ~ 150 µm. In a more approximate way, we can use natural biology to estimate the proper spacing of channels as there are capillaries within 150 µm of any cell within the body. By using a commercially available stainless steel filtering mesh, we can set up the microchannels in the template for the proper spacing. We measured the spacing and diameters of the microchannels from the fiber cast in a calibrated optical micrograph to have a spacing of 300 µm and a diameter of 100 µm (Figure 29).

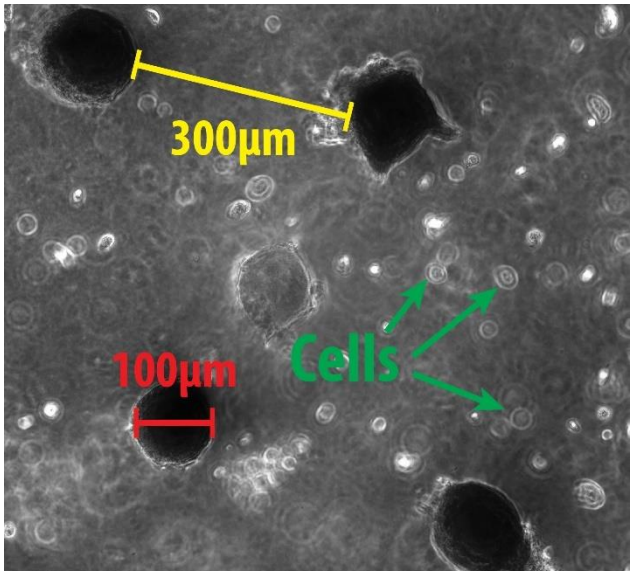

Figure 29: Optical micrograph of microchannels within a hydrogel scaffold. The channels are spaced 300 µm apart and the channels are 100 µm in diameter. Cells can be seen throughout the scaffold.

The flow rate through the system was calibrated with just tubing and in a blank (non-cell) scaffold to be 150 µL per minute. Throughout the experiment we saw no leakage around the perfusion cap leading to the conclusion that all of the flow through the pump is directed through the microchannels (Figure 30).

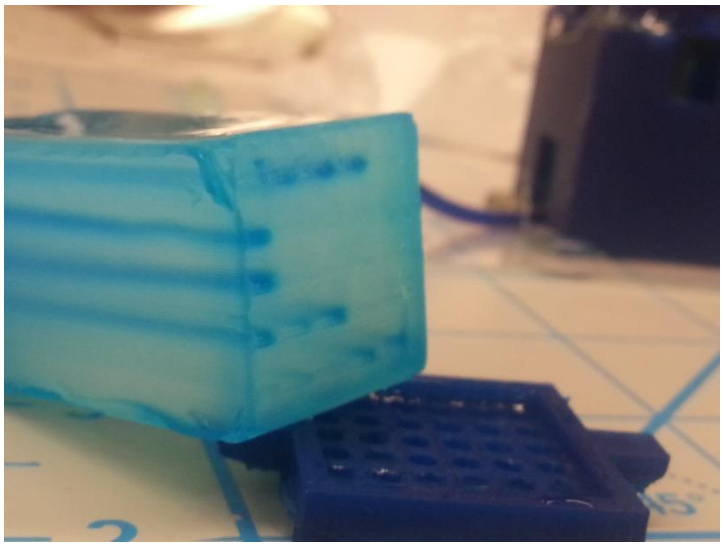

Figure 30: An agarose construct that has had blue dye perfused through the regularly spaced microchannels. Uneven perfusion is due to using a syringe to perfuse one channel at a time.

i. Endothelial Cells

The viability and cell numbers for a static construct of embedded HUVECs were quantified after 6, 24, and 48 hours. In this experiment, we used a microchannel spacing of 1.5 mm, 100 µm microchannel diameter, and a flow rate of 150 µL/min in the construct. Over 48 hours, we saw a decrease in cell viability and saw no proliferation of the cells (Graph 7).

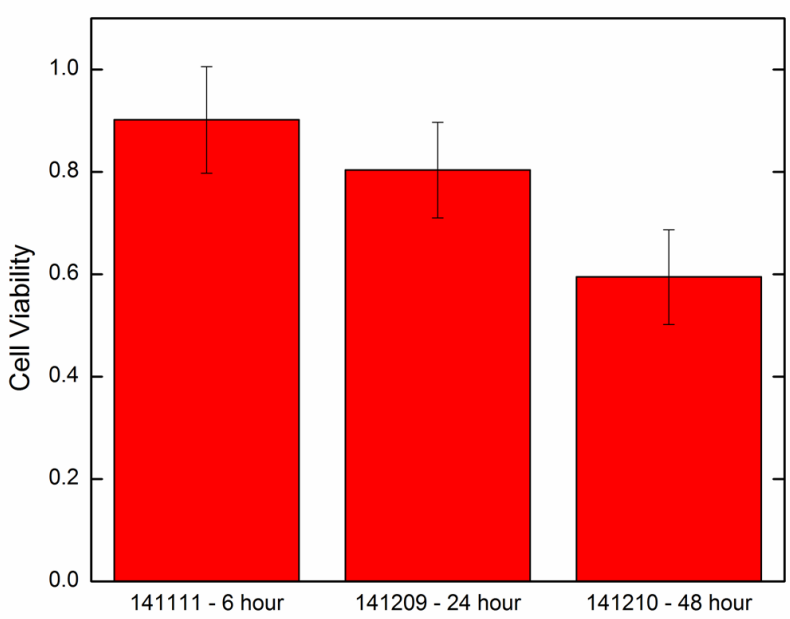

Graph 7: The viability of endothelial cells in a perfused tissue construct over 6, 24, and 48 hours.

We next quantified the cell viability and number between the edges of the construct and the middle of the construct. Qualitatively, cells toward the middle of the construct were less viable than those on the edge of the construct (Figure 31). We were able to quantify this result by comparing a section edge of the scaffold to middle sections. The diffusion through the edge of the piece was enough to create more viable cells over 6, 24, and 48 hours (Graph 8).

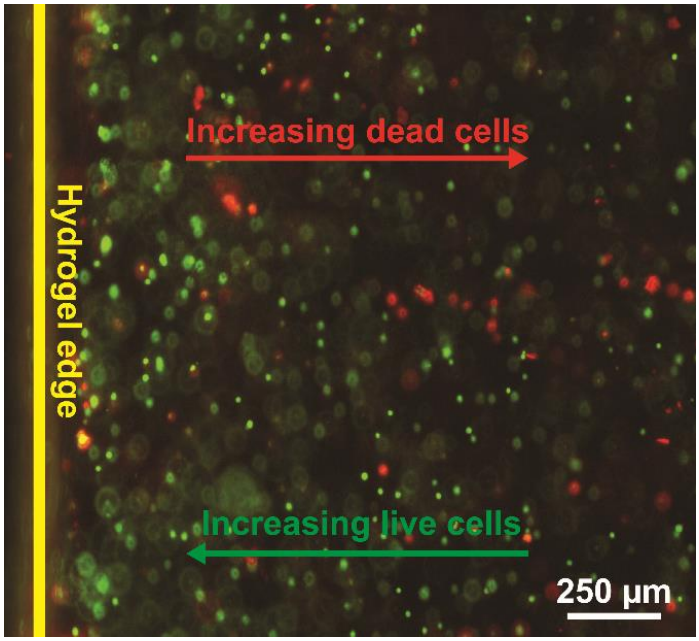

Figure 31: A combination of the live and dead micrographs from a static hydrogel construct. Nearer the hydrogel edge, shown in yellow, has a higher viability than the center of the construct. This is due to the diffusion limits of nutrients and waste limiting their transport to the core of the scaffold.

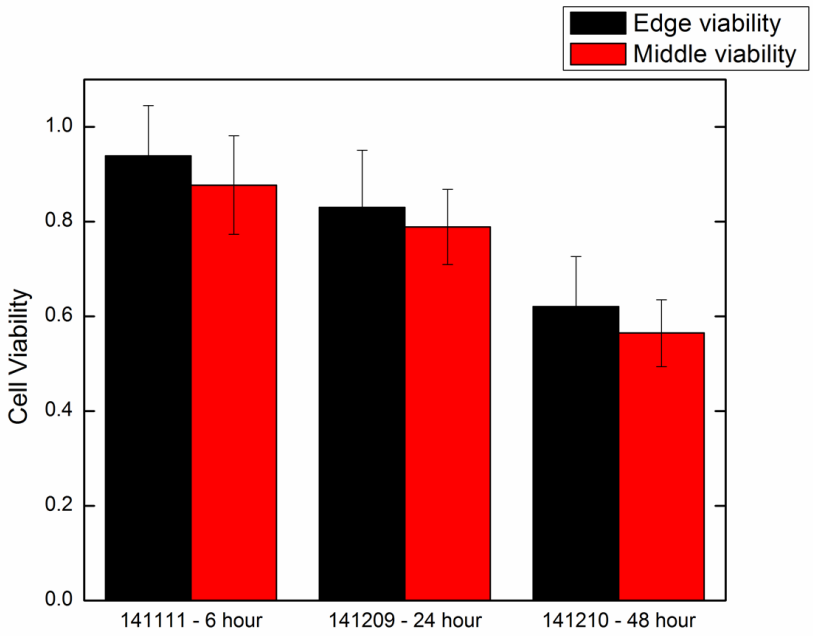

Graph 8: A comparison of the viability at the edge and middle of a tissue construct over 6, 24, and 48 hours.

Comparing the cellular viability of the flow tissue construct and the static tissue construct at 6 hours, there was no statistical difference in the two groups. This trend was repeated in the 24

hour experiments. At 48 hours, however, there was a statistically significant increase in the cell viability of the flow constructs compared to the static samples. We repeated this difference over three tissue construct samples (Graph 9).

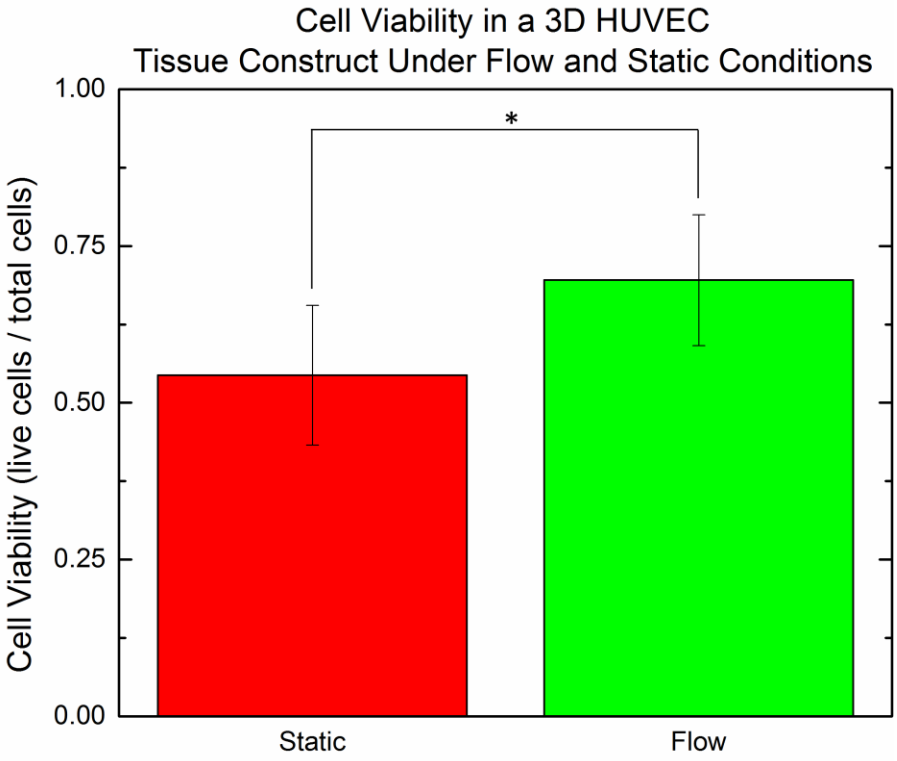

Graph 9: Comparison of the HUVEC tissue construct under static and flow conditions in three experiments. Each of the experiments showed statistically significant differences in viability between the static and the flow conditions (n = 3).

ii. Fibroblasts

To continue our understanding of this tissue construct we next tried to optimize the technique for use with HDFs. We began our experiments with the HDFs by replicating the experimental conditions of the HUVECs, a microchannel spacing of 1.5 mm, 100 µm microchannel diameter, and a flow rate of 150 µL/min.

However, even after 48 hours, we saw no difference between the static and flow constructs. We have seen some promising results with HDFs, where they showed statistically

significant differences between the static and flow samples (Graph 10). However, we have been unable to repeat this difference. Instead, after 8 days of culture we see virtually no differences in viability between the static and flow conditions within the tissue construct (Graph 11).

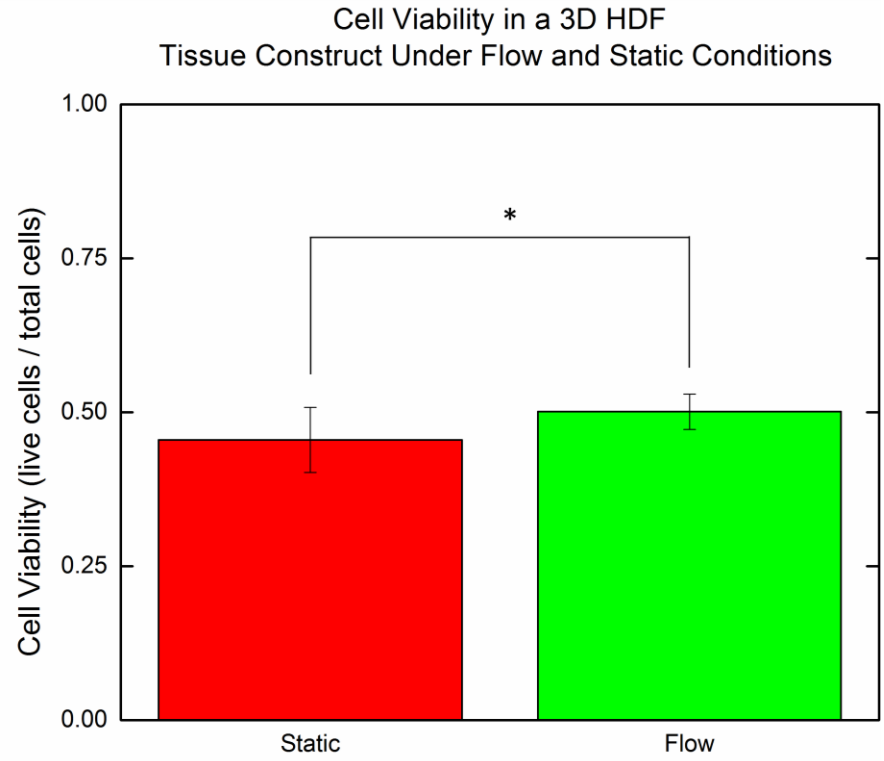

Graph 10: Statistically significant differences in viability of HDFs within the tissue construct under static and flow conditions (n = 1).

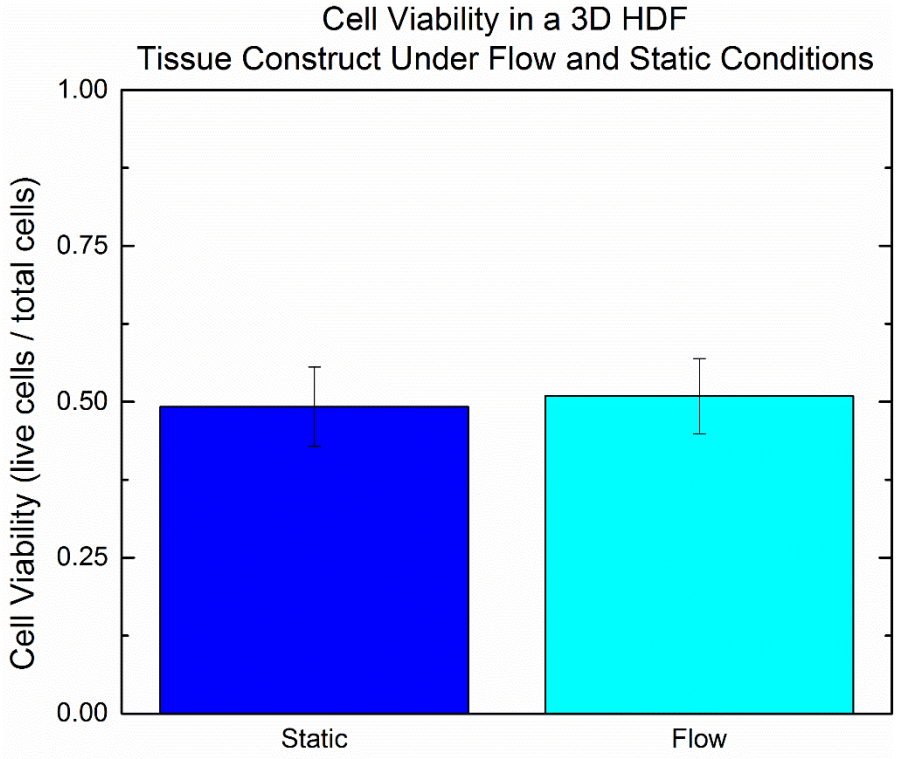

Graph 11: Comparison of the HDF tissue construct under static and flow conditions in three experiments. Each of the experiments show virtually no difference in viability between the two conditions (n = 3).

D. Discussion

In this proof-of-principle experiment we proved that our 3D tissue construct created an almost exact cast of the fiber, that it could sustain flow over the course of several days, and that the viability of the cells embedded in the construct was greater than that in the control construct.

i. Materials Justification

In our 3D tissue construct experiment, we used agarose as a scaffold for the cells. We used agarose because of its material properties, previous use as cell scaffolds, and advantageous polymerization pathway. Agarose can be a stiff hydrogel, even at the lower concentrations we used to make the scaffold; at a concentration of 1.5% agarose, the gel has a strength of 1500 g/cm^2.

Adjusting the percentage of gel can affect gel stiffness so it can be tuned to mimic target tissue stiffnesses. Agarose has also been used in blends with other hydrogel to increase cytocompatibility. For large tissue constructs, where the smallest dimension is larger than the penetration depth of UV, such as our construct, photo-polymerization cannot be used. Instead we relied on the reversible hydrogen bonding of agarose to create crosslinks in the gel.

In this construct we focused on culturing fibroblasts and HUVECs. These types of cells are ubiquitous in biology and form the backbone of tissue structures so it is important to ensure that they can grow in a construct before pursuing further studies. The cell lines we used in these experiments only maintain correct phenotypes for certain numbers of passages, we ensured that the cells are used within that range. Different experimental results can be attributed to older generations of cells, and we must ensure that we only use cells that are growing within normal parameters. Additionally, the gelling process of the agarose requires high temperature (> 40ºC), and the cells may not grow as well after being exposed to that high of temperature.

The PLA used to 3D print the mold that is used to cast the tissue construct was sterilized before use, but is notably biocompatible. The nylon fibers have diameters that mimic physiological capillary sizes and do not adhere to the agarose, allowing for easy removal. The stainless steel mesh is not compatible with cell culture for long periods of time, but the cells are only in the mold with the mesh for 30 minutes. The fibers are cut from the frame and the hydrogel removed from contacting the mesh, minimizing the effect of the mesh on cellular viability.

The PDMS used in the perfusion cap is sterilized before use and does not have any biocompatibility issues. The mold of the PLA print includes columns to create space between the cap and the surface of the tissue construct. This is to facilitate even perfusion through all of the

channels within the construct. A similar cap can be put on the exit of the microchannels in the construct, but was not used in these experiments. A peristaltic pump was used to allow for continuous perfusion of the construct over the course of several days. This allows less interaction with the construct during the experiment as media must be changed every 2 days. Syringe pumps could be used, but media must be exchanged or reloaded in to the syringe must more often at the flow rates we set.

When creating a 3D tissue construct it is difficult to monitor the inner workings of the construct during the experiment. Therefore, several end points are needed to measure the viability of the cells as there is no time lapse to monitor cells morphology.

ii. Template Casting as an Engineered Tissue Platform

The first step in building our construct template is to determine the diameter of the microchannels. The way we create the microchannels is to cast a hydrogel around them. Therefore, whatever the diameter of the fiber we embed will determine the size of the microchannel within the scaffold. We can use any monofilament fiber for this use as long as it does not adhere to hydrogels, is not acutely cytotoxic, and does not leave a residue within the microchannel. For our purposes, we focus on nylon monofilament suture. Nylon suture ensures that the fiber we get will not be cytotoxic, and comes in well-defined gauges. Larger diameter microchannels allow for more fluid flow, but increase the remodeling required for cells to form a lumen. Smaller diameter microchannels minimize the number of cells required to form a lumen, but increase the chance of an occlusion within the channel. The 50 and 100 μm suture suits our purpose.

A distinction between our method of creating a tissue construct and previous methods is our ability to create precisely arbitrarily oriented channels in a large volume construct all at once.

To this end, we measured our ability to create close-packed channels in a large volume (> 3 cm^3) construct. We were able to achieve a channel spacing of 300 μm and maintain the channel diameter of 100 μm throughout the construct. According to our model of nutrient transfer through the construct, this spacing is required throughout the construct to sustain cells and minimize zones of necrotic cells. Additionally, this spacing matches the physiological geometry seen in capillary beds. We use a flow rate of 150 μL per minute to replicate the flow rate in previous 3D culture experiments and be in a similar range to physiological flow rates.

iii. Visualizing Mass Transfer with HUVECs

To understand how a large volume tissue construct like ours limits the diffusion of nutrients into the core, we stained and quantified the viability of cells in different areas of the construct. This can be most easily seen near the edge of the hydrogel (Figure 31). Qualitatively, we can see the trend of increasing live cells nearing the edge of the hydrogel where mass transfer can most readily occur. The trend continues where cells nearing the center of the hydrogel show increasing numbers of dead cells. The population of cells in this gel does not approach the physiological levels in tissues, so the Krogh length into hydrogel is extended. There is no sharp cutoff where cells die, but a trend of less nutrients and decrease cell viability further into the hydrogel, consistent with a dying cell population within the tissue construct

We quantified the viability of cells in the center (minimal mass transfer) and on the edge (maximal mass transfer) of a non-flow sample. Over time we see decreasing viability of the cells, but also a clear difference between the viability of the cells near the edge with the ability to exchange nutrients and those cells in the center with limited ability to do so. As time goes on we see the difference in these two populations increasing. Because HUVEC populations double every 48 hours, we would not expect to see a large difference in cell number between these

populations for at least a few days. At these short time points, there may not be enough time for the cells within the static construct to die.

Next we wanted to understand the difference between the static, no flow with channels, tissue construct and the experimental, flow with channels, construct. To understand how many cells that went into a tissue scaffold, we counted 75 µL of re-suspended cell solution (ORFLO, Moxi). We had to dilute the re-suspended cell solution 4-fold to ensure that the counter would get an accurate count. The solution of cells we put into the tissue construct had 2×10^6 cells/mL and was diluted by two when mixed with the agarose. We use 4 flasks of cells, so there are approximately 5×10^5 cells per flask of cells.

We used larger spacing between the channels throughout our large (> 3 cm^3) construct than the decay length indicates we need. Even still, the HUVECs showed statistical differences between flow and static constructs even with large microchannel spacing. To provide 80% statistical power to this test given an expected viability of 60% for an un-perfused construct after 48 hours, we need a sample size of 3 at 75% viability with ~10% standard deviation. We were able to show this statistical difference in three experiments.

Part of the reason we saw this difference in the populations even with the channels being sparse, is due to the lower starting cell population within the 3D tissue construct. One of the factors limiting mass transfer is the consumption of the nutrients by the cells, and if there are less cells to consume the nutrients then the mass transfer can occur over longer lengths. We expect that decreasing the channel spacing to physiological spacing (~300 µm apart) would further increase the viability of the HUVECs under flow.

iv. Fibroblast Proliferation

We furthered our experiments on a large 3D tissue construct by continuing with a different cell line, fibroblasts. Fibroblasts are heartier than HUVECs, but have a similar population doubling time. We made this change because while HUVECs did show statistical differences in the viability of flow versus static populations, the viability and population of the cells was generally low. To combat this, we decreased the fiber spacing from 1.5 mm used in the HUVEC experiments to 300 μm and switched cell types.

The flow rate for these experiments was kept the same as before, 150 μL per minute. The exact number of cells used in a given experiment fluctuated, but was on average 1×10^6 cells per mL. This was similar to the number of cells used in other 3D cell culture experiments and was deemed an appropriate number of cells. The concentration of cells can be tweaked by changing the construct volume. Under these conditions, we saw a difference in the static and flow populations in initial experiments. However, upon replication of these experiments we saw no differences in population and similar viability to that of the HUVEC experimental groups even with increase experimental length.

Even though we expected the HDFs to be able to survive more adverse conditions than the HUVECs, it has been more difficult to show difference between the two groups. Our hypothesis for the difference in the viability of these two cell types is the difference in migration patterns of each. Endothelial cells tend to migrate slower and over shorter distances than fibroblasts.[243] Agarose lacks abundant adhesions sites for cells and therefore fibroblasts are more negatively affected by their confinement within the gel space. Increasing the experiment length has been considered, but there is too big of a risk of contamination at those time scales. Instead, we are attempting to sustain the flow construct by increasing the density of microchannels within

the scaffold. Stringing each of the high density fiber arrays takes significantly longer because of the complexity involved.

The lack of difference between the two samples was attributed to the heartiness of the fibroblasts. By increasing the length of the experiment, we hoped to let the cells within the static sample die while sustaining the flow construct. We increased the experimental time to 8 days, or 192 hours. Unfortunately, by increasing the time of the experiment, possibility of contamination also increased.

v. Lessons Learned

We did optimize the experiments along the way. We started by having the flow construct suspended above a surface of media, and switched to having it immersed in media to more closely resemble the control perfusion chamber and limit evaporation and contamination on the sides of the construct. We also increased the number of seeded cells. We began experiments only using one flask of cells, and quickly moved towards using more flasks of cells because cellular communication is important in maintaining cell viability.

The ability to resolve channels, even at small spacing remains elusive. In certain experiments, some of the channels have been easily observable, and we could quantify the spacing and diameter of the fibers. In other experiments the microchannels could not be found at all under bright field microscope illumination. As we move to smaller channel spacing, localizing each microchannel becomes less important because the whole area should be perfused, but it is still a factor when assessing the distribution of the channels within the construct.

Placing enough nylon fibers to fill a sufficient cross-sectional area with 300 μm spaced microchannels is a daunting task. There are several steps involved in the threading process. First, the thread must be cut to an appropriate length, here we cut them to 2 inches in length. Next each

fiber must be knotted with a square knot on one end. The knot must be big enough to resist going through the pore in the mesh. Finally, using a stereomicroscope, a pair a precise forceps, and a steady hand, each fiber must be threaded through the same aligned hole in the two meshes. Care must be taken during this process to not miss a hole and leave a portion of the construct un-perfused. This mold is not reusable, so each additional experiment requires re-stringing and creating this template.

We tried to make the construct as large as feasible given time constraints in threading the mesh. While theoretically we could thread a mesh as large as we care to, time and sanity must be checked to determine the construct size. In the end we chose a construct with dimensions of 1.5 cm x 1.5 cm x 3 cm to create our template cast. This is sufficiently larger than previous attempts at tissue constructs and demonstrates our ability to create highly ordered, tightly spaced, microchannels in such a construct.

Determining the timing to create a cell-laden agarose relied on a guess and check method. While the temperature that the gel polymerizes at is well-defined, there are temperature gradients introduced when transferring the gel to different vessels, especially those with large surface areas. Therefore, when using the gel all equipment must be pre-heated to prevent premature gelling of the agarose. To offset this requirement, higher gel temperatures could be used at the cost of cell viability. In the end, we found that by timing the time the gel had to cool before mixing with the gel produced the best results.

This type of proof of principle experiment meant that some of the materials we used could not be reliably sterilized before use. As to minimize the contamination of an incubator with cell lines we used a separate incubator where sterility was not as big of a concern. This meant that there were instances of contamination during the experiment, specifically in the cell media.

We found that regular exchanges of media and sterilizing as many aspects of the construct mold and perfusion apparatus as possible before use minimized the chance of contamination.

With such a large tissue construct, it is difficult to visualize any of the cells inside. This is due to both small working distances and the opaqueness of the gel used. Rather than try to visualize the tissue construct as a whole, we printed a cutting guide to section the tissue construct in as thin of slices as possible for visualization. A microtome could not be used because the gel was too soft to be cut evenly, and the gel itself could not be fixed or frozen without damaging either the gel structure or the cell viability. We found a compromise by sectioning by hand, which led to slight thickness variations.

vi. Limitations

Our results show that there is higher viability of cells in flow rather than static, but we do not see an increase in cell number as we would expect if the cells were proliferating. This could be due to a lack of nutrients in the case of the HUVEC experiments, and the experiments can be repeated with the higher density tissue constructs. As for the HDFs, the procedure to proliferate the cells may not be optimized and different flow rates, gas conditions, and percentage hydrogels can be attempted.

The hydrogel we used in this study is not the most amenable to cell adhesion. Preferable hydrogels include collagen, gelatin, PEG, and mixtures of these hydrogels. In this instance, they were not used because they lack the ability to be polymerized in a large volume. Further experiments can use a photo-crosslinkable hydrogel and polymerize one layer at a time to polymerize the whole construct, but they run the risk of damaging the cells from UV exposure.

E. Conclusion

Our novel template casting technique can create high aspect ratio and high density microchannels within hydrogels for use as a tissue construct. We have shown that HUVECs can be sustained using this agarose tissue construct.

We have shown that even with 1.5% agarose, the sacrificial template casting technique still produces high fidelity molds of the nylon fibers in the template. None of the materials we use are acutely cytotoxic and the template method is a quick and cost effective method to creating top-down tissue constructs with high density of pre-vascularization. We have successfully created a regular array of microchannels within agarose that agree with physiologic microvasculature spacing.

We have proven that the tissue construct has sustained the HUVECs more effectively than diffusion. Embedding endothelial cells is a vital step in any tissue engineering project, as they are vital to the creation of any vessels. The next step is to prove the tissue construct can sustain HDFs. HDFs are easier to culture, which makes it more difficult to see difference between samples. We hope that by using even higher density microchannels we can induce the fibroblasts to proliferate within the construct.

Overall, our template casting technique for tissue constructs in agarose can be used to sustain cells *in vitro* moving towards growing a whole organ.

5. Conclusions

We have created a technique to create arbitrarily complex microchannels in polymers for dMRI and tissue engineering applications. This technique of removing molded fibers to create microchannels is flexible, low cost, and scalable. We have used our technique to create a platform that fills the scale gap in current techniques between top-down and bottom-up applications. This type of platform can be used to better understand tissue biology, angiogenesis, and disease pathology. We have demonstrated its use in both dMRI applications and tissue culturing techniques.

We have shown that this technique can be used in the fabrication of a phantom for MR imaging studies with channels that are 20 μm at a volume fraction of 50%, similar to physiologically relevant numbers. This phantom is both more complex in the fiber crossing and a more accurate model of the white matter.

Here we have expanded our template casting technique from use in PDMS, a commonly used casting polymer, to use with a hydrogel. Most notably, we can create microchannels on size order of capillaries and place them in arbitrary geometries with high fidelity in the tissue construct.

Using this 2D model of a tissue as a research platform has several advantages over creating a 3D tissue. First, it allows for easier study as the preparations are less complex and there are not as many variables when designing studies. Second, the thin nature of the construct allows us to have continuous viewing of the cells within and observe and morphology or phenotypic changes that are happening. By flowing a cell stain within the media, this platform

could conceivably take time lapse fluorescent images to increased contrast and looking at more specific markers.

Our novel template casting technique can create high aspect ratio and high density microchannels within hydrogels for use as a tissue construct. We have proven that HUVECs can be sustained using this agarose tissue construct. Overall, our template casting technique for tissue constructs in agarose can be used to sustain cells *in vitro* moving towards growing a whole organ.

With our platform we can create the detailed features that are evident in biological structures over similar scales to their biological counterparts. We can create something beyond simple linear channels and create biologically relevant complex 3D systems.

A. Future Work

There are several ways this work can be expanded into other fields of study.

We envision that more complex geometries can be created using the PDMS dMRI phantom. With enough tenacity, smaller bundles of fibers could be placed at a time, making the arrangement of the fibers in the mold more specific to certain physiological areas. Additionally, a more precise mold would allow multiple phantoms to have the same ground truth, something not possible with the current molding process. But one of the biggest issues with our current phantom model, the large microchannel size, can potentially be addressed. We have begun experimentation into using carbon fibers, with diameters of 4 μm, in the mold. Not only as these fibers straight, as they do not come braided, but they are not affected by the solvent that is used to swell the PDMS. The limitation with using such fibers, however, is that while they have high tensile strength, they do not have any shear strength. Therefore, any twisting or off-center forces

on the fiber can cause them to break, and become permanently embedded in the PDMS phantom. Research into other viable fibers or into using carbon fibers successfully would allow this phantom to become one of the physiologically accurate methods of creating a stable dMRI phantom.

Other ways of minimizing the microchannel size also include moving away from PDMS as a substrate for the phantom. Biaxially oriented polystyrene sheets have been used previously in microfluidics as a way to create micro channels with macro techniques. A similar method could be employed when casting fibers. In this case, larger fibers could be cast in a polystyrene substrate and selectively etched away after the polystyrene has set. The phantom as a whole and the microchannels within could then be shrunk up to 50% by placing it in a 163ºC oven.

Our 2D tissue culture has applications beyond research into tissue growth. Recently research on tumor cell phenotypes has shown that mutagenic events alter multiple signaling pathways and are more numerous and heterogeneous than previously though. What is clear is that there many pathways that converge to adapt tumor cell metabolism to support their prolific growth and survival. Such a phenomenon was characterized in the 1920s by Otto Warburg. He noted that tumor cells consume glucose at a higher rate than normal cells, but secrete lactate, an incompletely oxidized form of glucose. The “Warburg Effect” then is the paradox of why cells that have great need for ATP have such a wasteful metabolism. By co-culturing cancerous and non-cancerous cell types in our 2D tissue culture device we can create a competition of nutrients between the cell populations when exposed to glucose rich vs. ketone rich media. By feeding ketones rather than glucose, we possibly favor non-cancerous cells over the glucose hungry cancer cells. The ability to quantitatively study this competition could open new ways of fighting cancer using dietary approaches.

Improvements in the microfabrication methods of the device may alleviate some of these constraints and can eliminate the need for alignment during assembly (Figure 32). Rather than sealing the ends of the slit after polymerizing the gel, a sealed container could be used to minimize leaks. Following such microfabrication techniques could lead to smaller slits (< 500 μm) which would increase the decay length of diffuse molecules within the model.

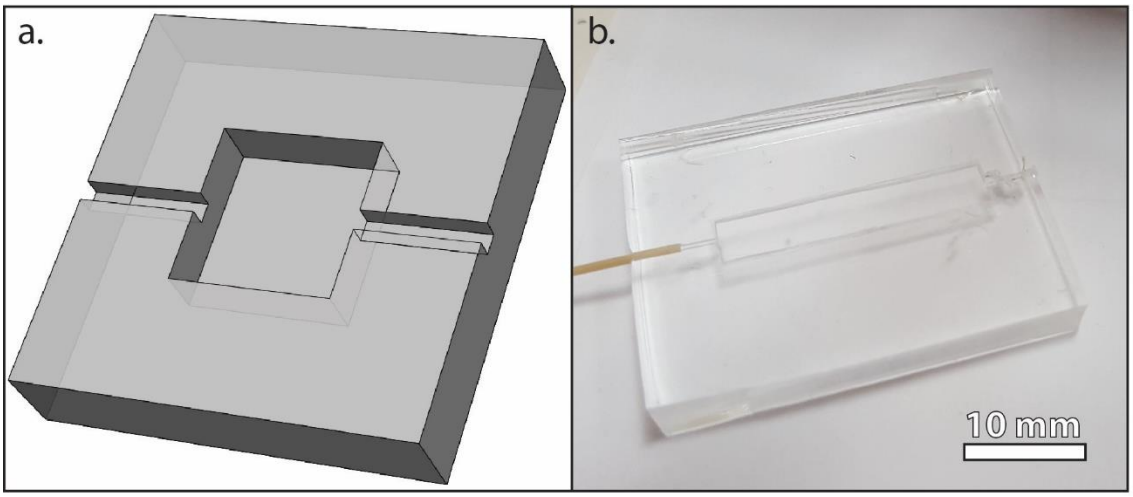

Figure 32: Schematic for the microfabrication of inlet and outlet for a tissue construct (a) and a prototype device with inlet tubing (b).

There has been work in the past on coating fibers with hydrogel. Selectively coating the fibers with a cell-laden hydrogel and filling the rest of the mold with normal agarose would dramatically increase the local concentration of cells around the microchannel after casting. By increasing this initial seeding density of cells, it may increase the speed of angiogenesis within the scaffold. Instead of filling the rest of the mold with cell-free agarose, a different cell type could be used to create a more representative tissue construct co-culture.

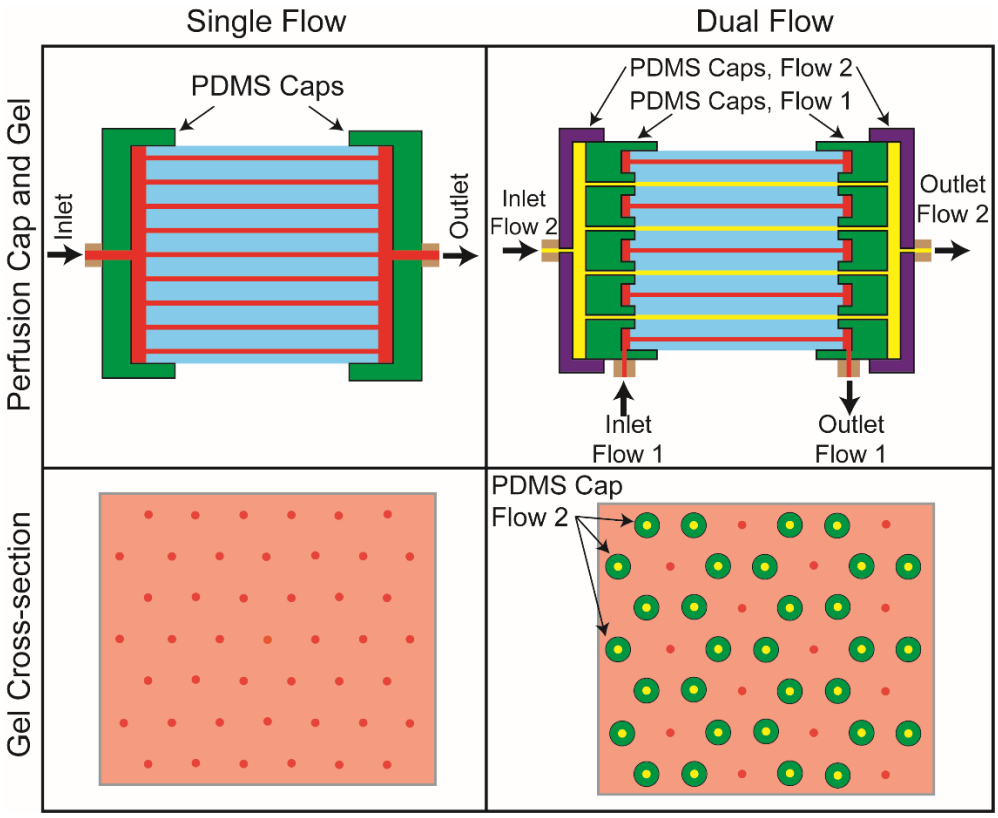

Figure 33: Envisioned two flow design for either end of the scaffold. The two flows (red and yellow) are flowed counter to one another through perfusion caps with nozzles. The nozzles form a tight seal on the agarose and allow individual microchannels to be perfused.

Rather than using identical strings in a square packing, different meshes could be used to have different diameter fibers in different orientations. This could lead to a more physiologically relevant sample. Even further, there are some interactions between the fibers that can be molded into the agarose. Creating different geometries within the scaffold opens up the possibilities for targeted growth. Livers have a hexagonal sub-structure that can easily be mimicked with properly oriented fibers. In addition to the hexagonal packing, livers have an interesting flow and counter flow within them. By creating two custom perfusion caps for either end of the scaffold, we can mimic these two flows to come even closer to the biological tissue (Figure 33).

6. Works Cited

1 Debanne, D., Campanac, E., Bialowas, A., Carlier, E. & Alcaraz, G. Axon Physiology. *Physiological Reviews* **91**, 555-602, doi:10.1152/physrev.00048.2009 (2011).

2 Basser, P. J., Mattiello, J. & LeBihan, D. MR diffusion tensor spectroscopy and imaging. *Biophys J* **66**, 259-267, doi:10.1016/s0006-3495(94)80775-1 (1994).

3 Basser, P. J. Inferring microstructural features and the physiological state of tissues from diffusion-weighted images. *NMR in Biomedicine* **8**, 333-344, doi:10.1002/nbm.1940080707 (1995).

4 Basser, P. J. & Jones, D. K. Diffusion-tensor MRI: theory, experimental design and data analysis - a technical review. *NMR Biomed* **15**, 456-467, doi:10.1002/nbm.783 (2002).

5 Basser, P. J. & Pierpaoli, C. Microstructural and physiological features of tissues elucidated by quantitative-diffusion-tensor MRI. *Journal of magnetic resonance. Series B* **111**, 209-219 (1996).

6 Giovannoni, G. *Education. Whats an MRI*, <http://multiple-sclerosis-research.blogspot.com/2015/01/education-whats-mri.html> (2015).

7 Moseley, M. E. *et al.* Diffusion-weighted MR imaging of anisotropic water diffusion in cat central nervous system. *Radiology* **176**, 439-445, doi:10.1148/radiology.176.2.2367658 (1990).

8 Moseley, M. E., Kucharczyk, J., Asgari, H. S. & Norman, D. Anisotropy in diffusion-weighted MRI. *Magnetic resonance in medicine* **19**, 321-326 (1991).

9 Sakuma, H. *et al.* Adult and neonatal human brain: diffusional anisotropy and myelination with diffusion-weighted MR imaging. *Radiology* **180**, 229-233, doi:10.1148/radiology.180.1.2052700 (1991).

10 Pierpaoli, C. & Basser, P. J. Toward a quantitative assessment of diffusion anisotropy. *Magnetic resonance in medicine* **36**, 893-906 (1996).

11 Pierpaoli, C., Jezzard, P., Basser, P. J., Barnett, A. & Di Chiro, G. Diffusion tensor MR imaging of the human brain. *Radiology* **201**, 637-648, doi:10.1148/radiology.201.3.8939209 (1996).

12 Nusbaum, A. O. Diffusion Tensor MR Imaging of Gray Matter in Different Multiple Sclerosis Phenotypes. *American Journal of Neuroradiology* **23**, 899-900 (2002).

13 Basser, P. J., Pajevic, S., Pierpaoli, C., Duda, J. & Aldroubi, A. In vivo fiber tractography using DT-MRI data. *Magnetic resonance in medicine* **44**, 625-632 (2000).

14 Conturo, T. E. *et al.* Tracking neuronal fiber pathways in the living human brain. *Proceedings of the National Academy of Sciences of the United States of America* **96**, 10422-10427 (1999).

15 Mori, S., Crain, B. J., Chacko, V. P. & van Zijl, P. C. Three-dimensional tracking of axonal projections in the brain by magnetic resonance imaging. *Annals of neurology* **45**, 265-269 (1999).

16 Catani, M., Howard, R. J., Pajevic, S. & Jones, D. K. Virtual in vivo interactive dissection of white matter fasciculi in the human brain. *NeuroImage* **17**, 77-94 (2002).

17 Hook, U. & Svalander, C. T. Agarose method for the preparation of isolated glomeruli from human renal biopsies. *APMIS* **99**, 844-848 (1991).

18 Caeyenberghs, K. *et al.* Brain-Behavior Relationships in Young Traumatic Brain Injury Patients: DTI Metrics are Highly Correlated with Postural Control. *Human Brain Mapping* **31**, 992-1002, doi:10.1002/hbm.20911 (2010).

19 Hulkower, M. B., Poliak, D. B., Rosenbaum, S. B., Zimmerman, M. E. & Lipton, M. L. A Decade of DTI in Traumatic Brain Injury: 10 Years and 100 Articles Later. *American Journal of Neuroradiology* **34**, 2064-2074, doi:10.3174/ajnr.A3395 (2013).

20 Wozniak, J. R. *et al.* Neurocognitive and neuroimaging correlates of pediatric traumatic brain injury: A diffusion tensor imaging (DTI) study. *Archives of Clinical Neuropsychology* **22**, 555-568, doi:10.1016/j.acn.2007.03.004 (2007).

21 Witwer, B. P. *et al.* Diffusion-tensor imaging of white matter tracts in patients with cerebral neoplasm. *Journal of neurosurgery* **97**, 568-575, doi:10.3171/jns.2002.97.3.0568 (2002).
22 Assaf, Y., Pianka, P., Rotshtein, P., Sigal, M. & Hendler, T. Deviation of Fiber Tracts in the Vicinity of Brain Lesions: Evaluation by Diffusion Tensor Imaging. *Israel Journal of Chemistry* **43**, 155-163, doi:10.1560/38QP-L6AV-V6KD-9V40 (2003).
23 Clark, C. A., Barrick, T. R., Murphy, M. M. & Bell, B. A. White matter fiber tracking in patients with space-occupying lesions of the brain: a new technique for neurosurgical planning? *NeuroImage* **20**, 1601-1608 (2003).
24 Sinha, S., Bastin, M. E., Whittle, I. R. & Wardlaw, J. M. Diffusion tensor MR imaging of high-grade cerebral gliomas. *AJNR. American journal of neuroradiology* **23**, 520-527 (2002).
25 Lee, J.-S., Im, I.-C., Kang, S.-M., Goo, E.-H. & Kwak, B.-J. Quantitative analysis of diffusion tensor imaging (DTI) using statistical parametric mapping (SPM) for brain disorders. *Journal of the Korean Physical Society* **63**, 83-88, doi:10.3938/jkps.63.83 (2013).
26 Maeda, T., Ishizaki, K.-i. & Yura, S. Can diffusion tensor imaging predict the functional outcome of supra-tentorialstroke? *Brain and Nerve (Tokyo)* **57**, 27-32 (2005).
27 Polan, R. M., Poretti, A., Huisman, T. A. G. M. & Bosemani, T. Susceptibility-Weighted Imaging in Pediatric Arterial Ischemic Stroke: A Valuable Alternative for the Noninvasive Evaluation of Altered Cerebral Hemodynamics. *American Journal of Neuroradiology* **36**, 783-788, doi:10.3174/ajnr.A4187 (2015).
28 Song, J. *et al.* DTI measures track and predict motor function outcomes in stroke rehabilitation utilizing BCI technology. *Frontiers in Human Neuroscience* **9**, doi:10.3339/fnhum.2015.00195 (2015).
29 Assaf, Y. & Cohen, Y. Assignment of the water slow-diffusing component in the central nervous system using q-space diffusion MRS: implications for fiber tract imaging. *Magnetic resonance in medicine* **43**, 191-199 (2000).
30 Assaf, Y. & Basser, P. J. Composite hindered and restricted model of diffusion (CHARMED) MR imaging of the human brain. *NeuroImage* **27**, 48-58, doi:10.1016/j.neuroimage.2005.03.042 (2005).
31 Beaulieu, C. The basis of anisotropic water diffusion in the nervous system - a technical review. *NMR Biomed* **15**, 435-455, doi:10.1002/nbm.782 (2002).
32 Jensen, J. H., Helpern, J. A., Ramani, A., Lu, H. & Kaczynski, K. Diffusional kurtosis imaging: the quantification of non-gaussian water diffusion by means of magnetic resonance imaging. *Magnetic resonance in medicine* **53**, 1432-1440, doi:10.1002/mrm.20508 (2005).
33 Jansons, K. M. & Alexander, D. C. Persistent Angular Structure: new insights from diffusion MRI data. Dummy version. *Information processing in medical imaging : proceedings of the ... conference* **18**, 672-683 (2003).
34 Tuch, D. S. *et al.* High angular resolution diffusion imaging reveals intravoxel white matter fiber heterogeneity. *Magn Reson Med* **48**, 577-582, doi:10.1002/mrm.10268 (2002).
35 Papadakis, N. G. *et al.* Study of the effect of CSF suppression on white matter diffusion anisotropy mapping of healthy human brain. *Magnetic resonance in medicine* **48**, 394-398, doi:10.1002/mrm.10204 (2002).
36 Assaf, Y. & Pasternak, O. Diffusion tensor imaging (DTI)-based white matter mapping in brain research: a review. *Journal of molecular neuroscience : MN* **34**, 51-61, doi:10.1007/s12031-007-0029-0 (2008).
37 Xu, J. *et al.* Mapping mean axon diameter and axonal volume fraction by MRI using temporal diffusion spectroscopy. *NeuroImage* **103**, 10-19, doi:10.1016/j.neuroimage.2014.09.006 (2014).
38 Moussavi-Biugui, A., Stieltjes, B., Fritzsche, K., Semmler, W. & Laun, F. B. Novel spherical phantoms for Q-ball imaging under in vivo conditions. *Magnetic resonance in medicine* **65**, 190-194, doi:10.1002/mrm.22602 (2011).

39 Yanasak, N. & Allison, J. Use of capillaries in the construction of an MRI phantom for the assessment of diffusion tensor imaging: demonstration of performance. *Magn Reson Imaging* **24**, 1349-1361, doi:10.1016/j.mri.2006.08.001 (2006).
40 Pullens, P., Roebroeck, A. & Goebel, R. Ground truth hardware phantoms for validation of diffusion-weighted MRI applications. *Journal of Magnetic Resonance Imaging* **32**, 482-488, doi:10.1002/jmri.22243 (2010).
41 Odom, T. W., Thalladi, V. R., Love, J. C. & Whitesides, G. M. Generation of 30-50 nm structures using easily fabricated, composite PDMS masks. *J Am Chem Soc* **124**, 12112-12113 (2002).
42 Ito, T. & Okazaki, S. Pushing the limits of lithography. *Nature* **406**, 1027-1031 (2000).
43 Whitesides, G. M. The origins and the future of microfluidics. *Nature* **442**, 368-373 (2006).
44 Samuel, R., Sant, H. J., Jiao, F., Johnson, C. R. & Gale, B. K. Microfluidic laminate-based phantom for diffusion tensor-magnetic resonance imaging (DT-MRI). *Journal of micromechanics and microengineering : structures, devices, and systems* **21**, 950271-9502711, doi:10.1088/0960-1317/21/9/095027 (2011).
45 Lee, J. N., Park, C. & Whitesides, G. M. Solvent Compatibility of Poly(dimethylsiloxane)-Based Microfluidic Devices. *Analytical Chemistry* **75**, 6544-6554, doi:10.1021/ac0346712 (2003).
46 Verma, M. K. S., Majumder, A. & Ghatak, A. Embedded Template-Assisted Fabrication of Complex Microchannels
in PDMS and Design of a Microfluidic Adhesive. *Langmuir : the ACS journal of surfaces and colloids* **22**, 10291-10295 (2006).
47 Descoteaux, M., Angelino, E., Fitzgibbons, S. & Deriche, R. Regularized, fast, and robust analytical Q-ball imaging. *Magn Reson Med* **58**, 497-510, doi:10.1002/mrm.21277 (2007).
48 Wedeen, V. J. *et al.* Diffusion spectrum magnetic resonance imaging (DSI) tractography of crossing fibers. *Neuroimage* **41**, 1267-1277, doi:10.1016/j.neuroimage.2008.03.036 (2008).
49 Yeh, F.-C., Verstynen, T. D., Wang, Y., Fernández-Miranda, J. C. & Tseng, W.-Y. I. Deterministic Diffusion Fiber Tracking Improved by Quantitative Anisotropy. *PLoS ONE* **8**, e80713, doi:10.1371/journal.pone.0080713 (2013).
50 Lee, J. N., Park, C. & Whitesides, G. M. Solvent Compatibility of Poly(dimethylsiloxane)-Based Microfluidic Devices. *Analytical Chemistry* **75**, 6544-6554 (2003).
51 Barazany, D., Basser, P. J. & Assaf, Y. In vivo measurement of axon diameter distribution in the corpus callosum of rat brain. *Brain* **132**, 1210-1220, doi:10.1093/brain/awp042 (2009).
52 Narayanan, R. T., Egger, R., Kock, C. P. J., & Oberlaender, M. in *Axons and brain architecutre* (ed K. S. Rockland) 183-202 (The Netherlands: Elsevier Academic Press, 2016).
53 Oruc-de Leon, J. *Development of a micromechanical computational finite element model of a brain axon*, The University of Texas at San Antonio, (2009).
54 Delannoy, J., Chen, C.-N., Turner, R., Levin, R. L. & Le Bihan, D. Noninvasive temperature imaging using diffusion MRI. *Magnetic Resonance in Medicine* **19**, 333-339, doi:10.1002/mrm.1910190224 (1991).
55 Daisne, J.-F. *et al.* Evaluation of a multimodality image (CT, MRI and PET) coregistration procedure on phantom and head and neck cancer patients: accuracy, reproducibility and consistency. *Radiotherapy and Oncology* **69**, 237-245, doi:http://dx.doi.org/10.1016/j.radonc.2003.10.009 (2003).
56 O'Brien, T. J. *et al.* Subtraction ictal SPECT co-registered to MRI improves clinical usefulness of SPECT in localizing the surgical seizure focus. *Neurology* **50**, 445-454 (1998).
57 Sollier, E., Murray, C., Maoddi, P. & Di Carlo, D. Rapid prototyping polymers for microfluidic devices and high pressure injections. *Lab on a chip* **11**, 3752-3765, doi:10.1039/C1LC20514E (2011).
58 UNOS. *Data*, <https://www.unos.org/data/> (2015).

59 Kittur, D. S., Hogan, M. M., Thukral, V. K., Johnson McGaw, L. & Alexander, J. W. Incentives for organ donation? *The Lancet* **338**, 1441-1443, doi:http://dx.doi.org/10.1016/0140-6736(91)92735-K (1991).
60 Becker, G. S. & Elías, J. J. Introducing Incentives in the Market for Live and Cadaveric Organ Donations. *The Journal of Economic Perspectives* **21**, 3-24, doi:10.2307/30033732 (2007).
61 Langer, R. & Vacanti, J. P. Tissue engineering. *Science (New York, N.Y.)* **260**, 920-926 (1993).
62 Khademhosseini, A., Vacanti, J. P. & Langer, R. Progress in tissue engineering. *Scientific American* **300**, 64-71 (2009).
63 Carmeliet, P. & Jain, R. K. Angiogenesis in cancer and other diseases. *Nature* **407**, 249-257 (2000).
64 mohanand09. *Blood vessels.2.*, 2011).
65 Lokmic, Z. & Mitchell, G. M. Engineering the microcirculation. *Tissue Eng Part B Rev* **14**, 87-103, doi:10.1089/teb.2007.0299 (2008).
66 Malda, J., Klein, T. J. & Upton, Z. The roles of hypoxia in the in vitro engineering of tissues. *Tissue engineering* **13**, 2153-2162, doi:10.1089/ten.2006.0417 (2007).
67 Wang, X., Yan, Y. & Zhang, R. Recent trends and challenges in complex organ manufacturing. *Tissue engineering. Part B, Reviews* **16**, 189-197, doi:10.1089/ten.TEB.2009.0576 (2010).
68 Ruoslahti, E. & Pierschbacher, M. D. New perspectives in cell adhesion: RGD and integrins. *Science* **238**, 491+ (1987).
69 Harris, A. K., Wild, P. & Stopak, D. Silicone Rubber Substrata: A New Wrinkle in the Study of Cell Locomotion. *Science* **208**, 177-179 (1980).
70 Oliver, T., Dembo, M. & Jacobson, K. Separation of propulsive and adhesive traction stresses in locomoting keratocytes. *The Journal of cell biology* **145**, 589-604 (1999).
71 Balaban, N. Q. *et al.* Force and focal adhesion assembly: a close relationship studied using elastic micropatterned substrates. *Nat Cell Biol* **3**, 466-472, doi:http://www.nature.com/ncb/journal/v3/n5/suppinfo/ncb0501_466_S1.html (2001).
72 Tan, J. L. *et al.* Cells Lying on a Bed of Microneedles: An Approach to Isolate Mechanical Force. *Proceedings of the National Academy of Sciences of the United States of America* **100**, 1484-1489 (2003).
73 Pelham, R. J. & Wang, Y.-L. Cell Locomotion and Focal Adhesions are Regulated by Substrate Flexibility. *Proceedings of the National Academy of Sciences of the United States of America* **94**, 13661-13665 (1997).
74 Wang, H. B., Dembo, M. & Wang, Y. L. Substrate flexibility regulates growth and apoptosis of normal but not transformed cells. *American journal of physiology. Cell physiology* **279**, C1345-1350 (2000).
75 Engler, A. *et al.* Substrate Compliance versus Ligand Density in Cell on Gel Responses. *Biophysical journal* **86**, 617-628, doi:http://dx.doi.org/10.1016/S0006-3495(04)74140-5 (2004).
76 Zhu, J. & Marchant, R. E. Design properties of hydrogel tissue-engineering scaffolds. *Expert review of medical devices* **8**, 607-626, doi:10.1586/erd.11.27 (2011).
77 Drury, J. L. & Mooney, D. J. Hydrogels for tissue engineering: scaffold design variables and applications. *Biomaterials* **24**, 4337-4351 (2003).
78 Kopecek, J. Hydrogel biomaterials: a smart future? *Biomaterials* **28**, 5185-5192, doi:10.1016/j.biomaterials.2007.07.044 (2007).
79 Chrobak, K. M., Potter, D. R. & Tien, J. Formation of perfused, functional microvascular tubes in vitro. *Microvascular research* **71**, 185-196, doi:10.1016/j.mvr.2006.02.005 (2006).
80 Wong, K. H., Truslow, J. G. & Tien, J. The role of cyclic AMP in normalizing the function of engineered human blood microvessels in microfluidic collagen gels. *Biomaterials* **31**, 4706-4714, doi:10.1016/j.biomaterials.2010.02.041 (2010).

81 Sakai, S., Hirose, K., Taguchi, K., Ogushi, Y. & Kawakami, K. An injectable, in situ enzymatically gellable, gelatin derivative for drug delivery and tissue engineering. *Biomaterials* **30**, 3371-3377, doi:10.1016/j.biomaterials.2009.03.030 (2009).
82 Paguirigan, A. & Beebe, D. J. Gelatin based microfluidic devices for cell culture. *Lab Chip* **6**, 407-413, doi:10.1039/b517524k (2006).
83 Ramamurthi, A. & Vesely, I. Ultraviolet light-induced modification of crosslinked hyaluronan gels. *Journal of biomedical materials research. Part A* **66**, 317-329, doi:10.1002/jbm.a.10588 (2003).
84 Kuo, C. K. & Ma, P. X. Ionically crosslinked alginate hydrogels as scaffolds for tissue engineering: Part 1. Structure, gelation rate and mechanical properties. *Biomaterials* **22**, 511-521, doi:http://dx.doi.org/10.1016/S0142-9612(00)00201-5 (2001).
85 Kim, I. Y. *et al.* Chitosan and its derivatives for tissue engineering applications. *Biotechnology advances* **26**, 1-21, doi:10.1016/j.biotechadv.2007.07.009 (2008).
86 Choi, N. W. *et al.* Microfluidic scaffolds for tissue engineering. *Nat Mater* **6**, 908-915, doi:http://www.nature.com/nmat/journal/v6/n11/suppinfo/nmat2022_S1.html (2007).
87 Ho, C. M. B., Ng, S. H., Li, K. H. H. & Yoon, Y.-J. 3D printed microfluidics for biological applications. *Lab on a Chip* **15**, 3627-3637, doi:10.1039/C5LC00685F (2015).
88 Cuchiara, M. P., Allen, A. C., Chen, T. M., Miller, J. S. & West, J. L. Multilayer microfluidic PEGDA hydrogels. *Biomaterials* **31**, 5491-5497, doi:10.1016/j.biomaterials.2010.03.031 (2010).
89 Chen, R. & Hunt, J. A. Biomimetic materials processing for tissue-engineering processes. *Journal of Materials Chemistry* **17**, 3974-3979, doi:10.1039/B706765H (2007).
90 Langer, R. & Tirrell, D. A. Designing materials for biology and medicine. *Nature* **428**, 487-492, doi:http://www.nature.com/nature/journal/v428/n6982/suppinfo/nature02388_S1.html (2004).
91 Borenstein, J. T. *et al.* Functional endothelialized microvascular networks with circular cross-sections in a tissue culture substrate. *Biomedical microdevices* **12**, 71-79, doi:10.1007/s10544-009-9361-1 (2010).
92 Fiddes, L. K. *et al.* A circular cross-section PDMS microfluidics system for replication of cardiovascular flow conditions. *Biomaterials* **31**, 3459-3464, doi:10.1016/j.biomaterials.2010.01.082 (2010).
93 McUsic, A. C., Lamba, D. A. & Reh, T. A. Guiding the morphogenesis of dissociated newborn mouse retinal cells and hES cell-derived retinal cells by soft lithography-patterned microchannel PLGA scaffolds. *Biomaterials* **33**, 1396-1405, doi:10.1016/j.biomaterials.2011.10.083 (2012).
94 Bettinger, C. J. *et al.* Three-Dimensional Microfluidic Tissue-Engineering Scaffolds Using a Flexible Biodegradable Polymer. *Advanced materials (Deerfield Beach, Fla.)* **18**, 165-169, doi:10.1002/adma.200500438 (2005).
95 Liu Tsang, V. *et al.* Fabrication of 3D hepatic tissues by additive photopatterning of cellular hydrogels. *FASEB journal : official publication of the Federation of American Societies for Experimental Biology* **21**, 790-801, doi:10.1096/fj.06-7117com (2007).
96 Buxton, A. N. *et al.* Design and characterization of poly(ethylene glycol) photopolymerizable semi-interpenetrating networks for chondrogenesis of human mesenchymal stem cells. *Tissue engineering* **13**, 2549-2560, doi:10.1089/ten.2007.0075 (2007).
97 Beamish, J. A., Zhu, J., Kottke-Marchant, K. & Marchant, R. E. The effects of monoacrylated poly(ethylene glycol) on the properties of poly(ethylene glycol) diacrylate hydrogels used for tissue engineering. *Journal of biomedical materials research. Part A* **92**, 441-450, doi:10.1002/jbm.a.32353 (2010).
98 Kloxin, A. M., Kasko, A. M., Salinas, C. N. & Anseth, K. S. Photodegradable hydrogels for dynamic tuning of physical and chemical properties. *Science (New York, N.Y.)* **324**, 59-63, doi:10.1126/science.1169494 (2009).

99 Sarig-Nadir, O., Livnat, N., Zajdman, R., Shoham, S. & Seliktar, D. Laser Photoablation of Guidance Microchannels into Hydrogels Directs Cell Growth in Three Dimensions. *Biophysical Journal* **96**, 4743-4752, doi:10.1016/j.bpj.2009.03.019 (2009).
100 Shalumon, K. T. *et al.* Fabrication of poly (l-lactic acid)/gelatin composite tubular scaffolds for vascular tissue engineering. *International Journal of Biological Macromolecules* **72**, 1048-1055, doi:10.1016/j.ijbiomac.2014.09.058 (2015).
101 Van Den Bulcke, A. I. *et al.* Structural and Rheological Properties of Methacrylamide Modified Gelatin Hydrogels. *Biomacromolecules* **1**, 31-38, doi:10.1021/bm990017d (2000).
102 Schuurman, W. *et al.* Gelatin-methacrylamide hydrogels as potential biomaterials for fabrication of tissue-engineered cartilage constructs. *Macromolecular bioscience* **13**, 551-561, doi:10.1002/mabi.201200471 (2013).
103 Bertassoni, L. E. *et al.* Hydrogel bioprinted microchannel networks for vascularization of tissue engineering constructs. *Lab on a chip* **14**, 2202-2211, doi:10.1039/c4lc00030g (2014).
104 Kolesky, D. B. *et al.* 3D bioprinting of vascularized, heterogeneous cell-laden tissue constructs. *Advanced materials* **26**, 3124-3130, doi:10.1002/adma.201305506 (2014).
105 Nichol, J. W. *et al.* Cell-laden microengineered gelatin methacrylate hydrogels. *Biomaterials* **31**, 5536-5544, doi:10.1016/j.biomaterials.2010.03.064 (2010).
106 Khor, E., Wu, H., Lim, L. Y. & Guo, C. M. Chitin-Methacrylate: Preparation, Characterization and Hydrogel Formation. *Materials* **4**, 1728 (2011).
107 Paepe, I. D., Declercq, H., Cornelissen, M. & Schacht, E. Novel hydrogels based on methacrylate-modified agarose. *Polymer International* **51**, 867-870, doi:10.1002/pi.945 (2002).
108 Leduc, E. H. & Bernhard, W. Recent modifications of the glycol methacrylate embedding procedure. *Journal of ultrastructure research* **19**, 196-199 (1967).
109 Mahaffy, R. E., Shih, C. K., MacKintosh, F. C. & Käs, J. Scanning Probe-Based Frequency-Dependent Microrheology of Polymer Gels and Biological Cells. *Physical Review Letters* **85**, 880-883 (2000).
110 Lo, C.-M., Wang, H.-B., Dembo, M. & Wang, Y.-l. Cell Movement Is Guided by the Rigidity of the Substrate. *Biophysical journal* **79**, 144-152, doi:http://dx.doi.org/10.1016/S0006-3495(00)76279-5 (2000).
111 Hu, S. *et al.* Mechanical anisotropy of adherent cells probed by a three-dimensional magnetic twisting device. *American journal of physiology. Cell physiology* **287**, C1184-1191, doi:10.1152/ajpcell.00224.2004 (2004).
112 Bao, G. & Suresh, S. Cell and molecular mechanics of biological materials. *Nat Mater* **2**, 715-725 (2003).
113 Engler, A. J. *et al.* Myotubes differentiate optimally on substrates with tissue-like stiffness: pathological implications for soft or stiff microenvironments. *The Journal of cell biology* **166**, 877-887, doi:10.1083/jcb.200405004 (2004).
114 Diridollou, S. *et al.* In vivo model of the mechanical properties of the human skin under suction. *Skin Research & Technology* **6**, 214 (2000).
115 Cukierman, E., Pankov, R., Stevens, D. R. & Yamada, K. M. Taking cell-matrix adhesions to the third dimension. *Science (New York, N.Y.)* **294**, 1708-1712 (2001).
116 Yeung, T. *et al.* Effects of substrate stiffness on cell morphology, cytoskeletal structure, and adhesion. *Cell Motility and the Cytoskeleton* **60**, 24-34, doi:10.1002/cm.20041 (2005).
117 Steinberg, M. S. Mechanism of Tissue Reconstruction by Dissociated Cells, II: Time-Course of Events. *Science* **137**, 762-763 (1962).
118 Trinkaus, J. P. & Lentz, J. P. Direct observation of type-specific segregation in mixed cell aggregates. *Developmental Biology* **9**, 115-136, doi:http://dx.doi.org/10.1016/0012-1606(64)90017-X (1964).

119 Arda, K., Ciledag, N., Aktas, E., Aribas, B. K. & Kose, K. Quantitative assessment of normal soft-tissue elasticity using shear-wave ultrasound elastography. *AJR. American journal of roentgenology* **197**, 532-536, doi:10.2214/ajr.10.5449 (2011).
120 Engler, A. J., Sen, S., Sweeney, H. L. & Discher, D. E. Matrix elasticity directs stem cell lineage specification. *Cell* **126**, 677-689, doi:10.1016/j.cell.2006.06.044 (2006).
121 Yeh, W. C. *et al.* Elastic modulus measurements of human liver and correlation with pathology. *Ultrasound in medicine & biology* **28**, 467-474 (2002).
122 Ahearne, M., Yang, Y., El Haj, A. J., Then, K. Y. & Liu, K.-K. Characterizing the viscoelastic properties of thin hydrogel-based constructs for tissue engineering applications. *Journal of the Royal Society Interface* **2**, 455-463, doi:10.1098/rsif.2005.0065 (2005).
123 Bryant, S. J., Bender, R. J., Durand, K. L. & Anseth, K. S. Encapsulating chondrocytes in degrading PEG hydrogels with high modulus: engineering gel structural changes to facilitate cartilaginous tissue production. *Biotechnology and bioengineering* **86**, 747-755, doi:10.1002/bit.20160 (2004).
124 Huang, G. *et al.* Engineering three-dimensional cell mechanical microenvironment with hydrogels. *Biofabrication* **4**, 042001, doi:10.1088/1758-5082/4/4/042001 (2012).
125 Miller, J. S. *et al.* Rapid casting of patterned vascular networks for perfusable engineered three-dimensional tissues. *Nat Mater* **11**, 768-774, doi:http://www.nature.com/nmat/journal/v11/n9/abs/nmat3357.html#supplementary-information (2012).
126 He, C., Kim, S. W. & Lee, D. S. In situ gelling stimuli-sensitive block copolymer hydrogels for drug delivery. *Journal of Controlled Release* **127**, 189-207, doi:http://dx.doi.org/10.1016/j.jconrel.2008.01.005 (2008).
127 Fisher, J. P., Mikos, Antonios G., Bronzion, Joseph D., Peterson, Donald R. *Tissue Engineering: Principles and Practices*. 1st edn, (CRC Press, 2012).
128 Farrell, M. J., Farrell, K. M., Riggin, C. N., Mauck, R. L. & Ieee. Mesenchymal Stem Cell Death in Three-Dimensional Agarose Culture for Cartilage Tissue Engineering Applications: Progression, Factors, and Prevention. *2012 38th Annual Northeast Bioengineering Conference (Nebec)*, 117-118 (2012).
129 Moskaluk, C. A. & Stoler, M. H. Agarose mold embedding of cultured cells for tissue microarrays. *Diagnostic Molecular Pathology* **11**, 234-238, doi:10.1097/00019606-200212000-00007 (2002).
130 Shapiro, P., Absher, P. M., Casty, F. & Evans, J. Maintaining intact mature lung tissue in culture using low melt agarose. *Methods in Cell Science* **17**, 245-249, doi:10.1007/bf00986229 (1995).
131 Rhodes, J. M. & Simons, M. The extracellular matrix and blood vessel formation: not just a scaffold. *Journal of cellular and molecular medicine* **11**, 176-205, doi:10.1111/j.1582-4934.2007.00031.x (2007).
132 Skardal, A. *et al.* Photocrosslinkable hyaluronan-gelatin hydrogels for two-step bioprinting. *Tissue engineering. Part A* **16**, 2675-2685, doi:10.1089/ten.TEA.2009.0798 (2010).
133 Hern, D. L. & Hubbell, J. A. Incorporation of adhesion peptides into nonadhesive hydrogels useful for tissue resurfacing. *Journal of biomedical materials research* **39**, 266-276 (1998).
134 Nicodemus, G. D. & Bryant, S. J. Cell encapsulation in biodegradable hydrogels for tissue engineering applications. *Tissue engineering. Part B, Reviews* **14**, 149-165, doi:10.1089/ten.teb.2007.0332 (2008).
135 Krogh, A. The number and distribution of capillaries in muscles with calculations of the oxygen pressure head necessary for supplying the tissue. *The Journal of physiology* **52**, 409-415 (1919).
136 Krogh, A. The rate of diffusion of gases through animal tissues, with some remarks on the coefficient of invasion. *The Journal of physiology* **52**, 391-408 (1919).

137 Artursson, P. & Borchardt, R. T. Intestinal Drug Absorption and Metabolism in Cell Cultures: Caco-2 and Beyond. *Pharmaceutical Research* **14**, 1655-1658, doi:10.1023/A:1012155124489 (1997).
138 Gallagher, R. & Appenzeller, T. Beyond Reductionism. *Science* **284**, 79 (1999).
139 Manson, S. M. Simplifying complexity: a review of complexity theory. *Geoforum* **32**, 405-414, doi:http://dx.doi.org/10.1016/S0016-7185(00)00035-X (2001).
140 Burdick, J. A. & Vunjak-Novakovic, G. Engineered Microenvironments for Controlled Stem Cell Differentiation. *Tissue Engineering Part A* **15**, 205-219, doi:10.1089/ten.tea.2008.0131 (2008).
141 Engler, A. J., Sen, S., Sweeney, H. L. & Discher, D. E. Matrix Elasticity Directs Stem Cell Lineage Specification. *Cell* **126**, 677-689, doi:http://dx.doi.org/10.1016/j.cell.2006.06.044 (2006).
142 Lutolf, M. P., Gilbert, P. M. & Blau, H. M. Designing materials to direct stem-cell fate. *Nature* **462**, 433-441 (2009).
143 Whiteside, T. L. The tumor microenvironment and its role in promoting tumor growth. *Oncogene* **27**, 5904-5912 (0000).
144 Kellner, K. *et al.* Determination of oxygen gradients in engineered tissue using a fluorescent sensor. *Biotechnology and Bioengineering* **80**, 73-83, doi:10.1002/bit.10352 (2002).
145 Glicklis, R., Merchuk, J. C. & Cohen, S. Modeling mass transfer in hepatocyte spheroids via cell viability, spheroid size, and hepatocellular functions. *Biotechnology and Bioengineering* **86**, 672-680, doi:10.1002/bit.20086 (2004).
146 Gebhardt, R. *et al.* New Hepatocyte In Vitro Systems for Drug Metabolism: Metabolic Capacity and Recommendations for Application in Basic Research and Drug Development, Standard Operation Procedures. *Drug Metabolism Reviews* **35**, 145-213, doi:10.1081/DMR-120023684 (2003).
147 Martin, Y. & Vermette, P. Bioreactors for tissue mass culture: Design, characterization, and recent advances. *Biomaterials* **26**, 7481-7503, doi:http://dx.doi.org/10.1016/j.biomaterials.2005.05.057 (2005).
148 Wang, D. W., Fermor, B., Gimble, J. M., Awad, H. A. & Guilak, F. Influence of oxygen on the proliferation and metabolism of adipose derived adult stem cells. *Journal of Cellular Physiology* **204**, 184-191, doi:10.1002/jcp.20324 (2005).
149 Zhao, F. *et al.* Effects of Oxygen Transport on 3-D Human Mesenchymal Stem Cell Metabolic Activity in Perfusion and Static Cultures: Experiments and Mathematical Model. *Biotechnology Progress* **21**, 1269-1280, doi:10.1021/bp0500664 (2005).
150 Radisky, D. C. *et al.* Rac1b and reactive oxygen species mediate MMP-3-induced EMT and genomic instability. *Nature* **436**, 123-127, doi:http://www.nature.com/nature/journal/v436/n7047/suppinfo/nature03688_S1.html (2005).
151 Janowska-Wieczorek, A., Majka, M., Ratajczak, J. & Ratajczak, M. Z. Autocrine/Paracrine Mechanisms in Human Hematopoiesis. *STEM CELLS* **19**, 99-107, doi:10.1634/stemcells.19-2-99 (2001).
152 Singh, A. B. & Harris, R. C. Autocrine, paracrine and juxtacrine signaling by EGFR ligands. *Cellular Signalling* **17**, 1183-1193, doi:http://dx.doi.org/10.1016/j.cellsig.2005.03.026 (2005).
153 DeWitt, A. *et al.* Affinity Regulates Spatial Range of EGF Receptor Autocrine Ligand Binding. *Developmental Biology* **250**, 305-316, doi:http://dx.doi.org/10.1006/dbio.2002.0807 (2002).
154 Cartmell, S. H., Porter, B. D., Garcia, A. J. & Guldberg, R. E. Effects of medium perfusion rate on cell-seeded three-dimensional bone constructs in vitro. *Tissue engineering* **9**, 1197-1203, doi:10.1089/10763270360728107 (2003).
155 Taylor, A. E. Capillary fluid filtration. Starling forces and lymph flow. *Circulation Research* **49**, 557-575, doi:10.1161/01.res.49.3.557 (1981).

156 Chary, S. R. & Jain, R. K. Direct measurement of interstitial convection and diffusion of albumin in normal and neoplastic tissues by fluorescence photobleaching. *Proc Natl Acad Sci U S A* **86**, 5385-5389 (1989).
157 Dafni, H., Israely, T., Bhujwalla, Z. M., Benjamin, L. E. & Neeman, M. Overexpression of vascular endothelial growth factor 165 drives peritumor interstitial convection and induces lymphatic drain: magnetic resonance imaging, confocal microscopy, and histological tracking of triple-labeled albumin. *Cancer research* **62**, 6731-6739 (2002).
158 Wilke, C. R. & Chang, P. Correlation of diffusion coefficients in dilute solutions. *AIChE Journal* **1**, 264-270, doi:10.1002/aic.690010222 (1955).
159 Vendruscolo, F. *et al.* Determination of Oxygen Solubility in Liquid Media. *ISRN Chemical Engineering* **2012**, 5, doi:10.5402/2012/601458 (2012).
160 Streeter, I. & Cheema, U. Oxygen consumption rate of cells in 3D culture: the use of experiment and simulation to measure kinetic parameters and optimise culture conditions. *The Analyst* **136**, 4013-4019, doi:10.1039/c1an15249a (2011).
161 Phillips, H. J. & Andrews, R. V. Instability of metabolic quotients obtained from tissue cultures. *Proceedings of the Society for Experimental Biology and Medicine. Society for Experimental Biology and Medicine (New York, N.Y.)* **103**, 160-163 (1960).
162 McCarthy, H. L. & Phillips, H. J. Oxygen uptake and lactate formation of HeLa cells. *Proceedings of the Society for Experimental Biology and Medicine. Society for Experimental Biology and Medicine (New York, N.Y.)* **93**, 573-576 (1956).
163 Green, M., Henle, G. & Deinhardt, F. Respiration and glycolysis of human cells grown in tissue culture. *Virology* **5**, 206-219 (1958).
164 Danes, B. S., Broadfoot, M. M. & Paul, J. A comparative study of respiratory metabolism in cultured mammalian cell strains. *Experimental Cell Research* **30**, 369-378, doi:http://dx.doi.org/10.1016/0014-4827(63)90308-2 (1963).
165 Lide, D. R. *CRC Handbook of chemistry and physics : a ready-reference book of chemical and physical data*. (Taylor and Francis, 2014).
166 Lemons, J. M. S. *et al.* Quiescent Fibroblasts Exhibit High Metabolic Activity. *PLoS Biol* **8**, e1000514, doi:10.1371/journal.pbio.1000514 (2010).
167 Lever, J. E. Modulation of glucose uptake in animal cells. Studies using plasma membrane vesicles isolated from nontransformed and simian virus 40-transformed mouse fibroblast cultures. *The Journal of biological chemistry* **254**, 2961-2967 (1979).
168 Chenyakin, Y. *Are diffusion coefficients calculated using the Stokes-Einstein equation combined with viscosities consistent with measured diffusion coefficients of tracer organics within organics-water mediums?* Master of Science - MSc thesis, University of British Columbia, (2015).
169 Choi, N. W. *et al.* Microfluidic scaffolds for tissue engineering. *Nat. Mater.* **6**, 908-915, doi:10.1038/nmat2022 (2007).
170 Griffith, L. G. & Swartz, M. A. Capturing complex 3D tissue physiology in vitro. *Nat Rev Mol Cell Biol* **7**, 211-224, doi:http://www.nature.com/nrm/journal/v7/n3/suppinfo/nrm1858_S1.html (2006).
171 Ago, H. *et al.* Mechanical immobilization of Hela cells on aligned carbon nanotube array. *Mater. Lett.* **60**, 3851-3854, doi:10.1016/j.matlet.2006.03.151 (2006).
172 Madhavan, H. N. *et al.* A study on the growth of continuous culture cell lines embedded in Mebiol gel. *Curr. Sci.* **87**, 1275-1277 (2004).
173 Ma, L. W., Liu, M. Z., Liu, H. L., Chen, J. & Cui, D. P. In vitro cytotoxicity and drug release properties of pH- and temperature-sensitive core-shell hydrogel microspheres. *Int. J. Pharm.* **385**, 86-91, doi:10.1016/j.ijpharm.2009.10.037 (2010).

174 Huang, T. Q., Qu, X., Liu, J. & Chen, S. C. 3D printing of biomimetic microstructures for cancer cell migration. *Biomed. Microdevices* **16**, 127-132, doi:10.1007/s10544-013-9812-6 (2014).
175 Mohanty, S. *et al.* 3D Printed Silicone-Hydrogel Scaffold with Enhanced Physicochemical Properties. *Biomacromolecules* **17**, 1321-1329, doi:10.1021/acs.biomac.5b01722 (2016).
176 Lee, J. N., Jiang, X., Ryan, D. & Whitesides, G. M. Compatibility of Mammalian Cells on Surfaces of Poly(dimethylsiloxane). *Langmuir : the ACS journal of surfaces and colloids* **20**, 11684-11691, doi:10.1021/la048562+ (2004).
177 McDonald, J. C. *et al.* Fabrication of microfluidic systems in poly(dimethylsiloxane). *Electrophoresis* **21**, 27-40, doi:10.1002/(sici)1522-2683(20000101)21:1<27::aid-elps27>3.0.co;2-c (2000).
178 Duffy, D. C., McDonald, J. C., Schueller, O. J. A. & Whitesides, G. M. Rapid Prototyping of Microfluidic Systems in Poly(dimethylsiloxane). *Analytical Chemistry* **70**, 4974-4984, doi:10.1021/ac980656z (1998).
179 Bodas, D. & Khan-Malek, C. Hydrophilization and hydrophobic recovery of PDMS by oxygen plasma and chemical treatment—An SEM investigation. *Sensors and Actuators B: Chemical* **123**, 368-373, doi:http://dx.doi.org/10.1016/j.snb.2006.08.037 (2007).
180 Hillborg, H. & Gedde, U. W. Hydrophobicity recovery of polydimethylsiloxane after exposure to corona discharges. *Polymer* **39**, 1991-1998, doi:http://dx.doi.org/10.1016/S0032-3861(97)00484-9 (1998).
181 Matsuda, S., Iwata, H., Se, N. & Ikada, Y. Bioadhesion of gelatin films crosslinked with glutaraldehyde. *Journal of Biomedical Materials Research* **45**, 20-27, doi:10.1002/(SICI)1097-4636(199904)45:1<20::AID-JBM3>3.0.CO;2-6 (1999).
182 Chen, Y.-C. *et al.* Functional Human Vascular Network Generated in Photocrosslinkable Gelatin Methacrylate Hydrogels. *Advanced Functional Materials* **22**, 2027-2039, doi:10.1002/adfm.201101662 (2012).
183 Gauvin, R. *et al.* Microfabrication of complex porous tissue engineering scaffolds using 3D projection stereolithography. *Biomaterials* **33**, 3824-3834, doi:http://dx.doi.org/10.1016/j.biomaterials.2012.01.048 (2012).
184 Pfeifer, G. P., You, Y.-H. & Besaratinia, A. Mutations induced by ultraviolet light. *Mutation Research/Fundamental and Molecular Mechanisms of Mutagenesis* **571**, 19-31, doi:http://dx.doi.org/10.1016/j.mrfmmm.2004.06.057 (2005).
185 Fedorovich, N. E. *et al.* The effect of photopolymerization on stem cells embedded in hydrogels. *Biomaterials* **30**, 344-353, doi:http://dx.doi.org/10.1016/j.biomaterials.2008.09.037 (2009).
186 Chuah, Y. J. *et al.* Simple surface engineering of polydimethylsiloxane with polydopamine for stabilized mesenchymal stem cell adhesion and multipotency. *Scientific Reports* **5**, 18162, doi:10.1038/srep18162 (2015).
187 Domansky, K. *et al.* Perfused multiwell plate for 3D liver tissue engineering. *Lab on a chip* **10**, 51-58, doi:10.1039/b913221j (2010).
188 Gos, M. *et al.* Cellular quiescence induced by contact inhibition or serum withdrawal in C3H10T1/2 cells. *Cell proliferation* **38**, 107-116, doi:10.1111/j.1365-2184.2005.00334.x (2005).
189 Maton, A. *Human biology and health.* (Prentice Hall, 1993).
190 Eckoldt, K. Biodynamics-circulation. Y. C. Fung. Springer-verlag New York-Berlin-Heidelberg-Tokyo 1984, 404 p., 189 illustr. Price: DM 92.00. ISBN 3–540–90867–6. *Crystal Research and Technology* **20**, 808-808, doi:10.1002/crat.2170200618 (1985).
191 Wang, S. S. *et al.* Functional trade-offs in white matter axonal scaling. *The Journal of neuroscience : the official journal of the Society for Neuroscience* **28**, 4047-4056, doi:10.1523/JNEUROSCI.5559-05.2008 (2008).
192 Goldman, D. Theoretical Models of Microvascular Oxygen Transport to Tissue. *Microcirculation (New York, N.Y. : 1994)* **15**, 795-811, doi:10.1080/10739680801938289 (2008).

193 Loh, Q. L. & Choong, C. Three-Dimensional Scaffolds for Tissue Engineering Applications: Role of Porosity and Pore Size. *Tissue engineering. Part B, Reviews* **19**, 485-502, doi:10.1089/ten.teb.2012.0437 (2013).
194 Murphy, C. M. & O'Brien, F. J. Understanding the effect of mean pore size on cell activity in collagen-glycosaminoglycan scaffolds. *Cell Adhesion & Migration* **4**, 377-381, doi:10.4161/cam.4.3.11747 (2010).
195 Lovett, M., Lee, K., Edwards, A. & Kaplan, D. L. Vascularization Strategies for Tissue Engineering. *Tissue engineering. Part B, Reviews* **15**, 353-370, doi:10.1089/ten.teb.2009.0085 (2009).
196 Guillotin, B. & Guillemot, F. Cell patterning technologies for organotypic tissue fabrication. *Trends in biotechnology* **29**, 183-190, doi:10.1016/j.tibtech.2010.12.008 (2011).
197 Sachlos, E. & Czernuszka, J. T. Making tissue engineering scaffolds work. Review: the application of solid freeform fabrication technology to the production of tissue engineering scaffolds. *European cells & materials* **5**, 29-39; discussion 39-40 (2003).
198 Mooney, D. J., Baldwin, D. F., Suh, N. P., Vacanti, J. P. & Langer, R. Novel approach to fabricate porous sponges of poly(D,L-lactic-co-glycolic acid) without the use of organic solvents. *Biomaterials* **17**, 1417-1422 (1996).
199 Thomson, R. C., Yaszemski, M. J., Powers, J. M. & Mikos, A. G. Fabrication of biodegradable polymer scaffolds to engineer trabecular bone. *Journal of biomaterials science. Polymer edition* **7**, 23-38 (1995).
200 Whang, K., Thomas, C. H., Healy, K. E. & Nuber, G. A novel method to fabricate bioabsorbable scaffolds. *Polymer* **36**, 837-842, doi:http://dx.doi.org/10.1016/0032-3861(95)93115-3 (1995).
201 Bellan, L. M. *et al.* Fabrication of an artificial 3-dimensional vascular network using sacrificial sugar structures. *Soft Matter* **5**, 1354-1357, doi:10.1039/B819905A (2009).
202 Mikos, A. G. & Temenoff, J. S. *Formation of highly porous biodegradable scaffolds for tissue engineering*. (2000).
203 McGuigan, A. P., Leung, B. & Sefton, M. V. Fabrication of cell-containing gel modules to assemble modular tissue-engineered constructs [corrected]. *Nature protocols* **1**, 2963-2969, doi:10.1038/nprot.2006.443 (2006).
204 McGuigan, A. P. & Sefton, M. V. Design and fabrication of sub-mm-sized modules containing encapsulated cells for modular tissue engineering. *Tissue engineering* **13**, 1069-1078 (2007).
205 McGuigan, A. P. & Sefton, M. V. Vascularized organoid engineered by modular assembly enables blood perfusion. *Proceedings of the National Academy of Sciences of the United States of America* **103**, 11461-11466, doi:10.1073/pnas.0602740103 (2006).
206 Fernandez, J. G. & Khademhosseini, A. Micro-Masonry: Construction of 3D Structures by Microscale Self-Assembly. *Advanced Materials* **22**, 2538-2541, doi:10.1002/adma.200903893 (2010).
207 Du, Y., Lo, E., Ali, S. & Khademhosseini, A. Directed assembly of cell-laden microgels for fabrication of 3D tissue constructs. *Proceedings of the National Academy of Sciences* **105**, 9522-9527, doi:10.1073/pnas.0801866105 (2008).
208 Abeyewickreme, A., Kwok, A., McEwan, J. R. & Jayasinghe, S. N. Bio-electrospraying embryonic stem cells: interrogating cellular viability and pluripotency. *Integrative biology : quantitative biosciences from nano to macro* **1**, 260-266, doi:10.1039/b819889f (2009).
209 Ravichandran, R. *et al.* Effects of nanotopography on stem cell phenotypes. *World Journal of Stem Cells* **1**, 55-66, doi:10.4252/wjsc.v1.i1.55 (2009).
210 Annabi, N. *et al.* Controlling the porosity and microarchitecture of hydrogels for tissue engineering. *Tissue engineering. Part B, Reviews* **16**, 371-383, doi:10.1089/ten.TEB.2009.0639 (2010).

211 Hacker, M. C. & Mikos, A. G. Trends in tissue engineering research. *Tissue engineering* **12**, 2049-2057, doi:10.1089/ten.2006.12.2049 (2006).
212 Song, Y. S. *et al.* Engineered 3D tissue models for cell-laden microfluidic channels. *Analytical and bioanalytical chemistry* **395**, 185-193, doi:10.1007/s00216-009-2935-1 (2009).
213 L'Heureux, N. *et al.* Human tissue-engineered blood vessels for adult arterial revascularization. *Nature medicine* **12**, 361-365, doi:10.1038/nm1364 (2006).
214 Buckley, C. T., Thorpe, S. D. & Kelly, D. J. Engineering of Large Cartilaginous Tissues Through the Use of Microchanneled Hydrogels and Rotational Culture. *Tissue Engineering Part A* **15**, 3213-3220, doi:10.1089/ten.tea.2008.0531 (2009).
215 Maidhof, R., Marsano, A., Lee, E. J. & Vunjak-Novakovic, G. Perfusion seeding of channeled elastomeric scaffolds with myocytes and endothelial cells for cardiac tissue engineering. *Biotechnol Prog* **26**, 565-572, doi:10.1002/btpr.337 (2010).
216 Nichol, J. W. & Khademhosseini, A. Modular Tissue Engineering: Engineering Biological Tissues from the Bottom Up. *Soft matter* **5**, 1312-1319, doi:10.1039/b814285h (2009).
217 Tan, W. & Desai, T. A. Layer-by-layer microfluidics for biomimetic three-dimensional structures. *Biomaterials* **25**, 1355-1364 (2004).
218 Shin, M. *et al.* Endothelialized networks with a vascular geometry in microfabricated poly(dimethyl siloxane). *Biomedical microdevices* **6**, 269-278, doi:10.1023/b:bmmd.0000048559.29932.27 (2004).
219 He, J., Zhu, L., Liu, Y., Li, D. & Jin, Z. Sequential assembly of 3D perfusable microfluidic hydrogels. *J Mater Sci Mater Med* **25**, 2491-2500, doi:10.1007/s10856-014-5270-9 (2014).
220 Liu, V. & Bhatia, S. Three-Dimensional Photopatterning of Hydrogels Containing Living Cells. *Biomedical microdevices* **4**, 257-266, doi:10.1023/A:1020932105236 (2002).
221 Hutmacher, D. W. Scaffold design and fabrication technologies for engineering tissues--state of the art and future perspectives. *Journal of biomaterials science. Polymer edition* **12**, 107-124 (2001).
222 Visconti, R. P. *et al.* Towards organ printing: engineering an intra-organ branched vascular tree. *Expert opinion on biological therapy* **10**, 409-420, doi:10.1517/14712590903563352 (2010).
223 Takei, T., Sakai, S., Yokonuma, T., Ijima, H. & Kawakami, K. Fabrication of Artificial Endothelialized Tubes with Predetermined Three-Dimensional Configuration from Flexible Cell-Enclosing Alginate Fibers. *Biotechnology Progress* **23**, 182-186, doi:10.1021/bp060152j (2007).
224 Takei, T., Sakai, S., Ono, T., Ijima, H. & Kawakami, K. Fabrication of endothelialized tube in collagen gel as starting point for self-developing capillary-like network to construct three-dimensional organs in vitro. *Biotechnology and bioengineering* **95**, 1-7, doi:10.1002/bit.20903 (2006).
225 Elloumi-Hannachi, I., Yamato, M. & Okano, T. Cell sheet engineering: a unique nanotechnology for scaffold-free tissue reconstruction with clinical applications in regenerative medicine. *Journal of internal medicine* **267**, 54-70, doi:10.1111/j.1365-2796.2009.02185.x (2010).
226 McAllister, T. N. *et al.* Effectiveness of haemodialysis access with an autologous tissue-engineered vascular graft: a multicentre cohort study. *Lancet (London, England)* **373**, 1440-1446, doi:10.1016/s0140-6736(09)60248-8 (2009).
227 Elloumi Hannachi, I. *et al.* Fabrication of transferable micropatterned-co-cultured cell sheets with microcontact printing. *Biomaterials* **30**, 5427-5432, doi:10.1016/j.biomaterials.2009.06.033 (2009).
228 Zheng, Y. *et al.* In vitro microvessels for the study of angiogenesis and thrombosis. *Proceedings of the National Academy of Sciences* **109**, 9342-9347, doi:10.1073/pnas.1201240109 (2012).
229 Ling, Y. *et al.* A cell-laden microfluidic hydrogel. *Lab Chip* **7**, 756-762, doi:10.1039/b615486g (2007).

230 Paguirigan, A. L. & Beebe, D. J. Protocol for the fabrication of enzymatically crosslinked gelatin microchannels for microfluidic cell culture. *Nature protocols* **2**, 1782-1788, doi:10.1038/nprot.2007.256 (2007).
231 Vijayakumar, K., Gulati, S., deMello, A. J. & Edel, J. B. Rapid cell extraction in aqueous two-phase microdroplet systems. *Chemical Science* **1**, 447-452, doi:10.1039/C0SC00229A (2010).
232 Hu, M. *et al.* Hydrodynamic spinning of hydrogel fibers. *Biomaterials* **31**, 863-869, doi:10.1016/j.biomaterials.2009.10.002 (2010).
233 Kelm, J. M. & Fussenegger, M. Microscale tissue engineering using gravity-enforced cell assembly. *Trends in biotechnology* **22**, 195-202, doi:10.1016/j.tibtech.2004.02.002 (2004).
234 Skardal, A., Zhang, J. & Prestwich, G. D. Bioprinting vessel-like constructs using hyaluronan hydrogels crosslinked with tetrahedral polyethylene glycol tetracrylates. *Biomaterials* **31**, 6173-6181, doi:10.1016/j.biomaterials.2010.04.045 (2010).
235 Guillemot, F., Souquet, A., Catros, S. & Guillotin, B. Laser-assisted cell printing: principle, physical parameters versus cell fate and perspectives in tissue engineering. *Nanomedicine (London, England)* **5**, 507-515, doi:10.2217/nnm.10.14 (2010).
236 Bohandy, J., Kim, B. F. & Adrian, F. J. Metal deposition from a supported metal film using an excimer laser. *Journal of Applied Physics* **60**, 1538-1539, doi:doi:http://dx.doi.org/10.1063/1.337287 (1986).
237 Hopp, B. *et al.* Survival and proliferative ability of various living cell types after laser-induced forward transfer. *Tissue engineering* **11**, 1817-1823, doi:10.1089/ten.2005.11.1817 (2005).
238 Gruene, M. *et al.* Laser printing of stem cells for biofabrication of scaffold-free autologous grafts. *Tissue engineering. Part C, Methods* **17**, 79-87, doi:10.1089/ten.TEC.2010.0359 (2011).
239 Othon, C. M., Wu, X., Anders, J. J. & Ringeisen, B. R. Single-cell printing to form three-dimensional lines of olfactory ensheathing cells. *Biomedical materials (Bristol, England)* **3**, 034101, doi:10.1088/1748-6041/3/3/034101 (2008).
240 Catros, S., Guillotin, B., Bačáková, M., Fricain, J.-C. & Guillemot, F. Effect of laser energy, substrate film thickness and bioink viscosity on viability of endothelial cells printed by Laser-Assisted Bioprinting. *Applied Surface Science* **257**, 5142-5147, doi:http://dx.doi.org/10.1016/j.apsusc.2010.11.049 (2011).
241 Mironov, V. *et al.* Organ printing: Tissue spheroids as building blocks. *Biomaterials* **30**, 2164-2174, doi:http://dx.doi.org/10.1016/j.biomaterials.2008.12.084 (2009).
242 Lee, V. K. *et al.* Creating perfused functional vascular channels using 3D bio-printing technology. *Biomaterials* **35**, 8092-8102, doi:http://dx.doi.org/10.1016/j.biomaterials.2014.05.083 (2014).
243 Absher, M. & Ryan, U. S. Comparison of pulmonary endothelial cell and fibroblast proliferation using time-lapse cinematographic analysis. *Tissue & cell* **13**, 645-650 (1981).